Rita Rodrigues Fernandes de Jesus

Licenciatura em Química Aplicada

Natural inspired small organic molecules for targeting aquaporins as a novel therapeutic approach to pancreatic cancer

Dissertação para obtenção do Grau de Mestre em Química Bioorgânica

Orientador: Carlos Alberto Mateus Afonso, Professor Catedrático, Faculdade de Farmácia da Universidade de Lisboa

Co-orientador: João Rafael Campos do Vale, Mestre em Química Bioorgânica, Faculdade de Farmácia da Universidade de Lisboa

Júri:

Presidente: Professor Doutor António Jorge Dias Parola
Arguente(s): Professora Doutora Paula Cristina de Sério Branco
Vogal(ais): Professor Doutor Carlos Alberto Mateus Afonso

FACULDADE DE CIÊNCIAS E TECNOLOGIA
UNIVERSIDADE NOVA DE LISBOA

Dezembro 2020

2020

Natural inspired small organic molecules for targeting aquaporins as a novel therapeutic approach to pancreatic cancer

Rita de Jesus

Rita Rodrigues Fernandes de Jesus

Licenciatura em Química Aplicada

Natural inspired small organic molecules for targeting aquaporins as a novel therapeutic approach to pancreatic cancer

Dissertação para obtenção do Grau de Mestre em Química Bioorgânica

Orientador: Carlos Alberto Mateus Afonso, Professor Catedrático, Faculdade de Farmácia da Universidade de Lisboa

Co-orientador: João Rafael Campos do Vale, Mestre em Química Bioorgânica, Faculdade de Farmácia da Universidade de Lisboa

Júri:

Presidente: Professor Doutor António Jorge Dias Parola
Arguente(s): Professora Doutora Paula Cristina de Sério Branco
Vogal(ais): Professor Doutor Carlos Alberto Mateus Afonso

FACULDADE DE CIÊNCIAS E TECNOLOGIA
UNIVERSIDADE NOVA DE LISBOA

Dezembro 2020

Natural inspired small organic molecules for targeting aquaporins as a novel therapeutic approach to pancreatic cancer

Copyright, Rita Rodrigues Fernandes de Jesus, Faculdade de Ciências e Tecnologia, Universidade Nova de Lisboa

"A Faculdade de Ciências e Tecnologia e a Universidade Nova de Lisboa têm o direito, perpétuo e sem limites geográficos, de arquivar e publicar esta dissertação através de exemplares impressos reproduzidos em papel ou de forma digital, ou por qualquer outro meio conhecido ou que venha a ser inventado, e de a divulgar através de repositórios científicos e de admitir a sua cópia e distribuição com objetivos educacionais ou de investigação, não comerciais, desde que seja dado crédito ao autor e editor"

Agradecimentos

Deixar a FCT-UNL que foi a minha casa durante 4 anos foi talvez a maior decisão que fiz até hoje. Custou admito, mas o facto de ter ido para um laboratório que me acolheu tão bem e ter comboios Fertagus várias vezes ao dia facilitou o processo de mudança. Este ano conheci pessoas maravilhosas e quero prestar-lhes o meu grande agradecimento.

Em primeiro lugar um obrigada á Professora Dr. Paula Branco que me aconselhou em ir conhecer o Professor Carlos Afonso e o seu laboratório.

Ao Professor Dr. Carlos Afonso, muito obrigada por me ter acolhido no seu laboratório. Obrigada por todas as conversas, pelo apoio e ajuda que me deu ao longo deste ano.

Tive a grande sorte de ter tido 2 grandes mentores que por mais que eu agradeça nunca vai ser suficiente: o Dr. Jaime Coelho e o MSc João Vale. Ao Dr. Jaime Coelho muito obrigada pela sua ajuda durante todo este ano. Embora tenha estado mais presente no segundo projeto da minha tese, foi uma pessoa sempre preocupada em me ajudar no que precisasse. Obrigada pelas discussões de química, por me ensinar a escrever em modo científico (ainda tenho muito para aprender é verdade) e por me fazer sonhar em ir cada vez mais longe. Ao MSc João Vale agradeço de coração o facto de me "aturar" diariamente no laboratório. Nunca me deixou a "nadar na maionese", ensinou-me a trabalhar num laboratório, apoiou-me e ajudou-me sempre que precisei, e graças a ele a Rita que entrou no laboratório há 1 ano não é a mesma. Obrigada por tudo.

Agradeço também às pessoas que mais me marcaram neste laboratório: Maria Beatriz pelo bullying; Milene obrigada por me chamares á Terra; ao meu vizinho Ricardo por me lembrar que tenho tapetes estendidos; ao Ravasco pelas discussões de química e "Chico da Tina"; á Mariama pela sua maneira bonita de ver a vida; Filipa Siopa pela "Gratidão de Luz"; Kessia e Juliana pelas boleias e gargalhadas a caminho de casa.

Um obrigada á Professora Graça Soveral e á MSc Catarina Pimpão pelos ensaios biológicos e por me esclarecer todas as dúvidas de biologia.

Um obrigada gigante a todos os meus amigos, vocês sabem quem são. Em especial á Paula Marques pela amizade que renasceu das cinzas neste mestrado; à Ana Mortinho pelas conversas internacionais; ao meu primo Cascais por ser uma inspiração, e ao meu melhor amigo Fernando por estar sempre presente e nunca se cansar dos meus desabafos.

E por último, aos meus pais e á minha mana. Obrigada pelo apoio incondicional, por acreditarem em mim e motivarem-me sempre a ir mais longe mesmo quando eu acho que não consigo.

Um agradecimento final à Faculdade de Ciências e Tecnologia da Universidade Nova de Lisboa, Faculdade de Farmácia da Universidade de Lisboa e ao iMED.ULisboa por cederem as infraestruturas necessárias à realização desta tese de mestrado e à Fundação para a Ciência e a Tecnologia (FCT) (PTDC/QUI-QOR/32008/2017, UID/DTP/04138/2019), COMPETE Programme (SAICTPAC/0019/2015) pelo apoio financeiro. *This project has received funding from the European Union's Horizon 2020 research and innovation programme under grant agreement No 951996.*

Resumo

O aproveitamento de productos naturais para uma potencial aplicação terapêutica e/ou catálise assimétrica é uma abordagem interessante para a valorização de produtos naturais. Assim sendo, neste trabalho dois projetos foram estudados: descoberta de novos agentes farmacológicos para o tratamento do cancro, e desenvolvimento de uma nova série de catalisadores assimétricos.

As aquaporinas (AQPs) são proteínas transmembranares envolvidas em processos metastáticos e de crescimento tumoral. Deste modo, o seu potencial como alvos terapêuticos levou ao estudo de moduladores de AQPs a partir de fontes naturais. Neste primeiro projeto, dois diterpenos do tipo lábdano presentes na planta *Cistus Ladaniferus* – ácido labdanólico a ácido-6-oxocativico – foram isolados e a sua atividade biológica estudada em três diferentes AQPs (AQP1, AQP3 e AQP5), com o objetivo de descobrir uma terapia inovadora para o tratamento do cancro. Através de estudos de permeabilidade usando a técnica de stopped flow, foi possível concluir que ambos os compostos não são promissores para o tratamento do cancro, visto que não é observado em nenhuma das AQPs em estudo uma diminuição da permeabilidade. Paralelamente, síntese do ácido-6-oxocativico partindo do ácido labdanólico foi desenvolvida, mas sem resultados promissores.

Tirando partido de outra planta — *Lupinus albus L.* — outra família de productos naturais é encontrada: alcalóides quinolizidínicos. A lupanina e a esparteina são compostos com conhecida atividade farmacológica e membros desta família de compostos. A esparteina é conhecida principalmente como base quiral em catálise assimétrica. Tendo em conta a possibilidade de desenvolver uma nova série de catalisadores assimétricos com uma enantiosselectividade superior á já conhecida esparteína, e com base em estudos previamente desenvolvidos no nosso grupo, neste segundo projeto foi iniciado o desenvolvimento de uma nova série de catalisadores assimétricos com base na funcionalização C-H eletroquímica da lupanina com um grupo nitrilo numa abordagem que até hoje não está reportada na literatura. Em batch, 17-ciano-*rac*-lupanina foi obtida com elevada seletividade e rendimento, enquanto que em química de fluxo, estudos adicionais devem ser efetuados para melhorar a seletividade da reação. Paralelamente, derivatizações foram efetuadas na 17-ciano-*rac*-lupanina e 17-ciano-*rac*-esparteina, levando à formação de produtos sinteticamente úteis. No âmbito de descobrir novos inibidores de aquaporinas, 17-ciano-*rac*-lupanina, 17-ciano-*rac*-esparteina e os derivados sintetizados ao longo deste trabalho foram estudados em três diferentes AQPs (AQP1, AQP3 e AQP5) usando a técnica de stopped flow. Os resultados indicam que todos os compostos em estudo não são promissores para o tratamento do cancro.

Ambos os projetos têm com objetivo valorizar a aplicação dos produtos naturais.

Palavras-chave: aquaporinas, moduladores, eletroquímica, alcalóides quinolizidínicos, química de fluxo

Abstract

Exploration of natural products for potential therapeutic use and asymmetric organic synthesis is an interesting approach for natural product valorisation. Therefore, in the present work, two projects were investigated: discovery of novel pharmacological agents for cancer treatment and development of a new series of asymmetric catalysts.

Aquaporins (AQPs) are transmembrane proteins involved in metastatic and tumour growth processes. Thus, their potential as a novel druggable cancer target prompted the study of AQPs modulators, from natural sources. In this first project, two labdane diterpenes present in Cistus Ladaniferus — Labdanolic acid (LA) and 6-oxocativic acid (OA) — were isolated and their biological activity was studied in three different AQPs (AQP1, AQP3, AQP5), aiming to unleash a new therapeutic application for cancer treatment. Through AQPs permeability assays using the stopped flow technique, results indicated that both compounds were not promising for cancer treatment, since a decrease in permeability is not depicted in any of the AQPs under study. In addition, a linear total synthesis of OA from LA was investigated but without promising results.

Using another natural source —Lupinus albus L. — another family of natural products is encountered: quinolizidine alkaloids. Lupanine and Sparteine are members of this family with known pharmacological activity. Sparteine is mostly known for its use in asymmetric catalysis as a chiral base. Considering the possibility of developing a new series of asymmetric catalysts with increased enantioselectivity comparing to the already known chiral base sparteine, and based on studies previously developed in our group, in this second project we envisioned the development of a new series of asymmetric catalysts via functionalization of lupanine with a nitrile functional group, through a yet unreported C-H activation electrochemical approach. In batch, 17-cyano-rac-lupanine was obtained in high yield and selectivity, whereas in flow, further studies need to be performed to improve reaction selectivity. Additionally, derivatizations of 17-cyano-rac-lupanine and 17-cyano-rac-sparteine were investigated, yielding new synthetically useful products. In the context of finding novel AQPs inhibitors, 17-cyano-rac-lupanine, 17-cyano-rac-sparteine and the derivatives synthetized throughout this work were studied in three different AQPs (AQP1, AQP3, AQP5) using the stopped flow technique. No promising results in regard to cancer treatment were obtained.

Both projects will add insight to natural product utility.

Keyword: aquaporins, modulators, electrochemistry, quinolizidine alkaloid, flow chemistry

Subject Index

Figure Index

Table index

Abbreviations:

^{13}C NMR – Carbon Nuclear Magnetic Resonance

^{1}H NMR - Proton Nuclear Magnetic Resonance

ACN - Acetonitrile

AQPs – Aquaporins

BOP - Basic organic phase

DMF - Dimethylformamide

EtOAc – Ethyl Acetate

Hex – Hexane

HRMS – High resolution mass spectrometry

IR – Infrared

LA – Labdanolic acid

MTBE - *tert*-Butyl methyl ether

NMO - N-Methylmorpholine N-oxide

NPA - asparagine-proline-alanine

OA – 6-oxocativic acid

PCC - Pyridinium Chlorochromate

PDC - Pyridinium Dichromate

PMA - Phosphomolybdic acid

RBCs - red blood cells

R_f – Retention factor

SF - selectivity filter

TLC – Thin Layer Chromatography

TPAP - Tetrapropylammonium perruthenate

1. Natural inspired small organic molecules for targeting aquaporins

According to the World Health Organization, Cancer is one of the major causes of mortality around the world[1]. Therefore, the urge to develop new therapies that inhibit growth and proliferation of cancer cells, metastasis and control invasion is of extreme importance[2].

The process of drug discovery begins with the choice of a target biomacromolecule, such as proteins and nucleic acids[3]. Ideally, a putative drug molecule will interact with these biomolecules, either provoking its activation or inhibition, leading to innovative medical treatments[4]. A promising drug-target are Aquaporins (AQPs): proteins responsible for the transport of water and other small molecules through the plasma membrane in response to osmotic or solute gradients[5]. Evidence shows their impact in various pathologies such as breast and lung cancer, highlighting their therapeutic potential[6].

1.1 Aquaporins

AQPs are a family of integral transmembrane protein channels identified in mammals and until now 13 isoforms are known (AQP0-12)[7]. All display high homology in protein sequence and there are three AQPs subfamilies, based on their primary sequence and channel selectivity: i) Orthodox AQPs, selective for water (AQPs0, 1, 2, 4, 5, 6, 8); ii) Aquaglyceroporins (AQPs3, 7, 9, 10), that besides water also present permeability to glycerol, urea, arsenite and hydrogen peroxide; and iii) S-aquaporins (AQP11, 12) which are characterized by a different signature pattern in the NPA motif [8] (*vide infra*). Noteworthy, AQP11 transports water and glycerol, and AQP12 permeability remains uncertain[5]. These proteins are composed by 4 identical monomers[2], and each monomer has 6 transmembrane domains (connected by 5 loops) with intracellular amino and carboxyl termini.[5]

The three-dimensional fold and oligomerization of AQPs' 13 isoforms is highly conserved **(Figure 1.1)**: all have a characteristic asparagine-proline-alanine (NPA) motif and a selectivity filter (SF) region.[9] The NPA motifs (present in cytoplasmatic loop B and extracellular loop E), contribute to a monomeric pore structure that provides the transport of water and other small polar solutes in a selective and bidirectional way. The SF region is what distinguishes the 13 isoforms, because the size of the pore will determine which type of molecule will pass through it.[2]

(A) **(B)**

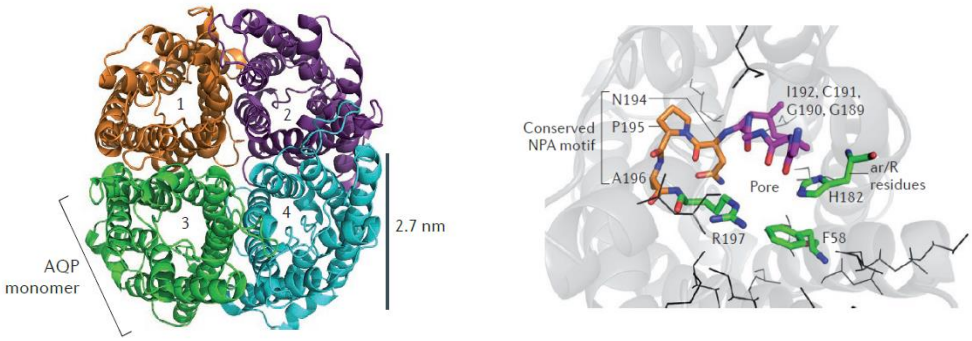

The transport rate of these molecules relies on the quantity of AQPs present in the cell membrane and in their single channel permeability. However, upon regulation[10], AQP permeability or AQP abundance can be changed leading to a shift in transport intensity.

1.1.1 AQP1, AQP3 and AQP5: function and modulation

AQPs' action mechanism is crucial in all living cells, especially in malignant cells. In this work we will focus our attention in two orthodox AQPs (AQP1 and AQP5) and in aquaglyceroporin AQP3.

AQP1 is expressed in several tumour cell types such as brain and in the pancreas intercalated ductal cells[11]. Studies have shown that reduced tumour growth and tumour necrosis were observed in mice lacking AQP1[12], as well as less aggressive metastatic processes in the absence of AQP1 expression.[13] AQP5 is overexpressed in various tumours like lung, breast and in pancreas intercalated ductal cells[11]. In lung tumours, when AQP5 gene is silenced, a decrease in cancer migration and proliferation is observed [14]. These data show that water permeability mediated by these macromolecules contributes to tumour development.

The aquaglyceroporin AQP3 is upregulated in skin tumours and in pancreatic islet cells[15] . Studies in mice lacking AQP3, show resistance to skin cancer development which can be explained by the lower intake in glycerol.[16] For a tumour to grow, tumour cells require a higher quantity of energy to divide more rapidly.[17] Since glycerol is used to produce adenosine triphosphate (ATP)[18], the more glycerol is provided, the more the tumour is going to develop.

The overexpression of AQP3 and AQP5 is a result of the epidermal growth factor receptor (EGFR) signalling pathway. In some tumours, such as pancreatic cancer, this receptor is highly expressed which upon activation prompts the transcription of genes involved in cell growth and proliferation[19].

Based on AQPs implication in physiological events suchlike tumour angiogenesis, cell migration and proliferation and metastasis[20], drug development using AQPs as target emerged[16]. Several molecules with distinct scaffolds have been identified as modulators of AQP1 and AQP3. In 1993, studies showed that mercury sulfhydryl reagents inhibit AQP1 due to its interaction with a specific cysteine residue[21]. However major drawbacks suchlike toxicity and lack of specificity, were not attractive for the development of suitable drug candidates. Another metal-based compound is Auphen **(Figure 1.2)**: a gold (III) center coordinated to two nitrogen atoms and a multidentate ligand. This gold compound can block AQP3 glycerol transport, probably due to the interaction between the gold center and sulfhydryl groups in proteins, namely thiolates groups of cysteines[22]. One derivative of Bumetanide named AqB013 inhibits water permeation in AQP1, which in turn suppress colon cancer migration and invasion in vitro.[2] Nature can also provide biologically active molecules as is the case with curcumins and resveratrol. Curcumins, present in the turmeric plant, besides possessing anti-inflammatory activity, can also decrease AQP1 expression.[23] The Stilbene resveratrol, known for its activity in preventing inflammation and carcinogenesis[24], can reduce the expression of AQP3, shedding light in solving skin disorders.[23] So far, no inhibitors or AQP5 have been identified.

By looking at the various scaffolds, it is possible to conclude that there is no structural similarity between them. Consequently, and considering the great source of inspiration that natural sources provide, the aim of this work was to isolate and investigate potentially biologically active molecules from a natural source for targeting pancreatic cancer. Due to the high mortality rate associated with pancreatic cancer[25], the urge to develop novel and effective approaches is of great importance. Considering the expression of AQP1,3 and 5 in the human pancreas, modulation of these AQPs could give valuable insight in tumour regression.

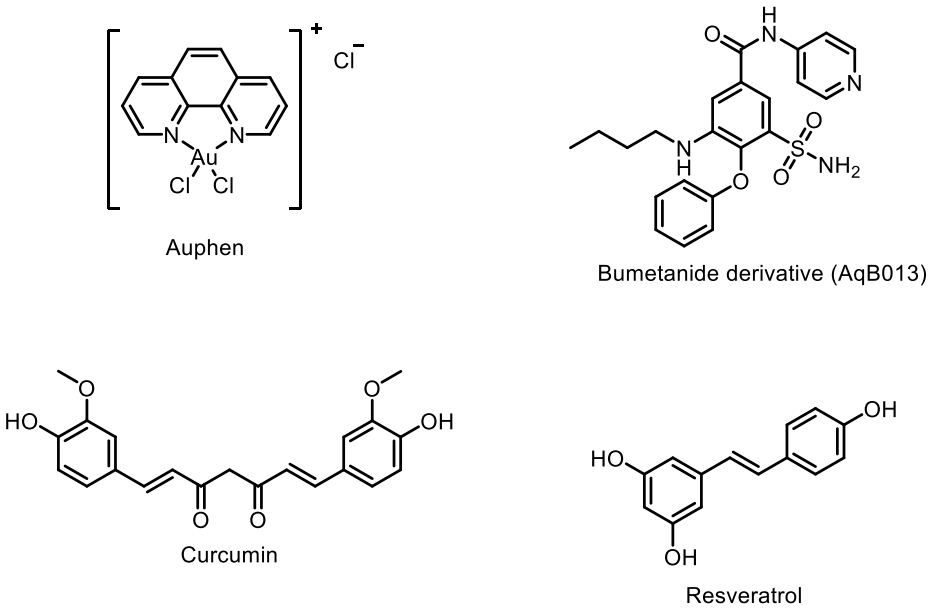

Figure 1.2: Structure of several inhibitors of AQP1 and AQP3.

1.2 *Cistus ladaniferus:* a natural source of Terpenes

Cistus ladaniferus (*C. ladaniferus*), known as “esteva” in Portugal, is a plant that grows in a lot of Mediterranean countries.[26] From its extract, nearly 300 compounds can be isolated, whose major compounds present belong to the terpene family.

Terpenes are molecules originated through the assembly of C5 isoprene units **(Figure 1.3)**, either in a head-to-tail or in a tail-to-tail fashion. Depending on the number of C5 units, terpenes can be classified as hemiterpenes (C_5), monoterpenes (C_{10}), sesquiterpenes (C_{15}), diterpenes (C_{20}), sesterterpenes (C_{25}), triterpenes (C_{30}) and tetraterpenes (C_{40}).[27]

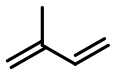

Figure 1.3: C_5 Isoprene unit.

The major compound present in *C. ladaniferus* is the diterpene Labdanolic Acid (LA). The presence of a labdane skeleton – decalin system with 5 chiral atoms – prompts pharmacological activity since several plants and marine sources with this skeleton show biological activity[28,29,30] **(Appendix 9)**.

Based on the therapeutic properties displayed, labdane diterpenes present in *C. ladaniferus* should be further studied. LA can be used as starting material for microbial transformations [31] and for the synthesis of small molecules with anti-inflammatory activity[30] such as labdanolic acid methyl ester **(Figure 1.4).** Ambrox is another compound present in *C. ladaniferus* and is acknowledged for its ambery note and fixative properties in the perfume industry. Its importance dates back to 1930s, when Firmenich – world´s largest company in fragrance and flavour business - invested in the synthesis of Ambrox instead of extracting it from a natural source[32]. (-)-sclareol continues to be a good starting material for Ambrox synthesis, however the use of LA as starting material provides a cheaper and more convenient synthesis, due to its abundance in nature.

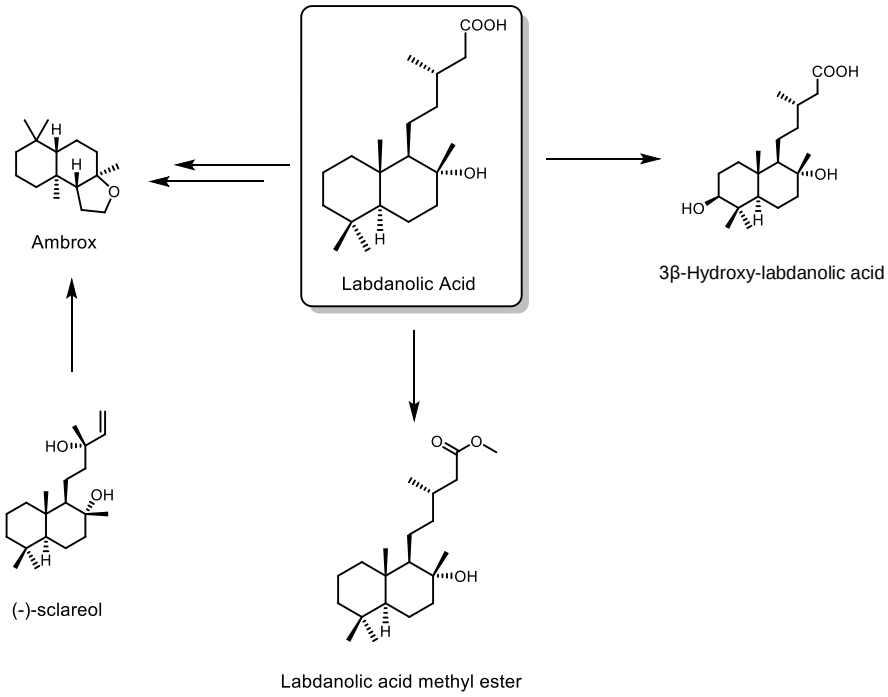

Figure 1.4: Possible transformations of Labdanolic acid: through microbial transformation, 3β-Hydroxy-labdanolic acid is obtained; labdanolic acid methyl ester has anti-inflammatory activity, and Ambrox synthesis instead of using (-)-sclareol as starting material.

Apart from Ambrox and LA, other minor compounds can be isolated as is the case of 6- oxocativic acid (OA) **(Figure 1.5)**. This α, β – unsaturated ketone had already been isolated and characterized, but pharmacological activity and potential uses such as starting material for the synthesis of small molecules has never been reported[33].

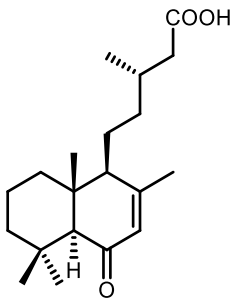

Figure 1.5: Structure of 6-oxocativic acid (OA).

Considering all the biological properties of labdane diterpenes, it is of great interest to study LA and OA pharmacological activity in a drug target. Since AQPs inhibitors reported in the literature, do not present a similar scaffold, labdane diterpenes may present a yet unexplored AQP modulation. Therefore, LA and OA were isolated from *C. ladaniferus* and biological assays against AQP1, AQP3 and AQP5 were performed, which may offer a novel therapeutic approach to several diseases. Additionally, and bearing in mind the possible applications of OA remaining to be discovered, synthesis of OA will be performed using LA as starting material.

1.3 Synthesis of 6-Oxocativic Acid

The linear synthesis planned started with a dehydration reaction yielding a mixture of olefins. Afterwards, allylic oxidation(s) can be performed to afford the desired α, β – unsaturated ketone **(Figure 1.6)**.

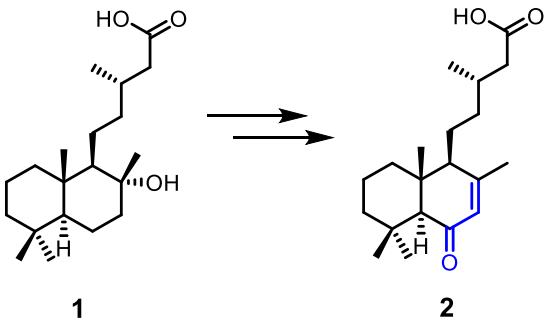

Figure 1.6: Structure of LA **(1)** and OA **(2)**, highlighting the desired α, β – unsaturated ketone

1.3.1 Dehydration reaction

Several reagents can be used for dehydration reactions such as Martin's sulfurane[34] or Burgess reagent[35] **(Figure 1.7)**. Even though they are selective reagents for the obtention of alkenes, more environmentally friendly alternatives can be explored. Amberlyst®-15(dry) is an heterogenous catalyst produced by the cross-linking of styrene with divinyl benzene and sulfonation with sulfonic groups (-SO_3H)[36]. Due to its macroreticular pore structure, this acidic resin can easily conduct the reactants to the hydrogen ion sites located across the bead[37]. This resin, not only is well tolerated by various functional groups (Boc and TBDMS) but also presents the advantage of being reused[37].

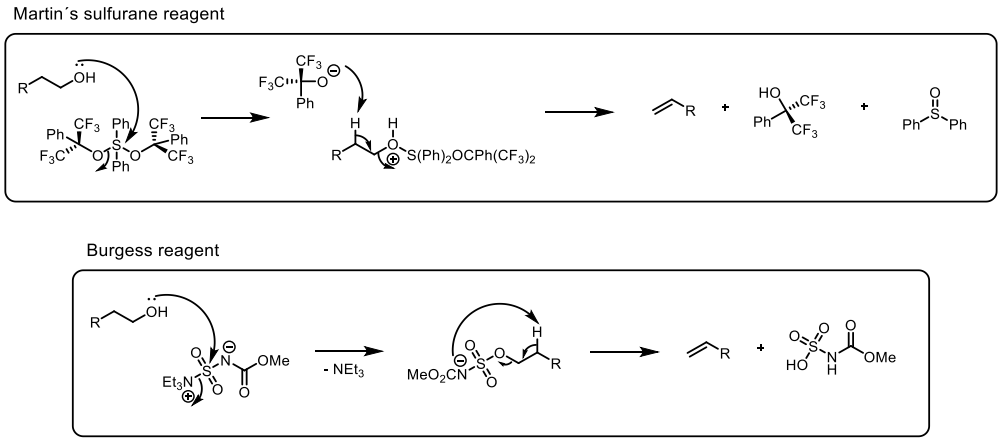

Figure 1.7: Dehydration mechanism using Martin´s sulfurane reagent (top mechanism) and Burgess reagent (bottom mechanism).

1.3.2 Allylic Oxidation

Alkene functionalization through hydroboration and allylic oxidation are just some useful examples to increase molecular complexity[38]. Since OA has an α,β-unsaturated ketone in its scaffold, an allylic oxidation was the next step of this synthesis. Depending on the reaction

conditions, the regioselective substitution of an allylic C-H bond for an oxygen provide allylic alcohols and/ or α,β-unsaturated compounds.

Chromium (VI) reagents like PCC (Pyridinium chlorochromate) or transition metal reagents such as rhodium complexes are useful reagents to yield enones[39]. Nevertheless, the most used reagent for allylic oxidation is Selenium Dioxide (SeO_2). Even though it presents hazardous effects towards health, this inexpensive and easy to handle reagent, yields the allylic alcohol in most cases[40]. As proposed by Sharpless in 1972[41], the allylic alcohol is obtained through an Alder-ene reaction. Then, a [2,3]-sigmatropic rearrangement followed by hydrolysis will yield the desired allylic alcohol[38] **(Figure 1.8)**. However, depending on reaction conditions – solvent, temperature, and stoichiometry – α, β-unsaturated compounds and ethers can be produced in addition to allylic alcohols[42], as a result of overoxidation.

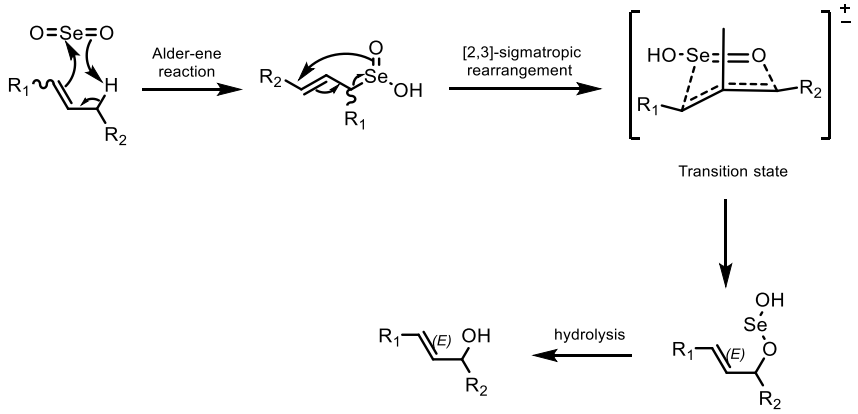

Figure 1.8: Allylic Oxidation mechanism with SeO_2.

In case overoxidation does not occur, the allylic alcohol needs to be further oxidized. MnO_2 is a selective reagent for the oxidation of primary/secondary allylic or benzylic alcohols to their corresponding aldehyde and ketone, even in the presence of saturated alcohols[43]. This transition metal oxide presents various advantages: it is a low cost and highly abundant reagent,[44] and work up procedure is simple. Its selectivity can be explained by the formation of a carbonyl in conjugation with an unsaturated system which is favourable thermodynamically **(Figure 1.9)**[43]**.** However, when the reaction is exposed to higher temperatures, this reagent becomes unselective, leading to side reactions like transforming aromatic primary amines into azo compounds[45].

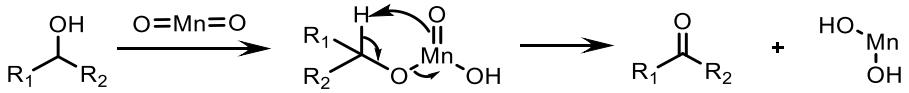

Figure 1.9: MnO_2 allylic oxidation mechanism

Another oxidizing reagent is Tetrapropylammonium perruthenate (TPAP). This ruthenium compound, also known as Ley–Griffith reagent, is a soluble, non-volatile and air stable oxidant[46]. It is highly selective to convert primary alcohols to aldehydes and secondary alcohols to ketones, and presents tolerance to a wide variety of functional groups and protecting groups[47] . Both allylic and secondary alcohols are oxidized with TPAP, however more sterically hindered alcohols react slower[48]. With a suitable co-oxidant, like N-Methylmorpholine N-oxide (NMO), this oxidation reaction can proceed catalytically **(Figure 1.10)**. The reaction is done in DCM or ACN with finely grounded molecular sieves, so that water formed during the catalytic cycle is removed, and the efficiency of the oxidation is not affected[48].

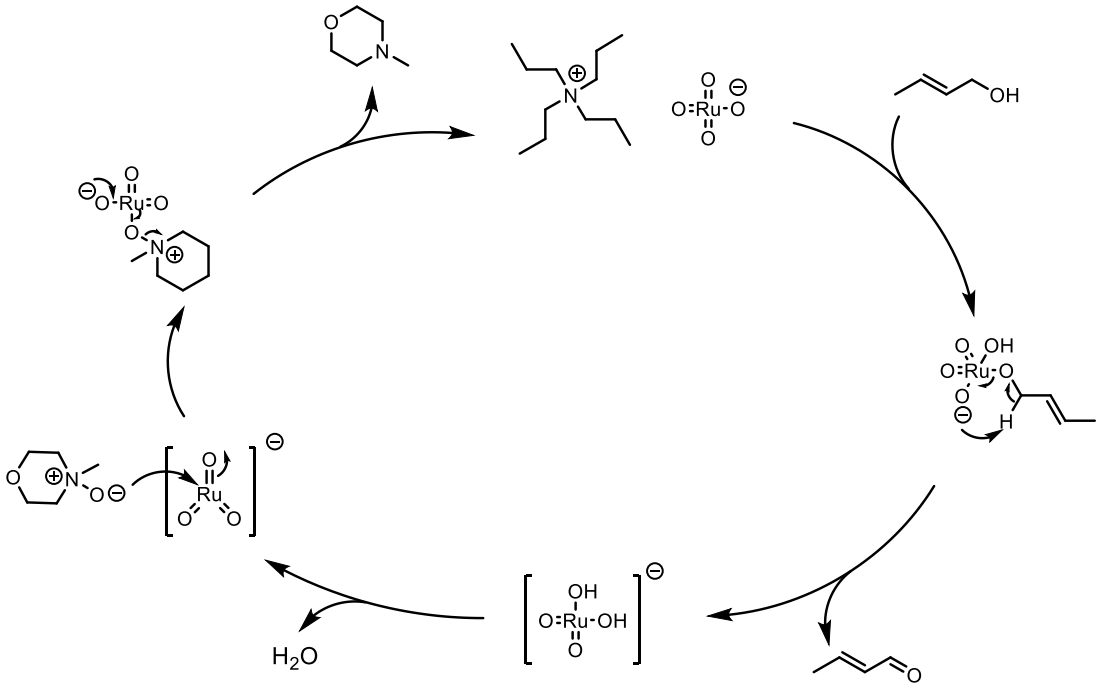

Figure 1.10: Ley-Griffith Oxidation Catalytic Cycle, using as co-oxidant NMO.

1.4 Objectives

Inspired by the therapeutic properties of labdane diterpenes, the objective of this work was to study the modulation of three AQPs (AQP1, AQP3 and AQP5) in the presence of LA and OA isolated from *C. ladaniferus*. The inhibitory effect in orthodox AQPs (AQP1 and AQP5) was measured using light scattering stopped-flow technique, and for aquaglyceroporins (AQP3) fluorescent stopped-flow technique was used.

After isolation of LA and OA, a linear synthesis of OA from LA was performed.

1.5 Results and Discussion

1.5.1 Extraction and Isolation of Labdanolic Acid and 6-Oxocativic Acid

To isolate LA and OA, an extraction methodology **(Figure 1.11)** previously reported in our group was followed **(Section 3.2)**.[49] The leaves were soaked in an ethanolic basic solution for 3 days, and after solvent evaporation and washes with an aqueous basic solution, the carboxylate form of LA and OA were present in the aqueous phase.

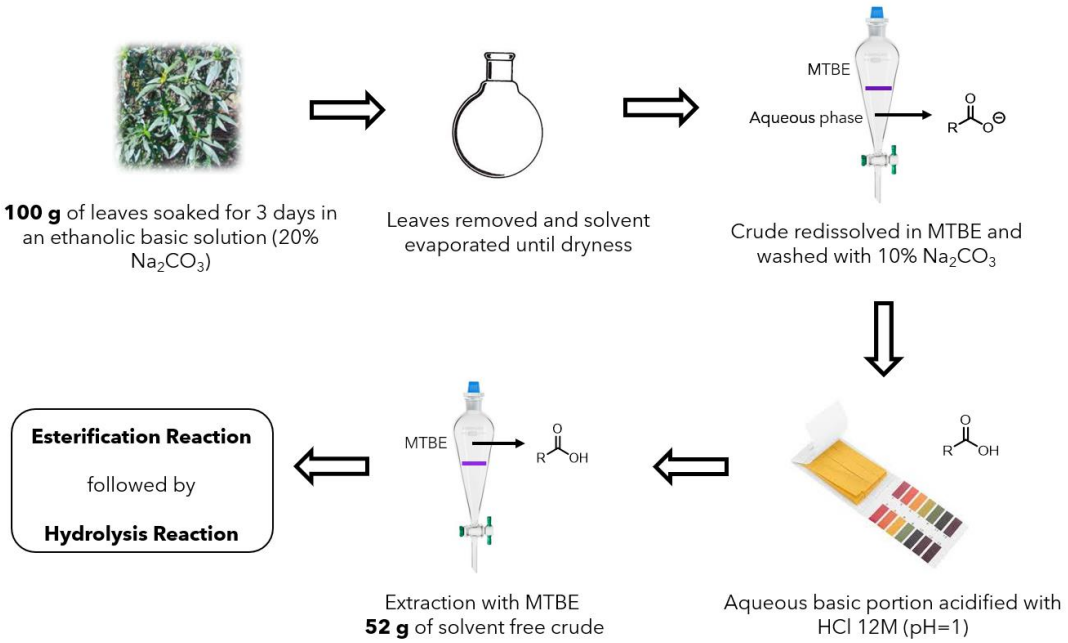

Figure 1.11: LA and OA extraction methodology.

The organic phase obtained from these washes was characterized **(Appendix 1),** presenting high structural diversity as depicted by Infrared Spectrometry (IR) **(Figure 1.12)**: broad band (3400 cm^{-1}) characteristic of O-H bonds; C-H aliphatic stretch band at 2800 cm^{-1}; *overtones* indicate the presence of aromatic compounds; C=O stretch band (1735 cm^{-1}) of carbonyl compounds and C=C stretch at 1657 cm^{-1} from olefins. This mixture can be seen as a renewable source for the production of valuable products: using microbial catalysts that gain energy from the degradation of aromatic molecules, a complex mixture can be *biologically funnelled* into useful reagents[50].

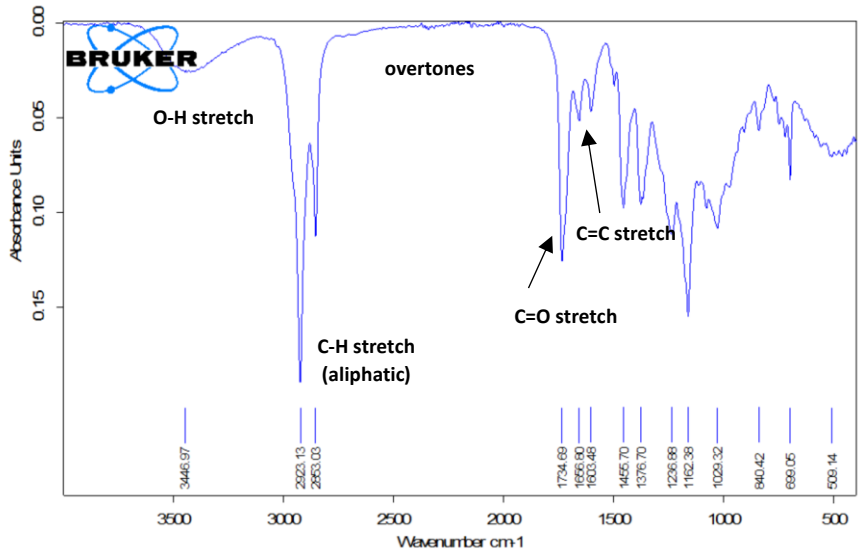

Figure 1.12: Infrared Spectra from Basic Organic Phase with the structure of some functional groups present in the mixture.

The aqueous phase was acidified to protonate LA and OA carboxylate, and then extractions were performed, affording 52 g of crude. After the extraction procedure, TLC analysis of the crude showed a high content of compounds which represented a challenge in isolating LA and OA. Considering that esters are less polar and water soluble than carboxylic acids, an esterification reaction was performed to facilitate isolation, which would be followed by a hydrolysis reaction to yield both compounds.

1.5.2 Esterification Reaction

The synthesis of esters using carboxylic acids as starting material can be done in two different approaches: using the carboxylic acid as electrophile or using the corresponding carboxylate as nucleophile. When acting as electrophile, Fisher reaction[51] or Steglich reaction[52] can be performed, however the traditional method consists in using an excess of the alcohol (reactant) under acid catalysis. As nucleophile, its acidity should be considered because in the presence of a base, the carboxylate ion reacts with alkyl halides via S_N2 reaction[53].

Taking into account that LA has a tertiary alcohol, to avoid its potential elimination under acidic conditions, esterification of the crude was performed under basic conditions, i.e, a S_N2 reaction between the corresponding carboxylate and methyl iodide **(Figure 1.13)**. Due to the absence of a tertiary alcohol in OA, basic medium is suitable for both compounds **(Section 3.3).**

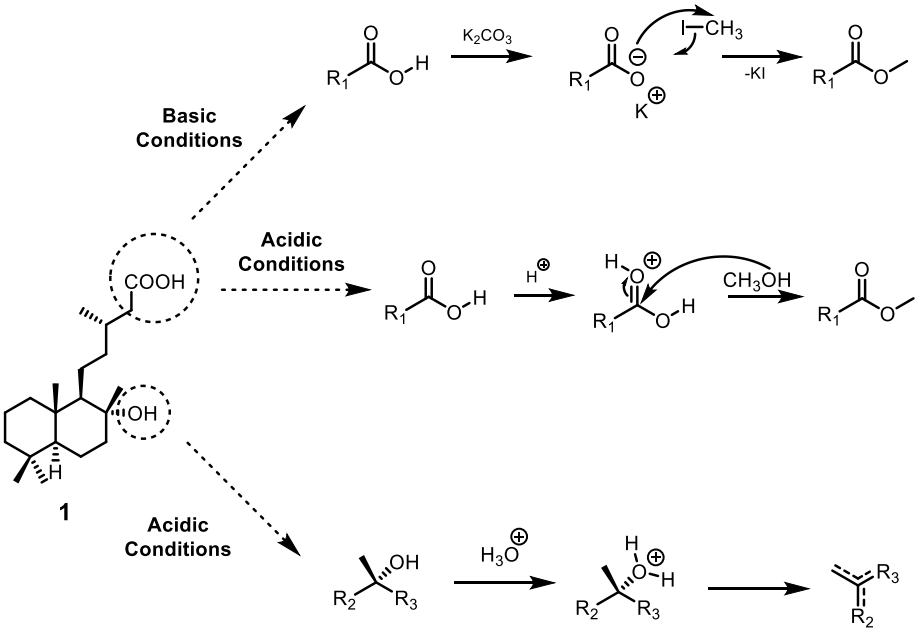

Figure 1.13: Esterification reaction under basic conditions and acidic conditions, using LA **(1)** as template. Acidic conditions are not desirable since the -OH group is turned into a good leaving group, being eliminated.

An adapted protocol for esterification was used[53] , resulting in the formation of several products which were isolated and characterized by ^{1}H NMR **(Appendix 2).** On agreement with reported values[54], one of the fractions contained LA methyl ester **(Appendix 2 - Figure 5.3)**, characterized by singlet at 3.65 ppm from the ester methyl group.

Comparing LA methyl ester **(3)** fraction with the ^{1}H NMR spectra from one of the remaining fractions **(Appendix 2 - Figure 5.4)**, signals in the range of 5 ppm-5.50 ppm characteristic of olefins were observed, indicating the possible presence of OA methyl ester **(4)**. Knowing the exact mass of OA methyl ester (334.25), high resolution mass spectrometry (HRMS) experiments were performed, and the peak observed at 335.25 *m/z* correspondent to $[M+H]^+$, indicated the presence of α, β – unsaturated ketone in that fraction.

The identification of both esterified compounds proved that the esterification reaction was a good starting point. For a better understanding each compound will have a name: LA methyl ester will be named *LA methyl ester-1*, and OA methyl ester will be *OA methyl ester-1.* Considering that prior to isolation no commercial standard was available in the laboratory that could be used on TLC to help identify both compounds in terms of Rf, the obtention of these 2 compounds is an achievement that was valuable across the whole isolation process. Having a standard of both esterified compounds in hands, a hydrolysis reaction was performed first with LA methyl ester, since it was the fraction obtained in higher amount.

1.5.3 Hydrolysis Reaction

Considering the presence of a tertiary alcohol in LA **(1)**, the reaction will proceed through base-catalysed hydrolysis **(Figure 1.14)**, since its displacement in acidic conditions would yield secondary products.

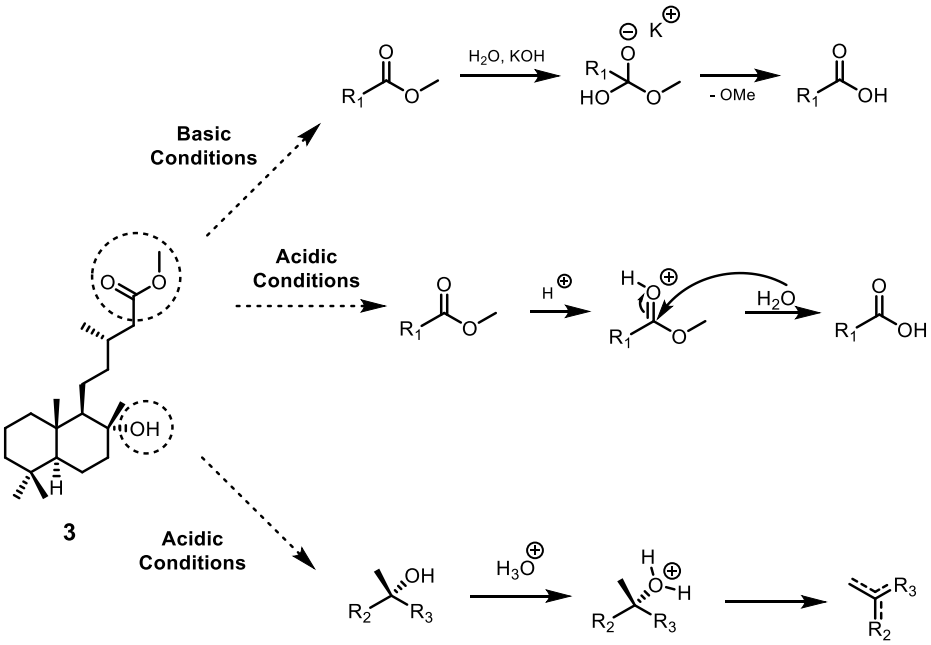

Figure 1.14: Hydrolysis reaction under basic conditions and acidic conditions, using LA methyl ester **(3)** as template. Acidic conditions are not desirable since the -OH group is turned into a good leaving group, being eliminated.

Using as starting material LA methyl ester-1, a hydrolysis reaction[55] was performed using potassium hydroxide (KOH) as base in mixture of THF and H_2O **(Section 3.4 – Procedure A)**, in order to obtain the carboxylic acid moiety. This methodology led to C-OMe bond cleavage, and formation of a new C-OH bond, as depicted in **Figure 1.15**, where the singlet at 3.65 ppm correspondent to the ester methyl group is absent. Despite the low yield (28%) which can be explained by the quantity of KOH used, this methodology proved to be useful in the hydrolysis of the ester. Since the esterification reaction yielded small quantities of LA methyl ester-1 and OA methyl ester-1, esterification reactions were upscaled, an optimized hydrolysis procedure was developed **(Section 3.4 – Procedure B)** and a series of flash chromatography were done in order to obtain both compounds in the purest form for the biological assays.

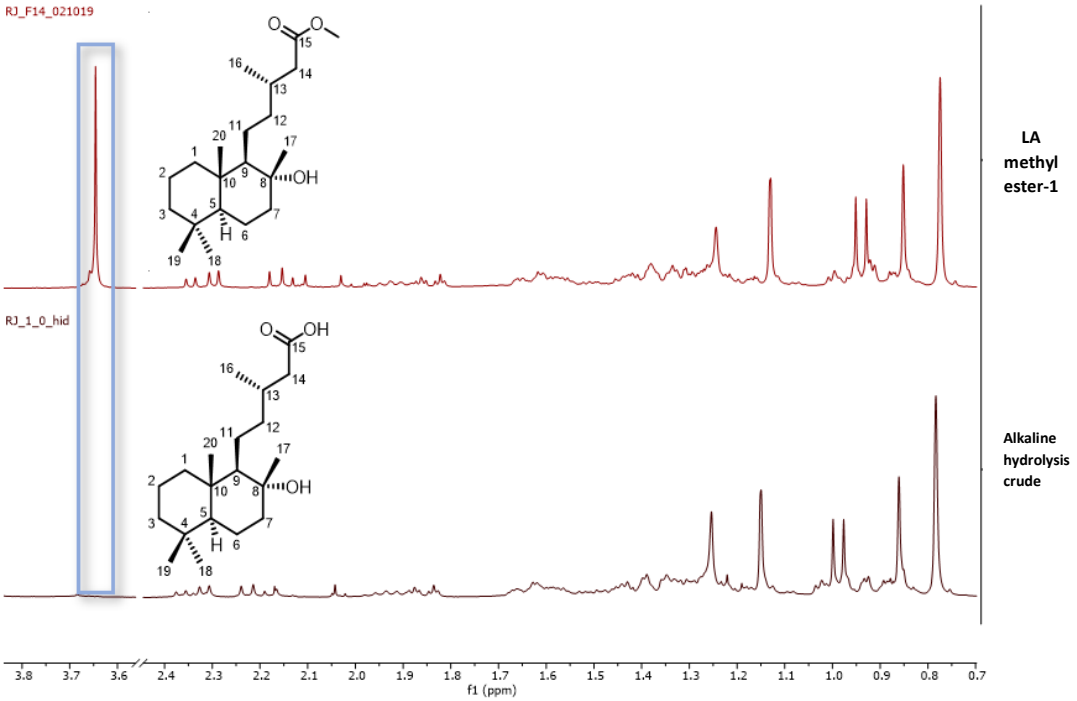

Figure 1.15: Comparison between the ^{1}H NMR of LA methyl ester-1 (top spectra) with the crude ^{1}H NMR from the alkaline hydrolysis reaction (bottom spectra), highlighting the disappearance of the singlet at 3.65 ppm.

1.5.4 Upscaled Esterification reactions and Hydrolysis Reaction

Throughout the isolation methodology, all upscaled esterification reactions were executed using 10 g of starting material, while the experimental procedure remains unchanged **(Section 3.3)**.

1.5.4.1 6-Oxocativic acid Isolation

In an upscaled esterification reaction the less polar compound – OA methyl ester **(4)** – was easily identified from the eluted fractions of a column chromatography, thanks to OA methyl ester-1 previously isolated. Due to the presence of impurities, column chromatography were performed using as mobile phase a mixture of EtOAc/Hex. This mixture of solvent did not lead to OA methyl ester in the purest state, meaning that a new mobile phase still needed to be optimized in order to improve and accelerate isolation. Other purification methods such as preparative chromatography could be used, however, both LA and OA do not contain an aromatic system in their structure, which means UV light will not be absorbed. Addition of a chromophore through a benzylation reaction can be a possibility if the shift of mobile phase does not improve isolation.

Using as new mobile phase a mixture of MTBE/Toluene, one fraction was obtained, which corresponded to the compound with less impurities so far **(Appendix 3 – Figure 5.5)** characterized by peak at 5.74 ppm from the vinylic proton. This compound will be the new standard, named OA methyl ester - 2. This change of standard shows that the level of purity is increasing, and its comparison with future compounds/fractions will result in a more accurate judgement.

Despite the presence of impurities in OA methyl ester-2, a hydrolysis reaction was performed **(Section 3.4 - Procedure B)**, since none of the mobile phases tested to purify the compound led to a good separation. After purification by column chromatography, 2 fractions were obtained, that after characterization, one of them corresponded to the desired compound **(Appendix 3 – Figure 5.6/Figure 5.11)**.

Through a combination of esterification reactions, hydrolysis reactions and purification steps, OA **(2)** was finally obtained **(Figure 1.16)** in 0.04 wt % (18.7 mg). The major difficulty encountered along the process was in identifying a good mobile phase for column chromatography's due to the presence of several compounds with the same R_f. It is important to point out that the whole isolation process did not rely in any commercial standard: all standards were acquired by a combination of nuclear magnetic resonance and HRMS information.

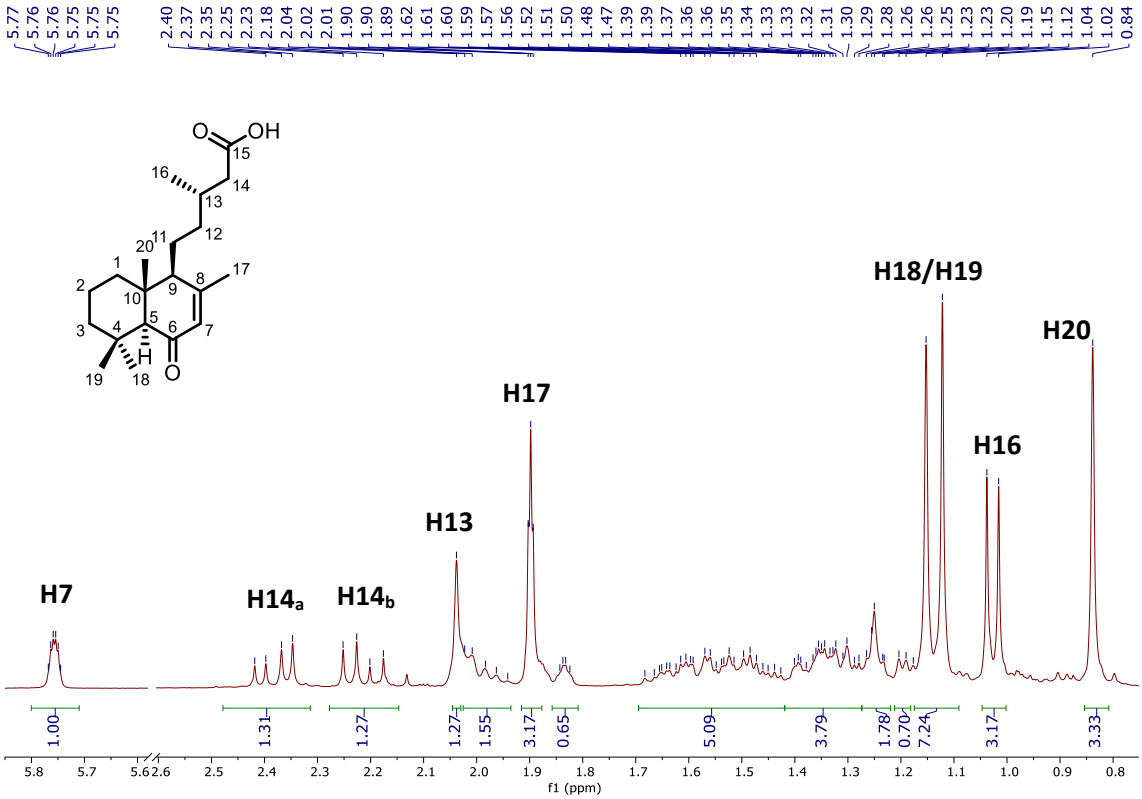

Figure 1.16: ^{1}H NMR spectrum of OA **(2)**

1.5.4.2 Labdanolic Acid Isolation

With LA methyl ester-1 standard, LA methyl ester was also easily spotted among the various fractions obtained from the upscaled esterification reaction **(Appendix 3 – Figure 5.12).** Bearing in mind the problems faced in OA isolation, instead of executing several purification steps, a hydrolysis reaction was performed **(Section 3.4 - Procedure B).** The success of the hydrolysis procedure was once again proven by C-OMe bond cleavage and C-OH bond formation **(Appendix 3 – Figure 5.13)**. To attain the labdane diterpene in its purest form, 2 column chromatographies were followed, yielding LA in 1.8 wt % **(Figure 1.17/Appendix 3 – Section 5.3.2).** LA **(1)** isolation was quicker comparing to OA **(2)** due to the absence of compounds with the same R_f.

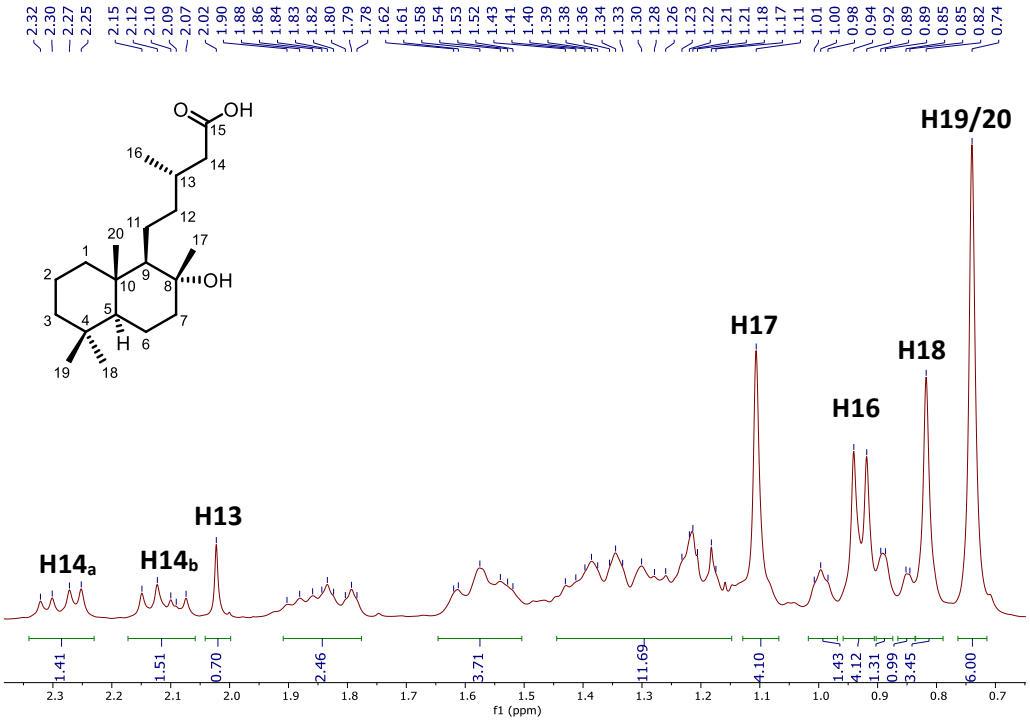

Figure 1.17: ^{1}H NMR spectrum of LA **(1)**

1.5.5 Characterization Analysis

After extraction and isolation, LA and OA were characterized by ^{1}H NMR and ^{13}C NMR. Both labdane diterpenes possess a carboxylic acid functional group (C15) depicted by peak 178.5 ppm in OA **(Table 1-Entry 1)** and peak at 178.2 ppm in LA **(Table 1-Entry 2)**.

Regarding OA **(Table 1-Entry 1)** the presence of an α, β – unsaturated carbonyl moiety is characterized by ketone carbonyl peak at 200.5 ppm (C6). Vinylic proton H7 is represented by the deshielded multiplet at 5.67 ppm along with carbon peak at 128.7 ppm (C7). Since diastereotopic protons H14 are adjacent to an electron-withdrawing group, they will be the most deshielded aliphatic protons in the molecule, depicted by 2 duplets of duplets at 2.38 ppm ($H14_a$) and 2.21 ppm ($H14_b$). H13 will present a lower shift (singlet at 2.04 ppm) comparing to H14 due to lower inductive effect. Attribution of the remaining aliphatic protons in OA were based upon 2D NMR analysis **(Appendix 3 – Figure 5.6/Figure 5.11)**.

Considering LA **(Table 1-Entry 2),** besides the presence of a carboxylic acid functional group (C15), an alcohol moiety is also present at C8 (peak at 75.1 ppm). From HMBC analysis **(Appendix 3 – Section 5.3.2)**, the adjacent protons from C17 are easily identified corresponding to the singlet at 1.11 ppm. Similarly to OA **(Table 1-Entry 1)**, the diastereotopic protons H14 are the most deshielded protons corresponding to 2 doublet of doublets at 2.29 ppm ($H14_a$) and 2.11 ppm ($H14_b$), and H13 presents a lower shift (singlet at 2.02 ppm). Attribution of the remaining aliphatic protons in LA were based upon 2D NMR analysis and reported spectral data **(Appendix 3 – Section 5.3.2)**[54]**.**

Table 1: ^{1}H NMR and ^{13}C NMR characterization of the OA (Entry 1) and LA (Entry 2), along with reported spectral data of LA.

Entry	Compound	^{1}H NMR	^{1}H NMR reported	^{13}C NMR	^{13}C NMR reported
1	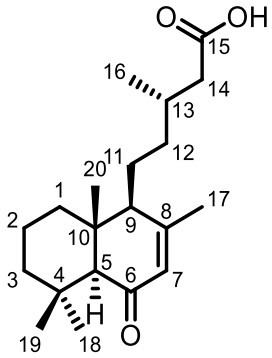 **2**	5.76 (m, 1H, H7) 2.38 (dd, J = 15.1, 6.3 Hz, 1H, $H14_a$) 2.21 (dd, J = 15.1, 7.7 Hz, 1H, $H14_b$) 2.04 (m, 1H, H13) 2.02-1.94 (m, 2H, H11,12) 1.90 (t, J = 1.4 Hz, 3H, H17) 1.70 – 1.42 (m, 3H) 1.41 – 1.22 (m, 3H) 1.14 (d, J = 9.2 Hz, 7H, H18/19) 1.03 (d, J = 6.7 Hz, 3H, H16) 0.84 (s, 3H, H20).	a	200.5 (C6) 178.5 (C15) 158.8 (C8) 128.7 (C7) 63.8 (C11/12) 56.9 (C11/12) 43.4 43.3 41.2 (C14) 39.4 38.9 33.6 32.4 (C18/18) 31.0 (C13) 24.7 (C18/19) 22.1 (C17) 21.6 19.9 (C16)	a

				18.3 14.8 (C20)	
2	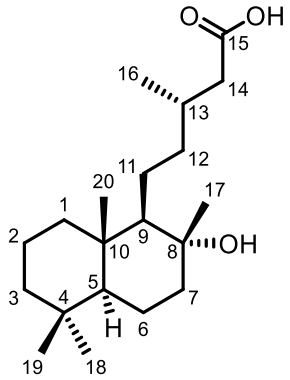 **1**	2.29 (dd, J = 14.8, 6.0 Hz, 1H, $H14_a$) 2.11 (dd, J = 14.7, 7.8 Hz, 1H, $H14_b$) 2.02 (s, 1H, H13) 1.90-1.78 (m, 2H, $H7_a$,11_a) 1.62 – 1.52 (m, 3H, $H1_a$, 2_a, 11_b) 1.44 – 1.16 (m, 11H, H3, 7_b, 2_b, 1_b, 6, 12) 1.11 (s, 3H, H17) 0.99 (m, 1H, H9) 0.93 (d, J = 6.6 Hz, 3H, H16) 0.89 (m, 1H, H5) 0.82 (s, 3H, H18) 0.74 (s, 6H, H19,20).	[b] 2.39 (dd, J = 14.7, 6.4 Hz, 1H, $H14_a$) 2.13 (dd, J =14.7, 7.6 Hz, 1H, $H14_b$) 1.97 (m, 1H, H13) 1.85 (dt, J = 12.2, 2.9 Hz, 1H, $H7_a$) 1.64 (m, 1H, $H6_a$) 1.60 (m, 1H, $H1_a$) 1.58 (m, 1H, $H2_a$) 1.42 (m, 2H, $H2_b$, 11_a) 1.40 (m, 2H, H12) 1.35 (m, 2H, $H3_a$, 7_b) 1.25 (m, 1H, $H6_b$) 1.24 (1H, m, $H11_b$) 1.15 (s, 3H, H17) 1.13 (m, 1H, $H3_b$) 1.03 (m, 1H, H9) 0.98 (, d, J = 6.5 Hz, 3H, H16) 0.93 (m, 1H, $H1_b$)	178.2 (C15) 75.1 (C8) 62.0 (C9) 56.0 (C5) 43.8 (C7) 42.0 (C3) 41.6 (C14) 40.6 (C12) 39.7 (C1) 39.2 (C10) 33.4 (C4/18) 33.2 (C4/18) 31.2 (C13) 23.8 (C17) 23.0 (C11) 21.5 (C19) 20.5 (C6) 19.9 (C16) 18.5 (C2)	[b] 178.4 (C15) 74.6 (C8) 61.7 (C9) 56.0 (C5) 44.2 (C7) 41.9 (C3) 40.9 (C14) 39.8 (C12) 39.6 (C1) 39.1 (C10) 33.3 (C18) 33.2 (C4) 30.7 (C13) 23.8 (C17) 21.9 (C11) 21.4 (C19) 20.4 (C6) 19.9 (C16) 18.4 (C2)

			0.91 (m, 1H, H5) 0.86 (s, 3H, H18) 0.78 (s, 6H, H19, 20)	15.5 (C20)	15.4 (C20)

a. Spectral data of 6-oxocativic acid is not available in literature.
b. ^{1}H NMR and ^{13}C NMR reported spectra of Labdanolic acid in $CDCl_3$ ((chemical shifts from TMS). ^{1}H NMR and 13C NMR spectra were performed on a on a Varian Mercury 300 spectrometer at a measuring frequency of 300 MHz for ^{1}H, and at 75.4 MHz for ^{13}C. [Adapted from Ref. 54]

1.5.6 Synthesis of 6-Oxocativic Acid

Taking into account that OA is a minor compound present in *C.ladaniferus* and its arduous isolation lead to a small quantity of compound, synthesis of OA was attempted using LA as starting material. The proposed linear synthesis consisted in three steps. Since LA has a tertiary alcohol, a dehydration reaction [37] would be the first step of the synthesis, yielding a mixture of olefins. Afterwards, two allylic oxidation reactions would be performed: the first oxidation to obtain the alcohol in the desired position, and then the second oxidation to give the α, β – unsaturated ketone. Even though rhodium complexes can directly oxidate olefins to enones [39], we focused on traditional approaches.

1.5.6.1 Dehydration reaction

Based on work previously reported by our group[37], the dehydration reaction was performed with Amberlyst®-15(dry). Given the conditions employed in this reaction **(Section 3.5)** and the stability of the carbocation, LA **(1)** dehydration reaction undergoes an E1 mechanism. With the formation of a tertiary carbocation, 3 β-protons can be abstracted, leading to the formation of 3 different alkenes, each with a different reactivity: tetrasubstituted olefin **(5)** as the most stable isomer, followed by the trisubstituted olefin **(6)** and then the exocyclic olefin **(7) (Figure 1.18).**

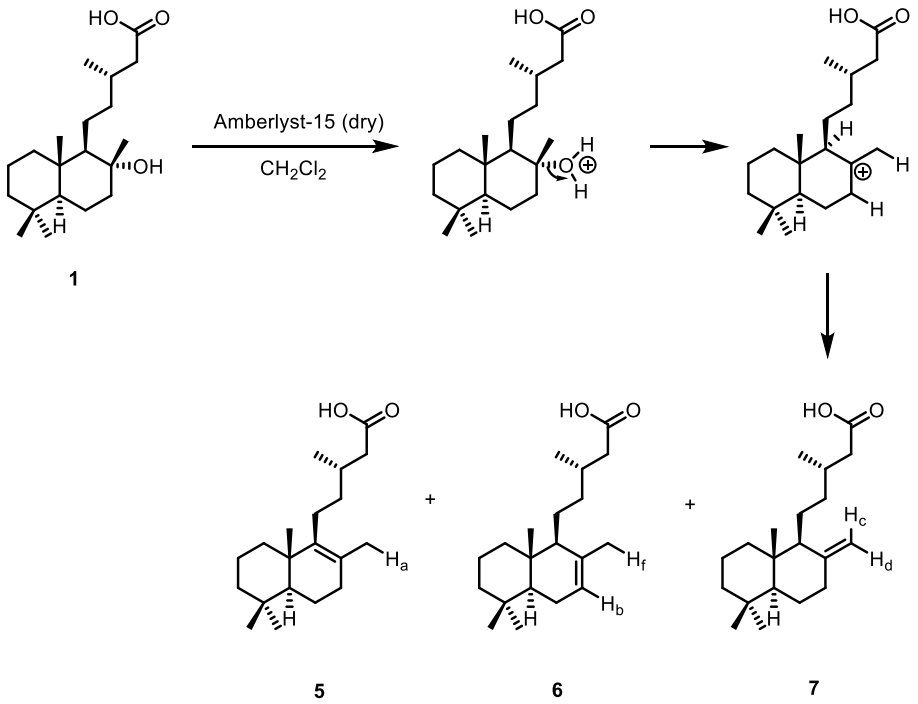

Figure 1.18: E1 mechanism of dehydration which can yield 3 types of olefins: tetrasubstituted **(5)**, trisubstituted **(6)** and exocyclic olefin **(7)**.

This reaction was performed in two different conditions: room temperature and at 0°C. In both conditions, and according to the literature[56,54] , it is possible to see the presence of the 3 isomeric unsaturated compounds in the ^{1}H NMR spectrum **(Figure 1.19)**: broad singlet at 5.38 ppm which corresponds to the vinylic proton H_b from the trisubstituted olefin; exocyclic vinylic protons H_c and H_d represented by the doublets at 4.80 ppm and 4.47 ppm; singlet at 1.54 ppm correspondent to allylic protons such as H_a and H_f.

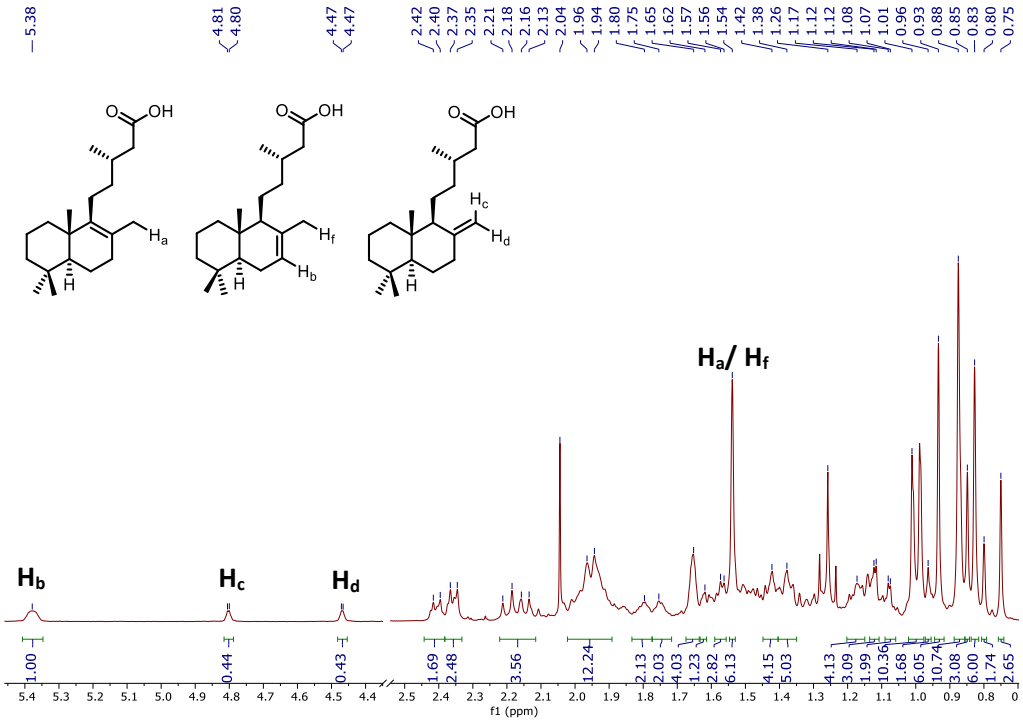

Figure 1.19: ^{1}H NMR from the dehydration reaction at 0°C, yielding three isomeric unsaturated compounds.

The difference between the 2 approaches is the percentage of each olefin in the mixture. Through a ratio calculated by ^{1}H NMR analysis, at 0°C, the mixture was composed predominantly by the 2 most stable isomers (tetrasubtituted and trisubstituted olefin) in a proportion of 53:34:15; whereas at room temperature, the ratio was more balanced, however tetrasubstituted olefin was present in higher quantity, followed by trisubstituted and tetrasubstituted (40:36:24). This indicates that the thermodynamic product is favoured despite the temperature applied in the system. Besides that Saytzeff´s rule was followed since the predominant alkene in the mixture is the more substituted[38]. Since the reaction performed at 0°C contained a higher percentage of stable compounds, this was the condition chosen to be reproduced throughout this synthesis.

Recalling the structure of OA - α,β-unsaturated ketone with a trisubstituted double bond – the next step could be the isolation of the trisubstituted olefin from the other isomers using silica gel impregnated with silver nitrate[57], or an allylic oxidation reaction of the olefin mixture, followed by isolation of the oxidated compounds. The second approach was selected.

1.5.6.2 Allylic Oxidation

The allylic oxidation was performed using SeO_2 **(Section 3.6.1)**. Since the starting material is a mixture of olefins, there are various potential oxidation sites, and therefore several products can be formed **(Figure 1.20).**

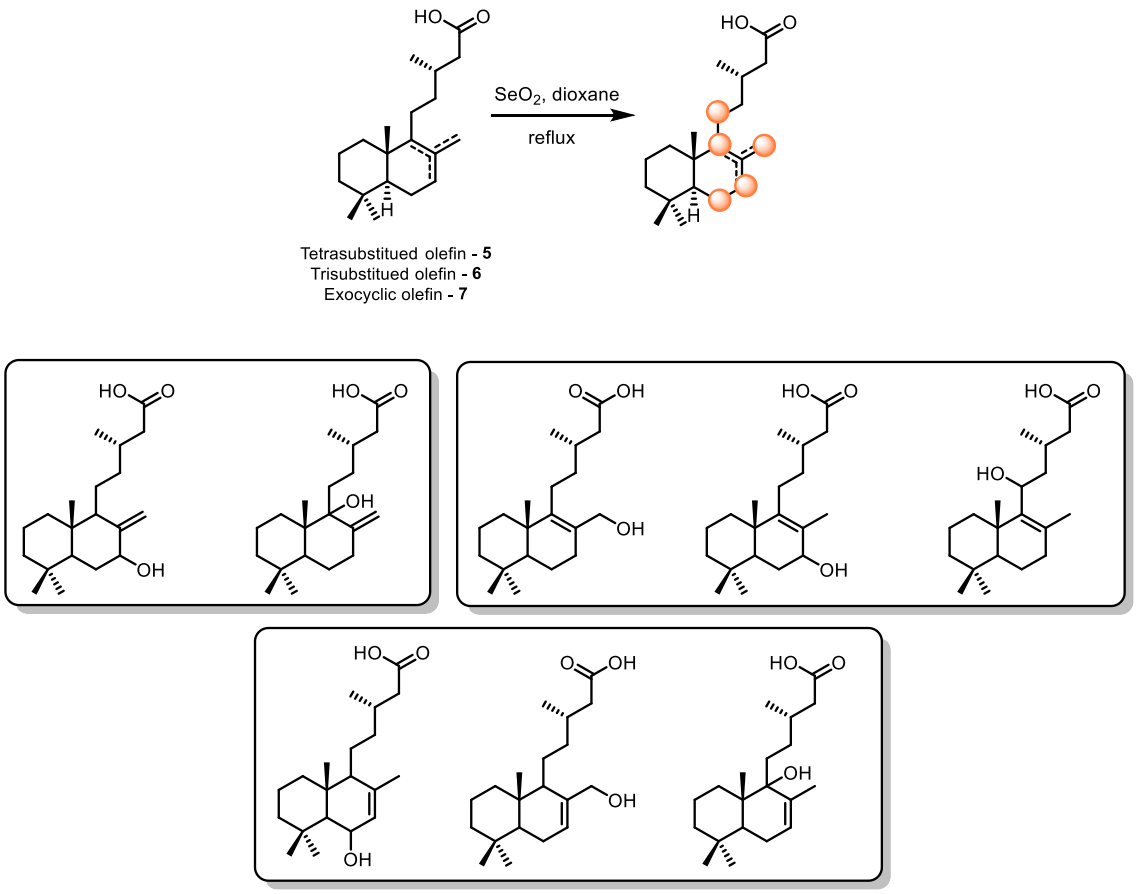

Figure 1.20: Potential sites for oxidation (marked in orange) and some possible products formed in the allylic oxidation with SeO_2.

Allylic oxidation ^1H NMR spectrum **(Figure 1.21)**, depicts full conversion of the starting material and singlet at 9.26 ppm, correspondent to an aldehyde proton, indicates overoxidation. Signals at lower yield (6-7 ppm) are attributed to vinylic protons.

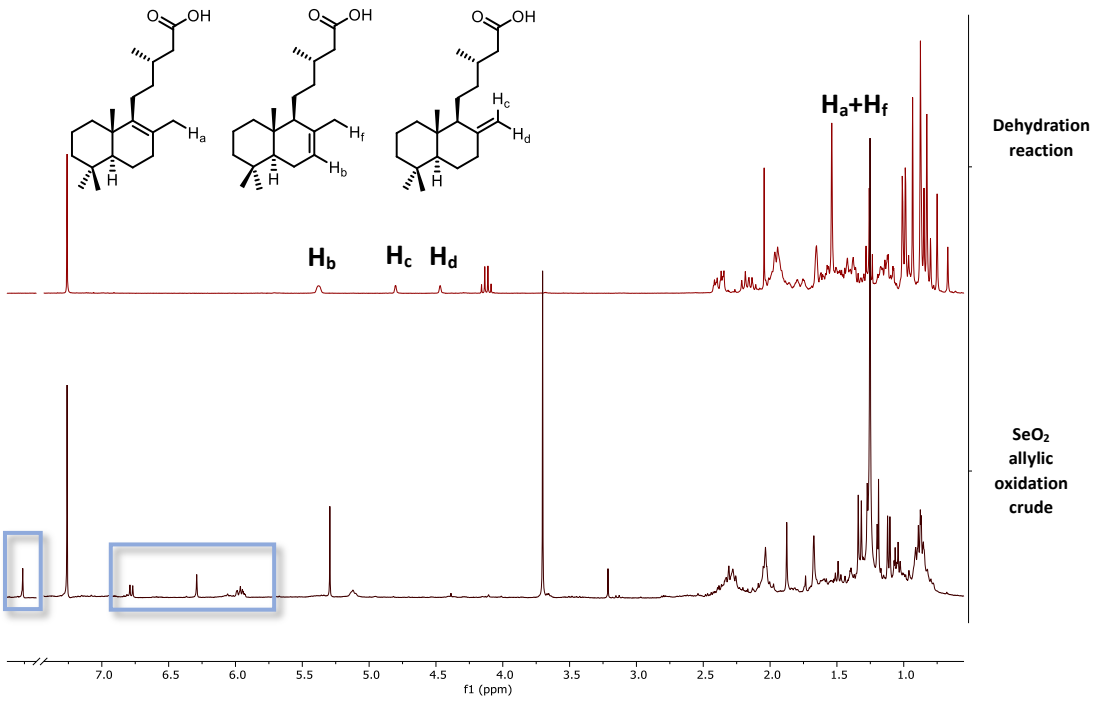

Figure 1.21: ^{1}H NMR of the dehydration reaction (top spectra) and crude from allylic oxidation (bottom spectra).

Purification of the olefin allylic oxidation was not done since no proper mobile phase was found that could separate all the obtained polar compounds with similar R_f. Therefore, a second allylic oxidation was performed to oxidize the primary and secondary allylic alcohols that might be present in the mixture. Besides that, since a second oxidation will decrease compounds polarity, we hoped this approach would facilitate further purification steps to yield the enone moiety.

1.5.6.3 Oxidation of Allylic Alcohols

Allylic alcohol oxidation was performed using MnO_2 in DCM **(Section 3.6.2)**. Comparison of crude ^1H NMR with starting material ^1H NMR **(Figure 1.22)**, it is possible to see that the starting material reacted to a certain extent. The peaks in the range of 7-5 ppm are no longer present, and several peaks at higher field have appeared (between 4.5-3 ppm).

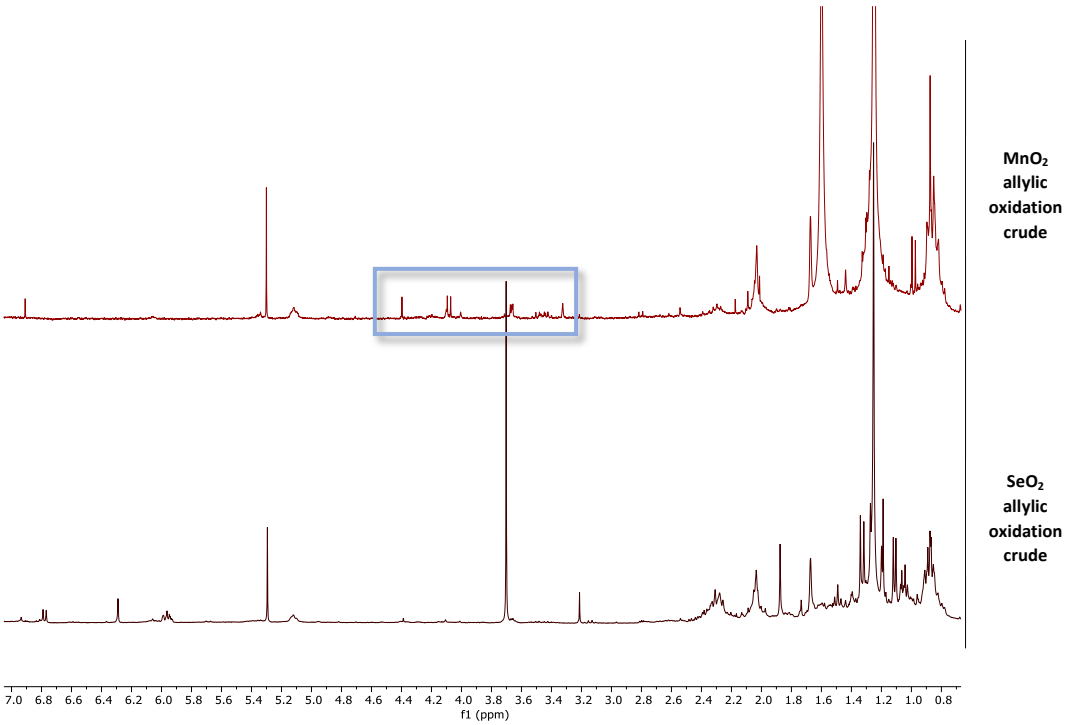

Figure 1.22: ^1H NMR comparison between crude from MnO_2 allylic oxidation (top spectra) and SeO_2 oxidation (bottom spectra).

The expected result from this oxidation is the presence of a carbonyl group, which will induce conjugation within the system. As a consequence, the peaks at lower field (7-5 ppm) that are supposedly from the starting material vinylic protons, will become less shielded. However, lack of signals at lower field in MnO_2 crude does not corroborate this hypothesis. With respect to the peaks between 3 ppm and 4.5 ppm, they can be attributed to the protons adjacent to alcohols that may be present in the mixture. Comparing ^1H NMR spectra of OA and the crude of this reaction **(Figure 1.23)**, it is possible to see the absence of peaks between 3-4.5 ppm on OA, which means the desired product was not obtained using this synthetic approach.

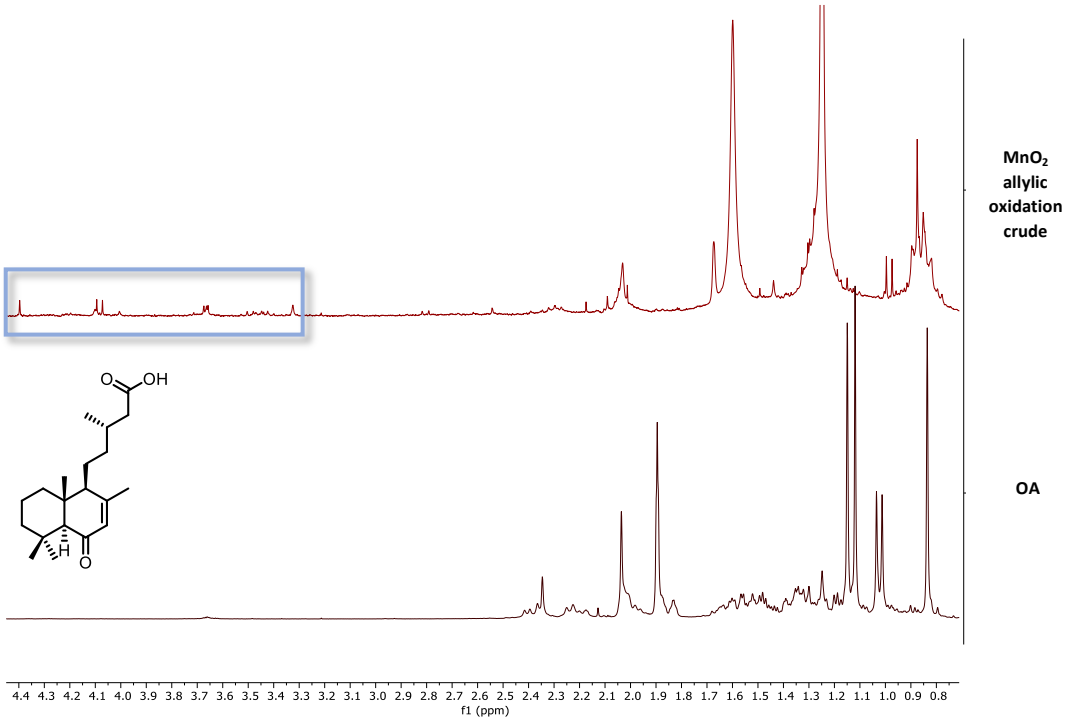

Figure 1.23: ^{1}H NMR comparison between crude from MnO_2 allylic oxidation (top spectra) and OA (bottom spectra).

This result can be explained by MnO_2 undermined oxidation power[43]. If the surface of the mineral contains impurities such as water molecules absorbed in its surface, competition reactions with the substrate can occur. Due to that reactions with MnO_2 are performed in apolar solvents (DCM or diethyl ether)[58].

Owning to the inconclusive results obtained from the allylic oxidation with MnO_2, Ley- Griffith oxidation was performed using as starting material the crude obtained from SeO_2 allylic oxidation. By ^{1}H NMR and ^{13}C NMR spectra **(Appendix 4 –Figure 5.19/Figure 5.20)** , several aspects can be highlighted: presence of starting material in the range between 5.5-7 ppm shows that full conversion was not achieved **(Figure 1.24)**; the aldehyde proton from the starting material at 9.26 ppm, supported by a carbon peak at 187 ppm; absence of signals above 200 ppm demonstrate that oxidation of secondary alcohols to ketone was not accomplished, indicating that these reactional conditions were not suitable for OA synthesis. By TLC analysis, it was visible the presence of 4 spots and purification was attempted. However, R_f similarity led to problems in purification, and no product was successfully isolated.

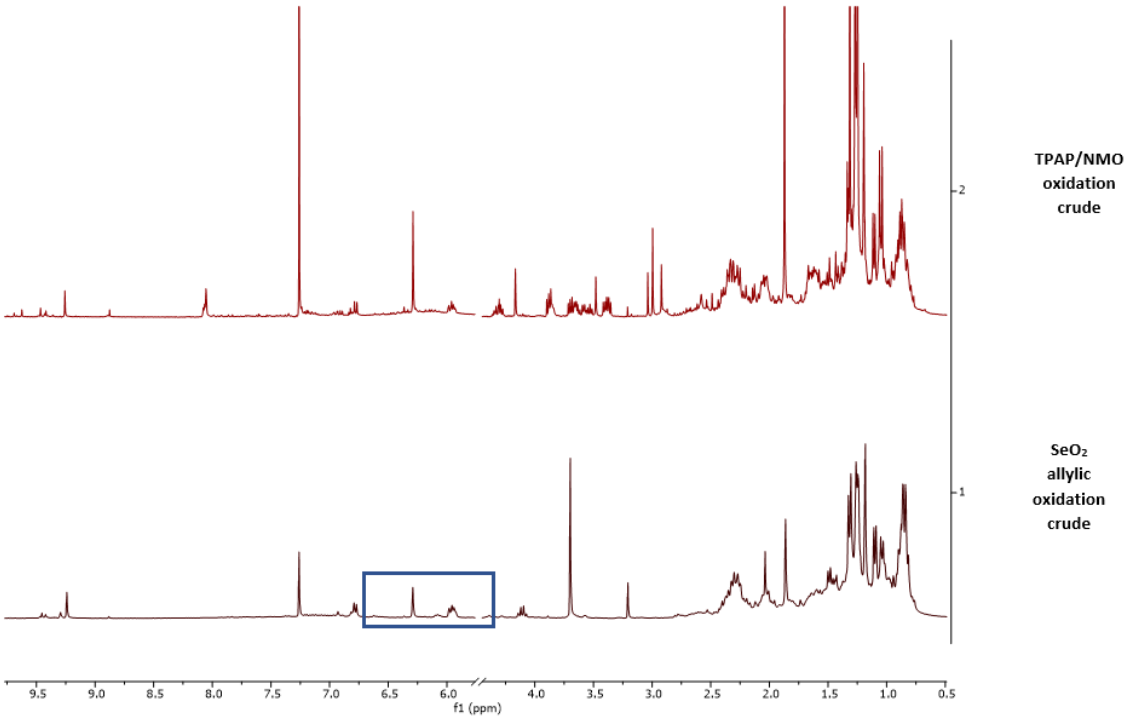

Figure 1.24: ^{1}H NMR comparison between crude from TPAP/NMO oxidation (top spectra) and crude obtained from the oxidation with SeO_2 (bottom spectra), with the starting material highlighted.

1.5.7 AQPs Biological Assays

Modulation of three AQPs were studied in the presence of LA and OA individually. Since AQPs are involved in the transport of small molecules across the cell membrane, their modulation can be evaluated by permeability assays using the stopped-flow technique. Since AQP1 and AQP3 are endogenously expressed in human red blood cells (RBCs), their permeability was assessed by light scattering stopped-flow experiences. Since AQP5 is absent in RBCs, this protein was expressed in yeast cells (*Saccharomyces cerevisiae* YSH 17770) transformed with a plasmid encoding human AQP5. To evaluate the effects of the compounds on AQP5 permeability, the permeability assays were performed using a fluorescence stopped-flow technique, where cells must be pre-loaded with a volume-sensitive fluorescence dye. Using a concentration of 25 µM of each compound to test permeability in AQP3 **(Figure 1.25 – A)**, AQP1 **(Figure 1.25 – B)**, and AQP5 **(Figure 1.25 – C),** it is possible to conclude that LA **(RJ_LA)** and OA **(RJ_OA)** do not modulate the permeability of the AQPs under study.

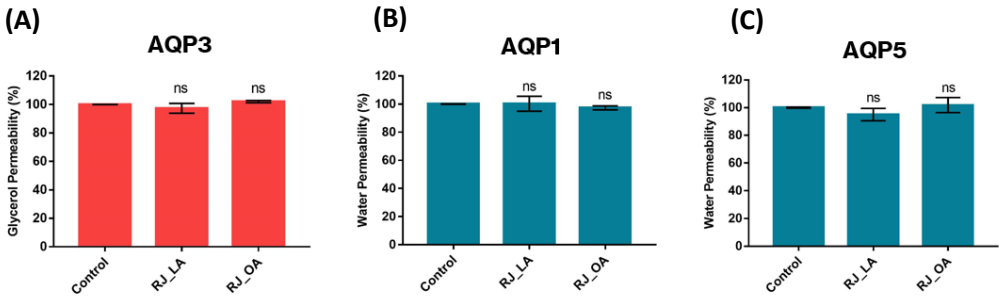

Figure 1.25: Modulation of AQP3 (A), AQP1 (B) and AQP5 (C) in the presence of LA (RJ_LA) and OA (RJ_OA). Both compounds do not exhibit modulation in the AQPs under study

1.6 Conclusions

Considering the wide range of pharmacological activity depicted by labdane diterpenes and in an attempt to valorise natural products, Labdanoic Acid and 6-Oxocativic Acid were isolated from *Cistus Ladaniferus*. Their activity was studied in three different AQPs with the purpose of discovering a novel therapeutic approach to cancer. Even though both compounds did not exhibit AQP modulation, a methodology for 6-Oxocativic Acid isolation was developed. As future prospects, other biological assays could be performed to see a possible disclosed activity.

An attempt to synthetize OA using LA as starting material was performed. With a synthesis consisting of 3 steps – dehydration with Amberlyst®-15(dry), allylic oxidation with SeO_2, and further oxidation with either MnO_2 or TPAP/NMO - it was not possible to obtain the desired compound. In the future, other oxidation reactions should be experimented such as Swern Oxidation and Dess-Martin oxidation. Isolation of each olefin isomer can also be attempted to avoid problems in further steps of the synthesis.

2. Functionalization of Quinolizidine Alkaloids

"Men argue. Nature acts"

Voltaire

We are living in a period where each of our actions have a deep impact in the environment[59]. So, as chemists, the search for alternatives that follow green chemistry principles such as development of safer methodologies and waste prevention[60] are extremely important. This is why we have been witnessing the renascence of Electrochemistry. The first milestone was in 1800, with the invention of the first electric battery named Volta Pile [61]. This device allowed Michael Faraday to perform the electrolysis of acetic acid in the early 19th [62] and since then the field has witnessed various achievements **(Figure 2.1)**: Kolbe reaction (1847) to form C-C bonds under mild conditions[63]; in the 1960s, the conversion of acrylonitrile to adiponitrile lead to the industrial development and commercialization of the Monsanto electrochemical adiponitrile process[64]; C-H activation using Shono Oxidation (1975), where a tertiary amide is oxidized to an N-acyliminium intermediate, and then trapped by several nucleophiles[65].

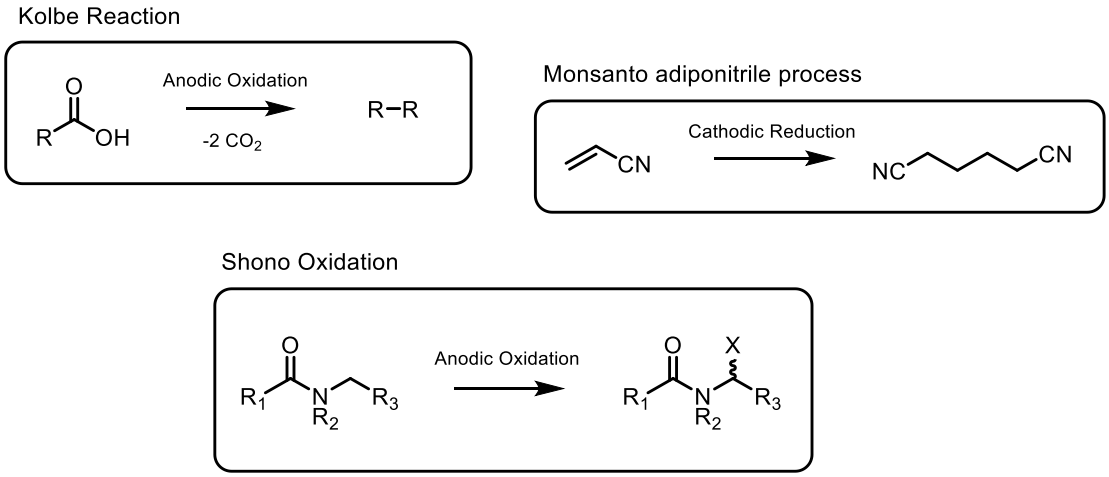

Figure 2.1: Some milestones in electrochemistry

2.1 Principles of electrochemical reactions

Electrochemistry offers a mild and efficient alternative to conventional oxidation/reduction procedures, without the use of dangerous reagents such as OsO_4 and $LiAlH_4$[66]. The reaction takes place in an electrochemical cell: a combination of electrodes connected by a power source, in contact with a solution composed of an electrolyte and a substrate. An electrochemical reaction is a redox reaction, consisting in 2 half-reaction: an oxidation that occurs at the anode, and a reduction reaction that occurs in the cathode. These 2 half-reactions are dependent of one another and both occur in the interface between the electrode and the solution[67]. This interface called double-layer, makes the reaction an heterogenous process[68] .

In the anode, one specie (reducing agent) is oxidized, and its electrons are transferred to another specie (oxidizing agent) at the cathode. Depending on the reaction conditions, sometimes a third electrode is used, called reference electrode. This electrode is used as a "quality control agent" to give an accurate measurement of the potential in the cell [69]. Electrodes exist in a wide variety of materials such as platinum, graphite, and vitreous carbon. Independently on which material

was chosen, electrodes must be (1) chemically stable in solution to avoid formation of undesirable species (oxides and hydrides) that can affect the outcome of the reaction; (2) resistant to erosion by the solution; (3) fairly conductive to maintain a steady current and potential in the circuit and (4) durable[70] .

The redox reaction occurs due to the use of a power source (battery, potentiostat, applied electricity): electrons are pushed form the anode to the cathode, creating a potential difference, also known as voltage. The voltage forces species to move within the circuit, creating a phenomenon called current[71].

Considering the Shono Oxidation reaction as a case study **(Figure 2.2)** - the first step consists in the proximity or absorption of the amide in the anode[72]. Then, a single electron transfer (SET) occurs from the lone pair of the amide nitrogen, transferring an electron to the anode, and generating a radical cation intermediate[73].The driving force of this transfer is based on the energy difference between the electrode and the substrate [74]. Since electrodes are electrical conductors, as the power source applies a specific potential to the electrodes, the energy of its electrons can be changed. Since the amide is going to be oxidized, the energy of the electron in the substrate is higher than the energy of the electrons in the electrode. Due to that, the electron in the highest occupied molecular orbital (HOMO) of the amide is going to be transferred to the anode, leading to an oxidation reaction[75].To generate the N-acyliminium ion, a second electron removal is done, along with proton elimination. This cation is then desorbed into the electrolyte, and trapped with a nucleophile, yielding the desired product[73]. In the cathode, the protons removed under the process were reduced generating hydrogen gas. In this example, the anode is called working electrode because it was where the reaction of interest (oxidation of the tertiary amide) took place, whereas the cathode is the counter electrode[71].

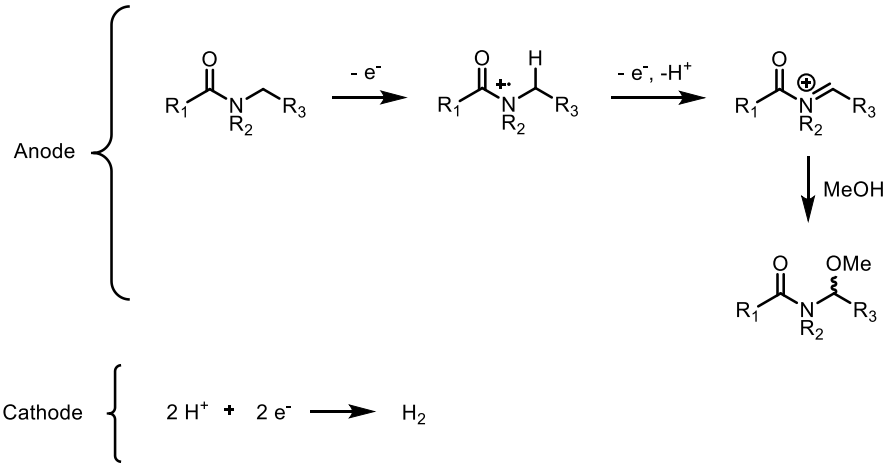

Figure 2.2: Half-reaction at the anode and cathode in Shono Oxidation.

In all electrochemical reactions, an electrolyte – combination of solvent and a supporting electrolyte - is used to maintain electric conductivity[76]. The solvent employed must (1) have a wide solvent window, i.e, must tolerate a wide range of potentials to avoid solvent degradation; (2) stabilize the intermediates formed in the reaction and (3) solubilize all the species in solution. Due to all these requirements, the most used solvents are the polar ones, because they present higher conductivity (and therefore lower resistance is experienced by the system) and are normally better in dissolving all species[77]. Supporting electrolyte such as tetrabutylammonium (TBA) salts are used to decrease the resistance of the system, increase conductivity, and stabilize neutral/charged species[72]. When is used, the electrochemical process gets more expensive (in case the supporting electrolyte is not recycled) and the work-up can become lengthy[78]. Additives can also be added to stabilize species or improve counter reaction[77].

An electrochemical reaction can be performed in a divided or in an undivided cell **(Figure 2.3)**. In an undivided cell, both half-reactions occur simultaneously in the cell since they do not interfere with one another. However, when a specie in solution can suffer a transformation in both

electrodes leading to secondary reactions, a divided cell should be used. The presence of a separator such as a glass-frit or a porous ceramic [79], enables the selective transport of ions to sustain the conductivity of the system[68] .

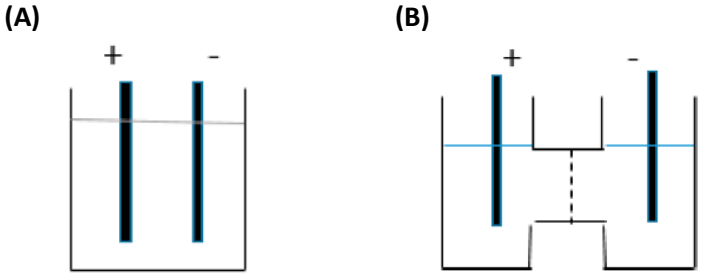

Figure 2.3: Typical cells used in electrochemistry, (A) an undivided cell and (B) a divided cell with a porous separator. [Adapted from Ref. 79]

2.1.1 Cyclic Voltammetry

Prior to an electrochemical reaction, Cyclic Voltammetry (CV) studies are performed to understand the reductive/oxidative behaviour of the substrates[80].The set-up of this technique consists in an undivided electrochemical cell, with 3 electrodes: working, counter and reference electrode[77]. A cyclic voltammogram of a molecule shows that as potential (*x*-axis) is being applied to the system, a variation of current (*y*-axis) is observed[43]. Depending on the molecule in study, a potential window is set with an initial and final value of potential. This initial value is where the forward scan begins with an oxidation (or reduction) reaction, whereas the final value of the potential window, is where the reverse scan begins with reduction (or oxidation) reaction[80]. There are various types of voltammograms depending on the type of reaction **(Figure 2.4).** Under a reversible reaction, two peaks are observed where the current is at a maximum: the anodic potential E^a, and the cathodic potential E^c [77]. These peaks are related to the Nernst equation **(Equation 1)**. This equation gives information about how the concentration of species in solution can be affected by the potential (energy) given to the system. Besides the values of anodic and cathodic potential, the value of potential required to undergo a redox reaction, $E_{1/2}$, can be obtained. According to the Nernst Equation, this value is when the concentration of oxidized and reduced species is equal to unity. Therefore, to perform an oxidation/reduction reaction, $E_{1/2}$ should be considered.

$$E = E^o + \frac{RT}{zF} ln \frac{c_{ox}}{c_{red}}$$

Equation 1: Nernst Equation (E, electrochemical potential of the cell; E^0, standard potential of a specie; F, Faraday´s constant; R, universal gas constant; z, number of electrons involved in the reaction; T, temperature)

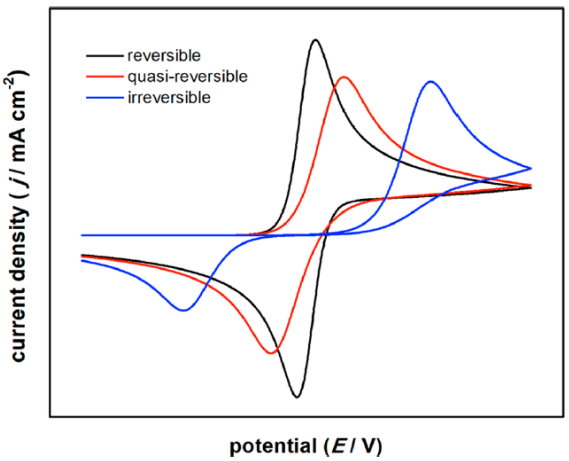

Figure 2.4: Types of cyclic voltammograms: reversible voltammogram in black; irreversible voltammogram in blue; "quasi-reversible" voltammogram in red. [Adapted from ref. 82]

2.1.2 Constant Current versus Constant Potential

The more energy is given to the cell, the higher the potential will be. This potential is what keeps electrons moving within the system, and as depicted by the **Equation 2**, as potential increases, so will current[77]. The value of resistance should be as low as possible, and that is dependent upon several factors like the choice of solvent, supporting electrolyte, and the type of cell used[71].

$$U = R.\mathrm{I}$$

Equation 2: Equation which relates current (*I*), potential (*U*) and resistance (R).

There are two modes of performing an electrochemical reaction: under constant current or under constant potential. In constant current (galvanostatic conditions) 2 electrodes are used (working and counter electrode). In this type of set-up, the current remains steady, while potential varies over time to maintain the selected current[81]. Based on the values obtained from CV, the first electrophore to undergo modification will be the one with the lower potential. Until there is substrate to be consumed and the current is maintained, the potential at the working electrode will be fixed. As the substrate is consumed, the potential will change according to the next electrophore to be oxidized/reduced. This methodology provides a good advantage: at a selected current, a vast selection of potentials can be traced[82]. However, lack of selectivity might occur since potential is not fixed[68].

To overcome selectivity issues, the use of constant potential (potentiostatic conditions) is the best mode to work. In some equipments, the use of a third electrode (reference electrode) is required[81]. Under constant potential, the potential is fixed, and current varies to maintain the potential value steady. As the substrate is being consumed, mass transfer can limit the progress of the reaction, so current will decrease, but the potential is maintained. This methodology provides higher selectivity, because the potential is set for a specific electrophore, despite the presence of others. However, this set-up might lead to lower yields comparing to constant current[69].

The rate-determining step of electrochemical reactions consist in the transport of substrate molecules from solution to the electrode surface. This phenomenon called mass transfer needs to be high in order to decrease reaction time. Therefore, high stirring and smaller gaps between

electrodes are advisable[77]. The greater the distance between the electrodes, the greater is the resistance experienced by the current to pass through the solution, and therefore the potential will decrease. This phenomenon known as Ohmic drop can be circumvented by using supporting electrolytes[78]. As stated above, the use of supporting electrolytes increases the cost of the reaction and generates additional waste therefore the development of greener electrochemical processes that require little or no use of supporting electrolyte would be of great interest. This is the reason why flow electrochemistry has been of great interest in recent studies.

2.1.3 Batch and Flow Electrochemistry

Batch presents some disadvantages, such as (1) large distance between electrodes, (2) mixing of species is made by stirring, which creates an uneven current and potential within the system, prompting side reactions and lower conversion; (3) scaling-up can be dangerous due to poor heat exchange (the distance between the electrodes creates a rise in the temperature of the system due to an increase in resistance)[83]. To overcome these downsides, flow electrochemistry can be a solution. Reactions are performed in a flow cell: combination of 2 half cells each equipped with an electrode, connected by a power supply with cords. Just as in batch electrochemistry, there are a wide variety of electrodes that can be used, and the set-up can be either a divided or an undivided cell. In flow, the reaction mixture is transported in tubes from the reaction vessel to the flow cell using a pump. The pump transports the reaction mixture at a pre-selected flow rate through the tubes, until the desired product leaves the cell.

The flow rate will determine the retention time - time period in which the reaction mixture stays inside the cell to react. Depending on how long the reaction stays inside the cell, conversion and selectivity issues may arise, indicating the flow rate readjustment.

The smaller distance between electrodes promotes faster reactions[84] and since the resistance experienced within the system is much lower, it facilitates the application of higher currents[85] . The presence of higher current means that the use of supporting electrolyte can be dramatically reduced or even neglected [66] turning the whole process more environmentally friendly. This technique is usually applied when scale-up is required: while electrochemical reactions in batch are dependent on the volume of the vessel, flow processes are dependent on time: as long as reagent in being pumped into the system, the chemical process continues [86]. Selectivity in flow is higher than in batch due to an efficient mixing of species which prevents the formation of side products[87]. However, cleaning problems (blocking of channels with solids) and limited flow rates due to the diameter of the channels employed in the system[86], are some disadvantages encountered in flow.

Since flow chemistry is a safer and greener alternative comparing to batch, developments have been made in several reactions such as organometallic and nitration reactions[88] . Furthermore, the synthesis of natural compounds can also benefit from flow chemistry: construction of bonds, multi-functional group tolerance and easy scale-up[89]. Due to these advantages and continuing with the purpose of adding value to natural compounds, the aim of this second project is to functionalize two quinolizidine alkaloids using the power of electrochemistry, in batch and flow.

2.2 Quinolizidine alkaloids

To defend themselves against insect pests, plants produce secondary metabolites, such as alkaloids.[90] These molecules are characterized by the presence of at least one nitrogen atom, conferring basicity to the molecule.[91] Depending on the precursor used in the alkaloid biosynthesis, several alkaloid sub-families arise. One of them are the Quinolizidine Alkaloids (QA), which have as precursor the protein amino acid L-lysine.[92] The union of 2 lysine molecules leads to the quinolizine ring, a bicyclic ring present in Lupinine. As more lysine molecules are

incorporated, more complex molecules arise, such as Lupanine and Sparteine, characterized by a bis-quinolizidine ring system **(Figure 2.5).**[27]

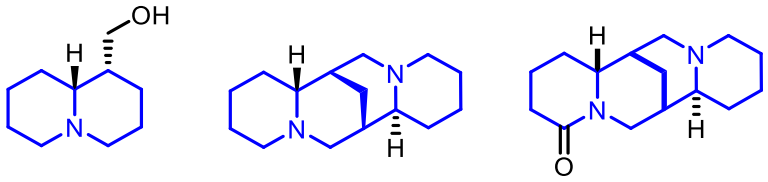

Lupinine (-)-sparteine *rac*-lupanine

Figure 2.5: Types of Quinolizidine Alkaloids. Quinolizine ring (highlighted in blue) in lupinine, and bis-quinolizidine ring (highlighted in blue) present in (-)-sparteine and *rac*-lupanine.

This class of alkaloids are one of the most abundant in the *Leguminosae* family[93], especially in the genera *Lupinus* and *Baptisia*[91]. One of the most cultivated species of *Lupinus* is *Lupinus albus L*. (*L.albus L.*), present in several countries across the globe [94]. The seeds of this species, known as "tremoço" in Portugal, have been a part of humans and animals' diet, due to its high source of protein, oil and carbohydrates. However, the usage of these seeds has been limited due to the presence of QA (nearly 1%)[95]. The higher the quantity of alkaloids present in the seeds, the more bitter and toxic they will be, so alkaloids removal prior to consumption is crucial[94].

One methodology to remove these compounds is called debittering which consists in leaching the seeds in water, generating at the end a great amount of water full of toxic compounds that is discarded as effluent wastewaters[96]. These wastewaters have the potential to be used: besides reducing the environmental impact of the overall process, QA would be available in large amounts that could be applied in total synthesis[97]. The most abundant QA in *L.albus L.* are Sparteine and Lupanine. Despite its toxicity, these compounds can be used for various purposes, from pharmacological activity to asymmetric synthesis.

2.2.1 Lupanine and Sparteine applications

The bis-quinolizidine system is composed by 4 rings that are divided in 2 systems: A/B system and C/D system[98]. Lupanine, a sparteine lactam, possesses anti-hyperglycemia properties and reduces high blood pressure[99]. In solution, it occurs in 2 conformations with dominance of ring C in a boat conformation[100] **(Figure 2.6)**. The presence of a tertiary amine and a lactim-lactam mesomerism, explains the high stability of this compound and also its difficulty in functionalization[101] . Upon its reduction with $NaBH_4/I_2$ [102], Sparteine is afforded, the second most encountered QA in plants.

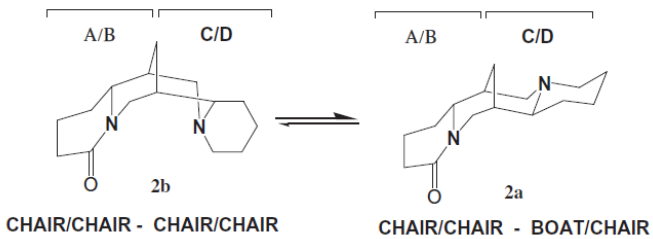

Figure 2.6: Conformational changes in Lupanine [Adapted from Ref. 100]

Besides possessing antiarrhythmic activity[103], Sparteine is known for its uses as chiral base in asymmetric lithiation-substitution reaction[104]. In its most energetic conformation, Sparteine acts as a bidentate ligand that upon interaction with aminophilic cations (lithium) present in bases like *sec*-BuLi, a complex is created that induces asymmetry in prochiral substrates[105]. This methodology affords products with high enantiomeric ratios which can be explained by 2 possible reaction pathways **(Figure 2.7)**. The first pathway consists in inducing asymmetry in the deprotonation step: the chiral base differentiates and abstracts one of the prochiral protons (pro-H_r and pro-H_s), affording an organolithium intermediate that will subsequently suffer a stereoselective electrophilic substitution. In the second pathway, the asymmetry is induced in the electrophilic substitution: formation of a racemic organolithium compound will then complex with the chiral base, which will then undergo electrophilic substitution[106]. The preferential path for a reaction is based on kinetic and thermodynamic factors[107]. Using this approach, formation of new bonds stereoselectively and in high enantiomeric excess can be formed using various electrophiles[108].

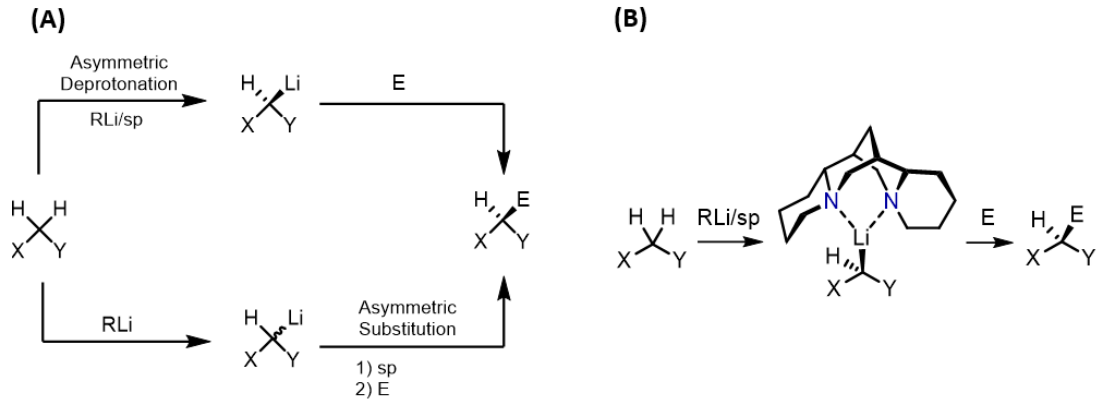

Figure 2.7: (A) Possible pathways for asymmetric induction, using sparteine (sp) as chiral ligand; (B) sparteine acting as a bidentate ligand in asymmetric deprotonation.

The use of natural products as catalysts dates to 1912 when cinchona alkaloids where used for cyanohydrin formation[109]. The success of sparteine as a catalyst for asymmetric reactions is attributed to its rigidity, binding, and steric features[110]. As an attempt to improve the existing methodologies in asymmetric synthesis, Sparteine and Lupanine will be functionalized in order to develop a new serie of catalysts for asymmetric catalysed reactions.

2.3 Lupanine and Sparteine Functionalization

C-H bond functionalization is a useful tool in drug design[111] and since nitrogen-containing moieties are abundant in feedstock chemicals and API synthesis, C-H bond functionalization adjacent to a tertiary amine is crucial[112] . α – Aminonitriles, firstly made by Strecker[113] are very versatile intermediates in the synthesis of various functional groups[114]. For the synthesis of primary amines, nitrile catalytic hydrogenation is a useful methodology, however unwanted products such as secondary and tertiary amines can arise **(Figure 2.8)**. This lack of selectivity can be solved using the appropriate solvent[115] and metallic catalyst[116].

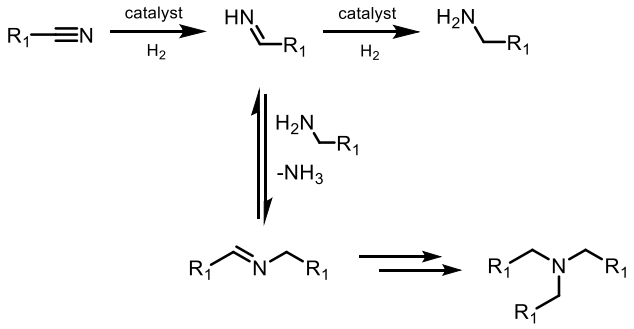

Figure 2.8: Nitrile catalytic hydrogenation and its possible products.

A less environmentally friendly approach to afford primary amines is using $LiAlH_4$. Depending on the structure of the α – aminonitriles, stereoelectronic effects and internal strain of the molecule[117], the nitrile functionality can be reduced to form 1,2-diamines or eliminated through a decyanation reaction. This competing reaction occurs when the nitrile moiety is antiparallel to the nitrogen-lone pair, affording an iminium cation that is further reduced by $LiAlH_4$ [118]. Reductive decyanation was also reported using DIBAL[119]. This electrophilic reducing agent reduces nitriles to aldehydes upon quench with water, however, if the nitrile reacts with a second equivalent of DIBAL, primary amines are obtained[120] **(Figure 2.9)** .

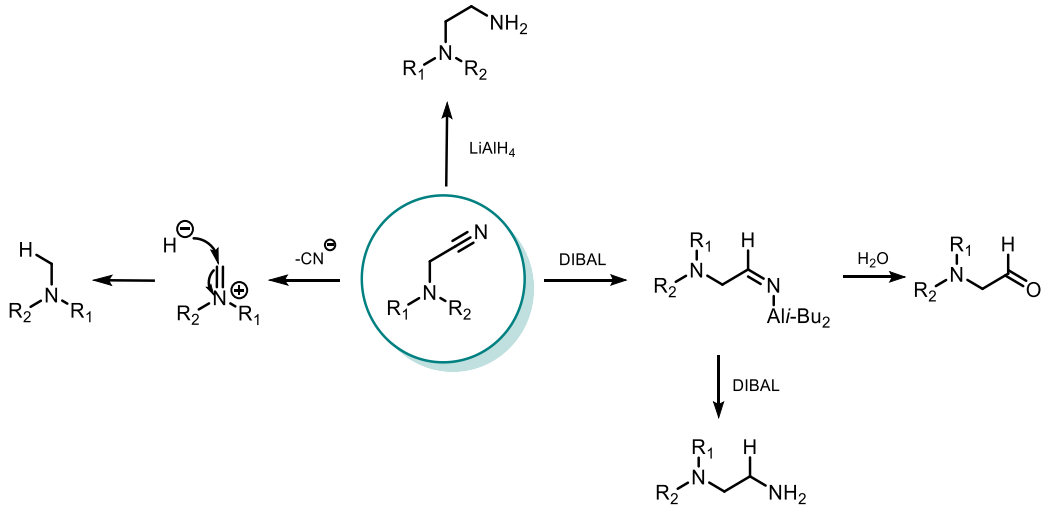

Figure 2.9: Reduction methodologies for α – aminonitriles, using $LiAlH_4$, DIBAL and reductive decyanation.

Nitrile hydration is usually performed under harsh conditions such as the use of concentrated H_2SO_4 to afford a primary amide[121] and mixture of H_2SO_4/MeOH to yield esters[122]. α – Aminoacids are commonly formed as a result of over-hydrolysis **(Figure 2.10)**[123]. Synthetic methodologies using transition metal complexes have been developed, using milder conditions and higher selectivity[123].

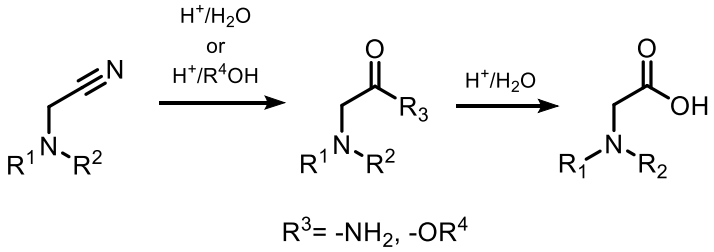

Figure 2.10: Nitrile hydration using acidic conditions.

Nitrogen heterocycles that provides scaffold rigidity and metabolic stability to many pharmaceuticals can also by synthetized from nitriles[124]. Oxazole is an unsaturated 5-membered ring containing in its structure an oxygen atom at position 1 and a nitrogen atom at position 3, each separated by a carbon atom. Upon substitution, pharmacological activity can arise, such as antitubercular and antitumoral activity[125] **(Figure 2.11).**

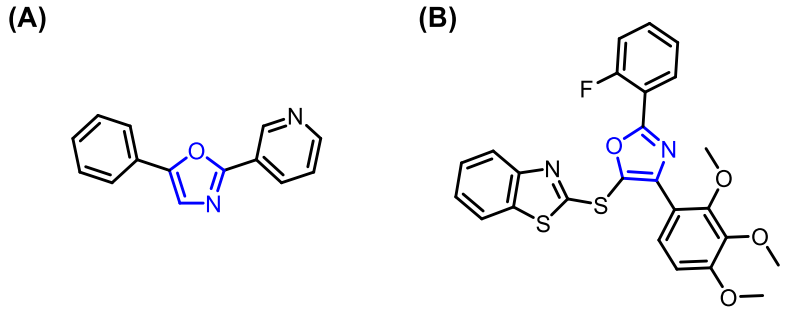

Figure 2.11: (A) Antitubercular and (B) Antitumoral drug, both containing the oxazole ring

An innovative approach to synthetize these N-heterocycles was reported by Nagib *et al*.[126] in which upon addition of an alcohol to an activated nitrile, a Pinner salt is formed. Subsequential hydrogen atom transfer (HAT) would occur leading to the desired product **(Figure 2.12).**

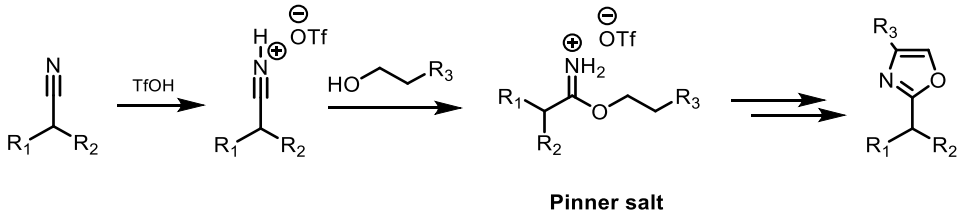

Figure 2.12: Nagib *et al.* approach to oxazole synthesis.

Tetrazole is another example of a N-heterocycle, composed by 4 nitrogen atoms and 1 carbon[127]. Present in antihypertensive drug losartan, this organic heterocycle can be synthetized by azide addition to nitriles. In case the substrate does not have strongly electron-withdrawing groups, the nitrile needs to be activated for azide nucleophilic attack. Using acid conditions, 3 different mechanisms can occur: concerted dipolar [2+3] cycloaddition; anionic 2 step [2+3] cycloaddition or by nitrile activation by proton, forming an imidoyl azide intermediate[128] **(Figure 2.13)**. However, based on transition state energies, the formation of an imidoyl azide intermediate is the preferential path for this reaction, compared to the high transition state energies in concerted and anionic cycloaddition[129] .

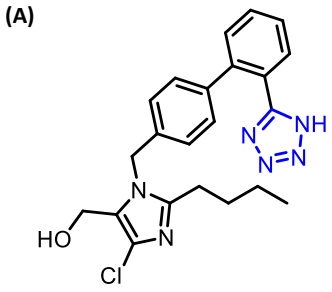

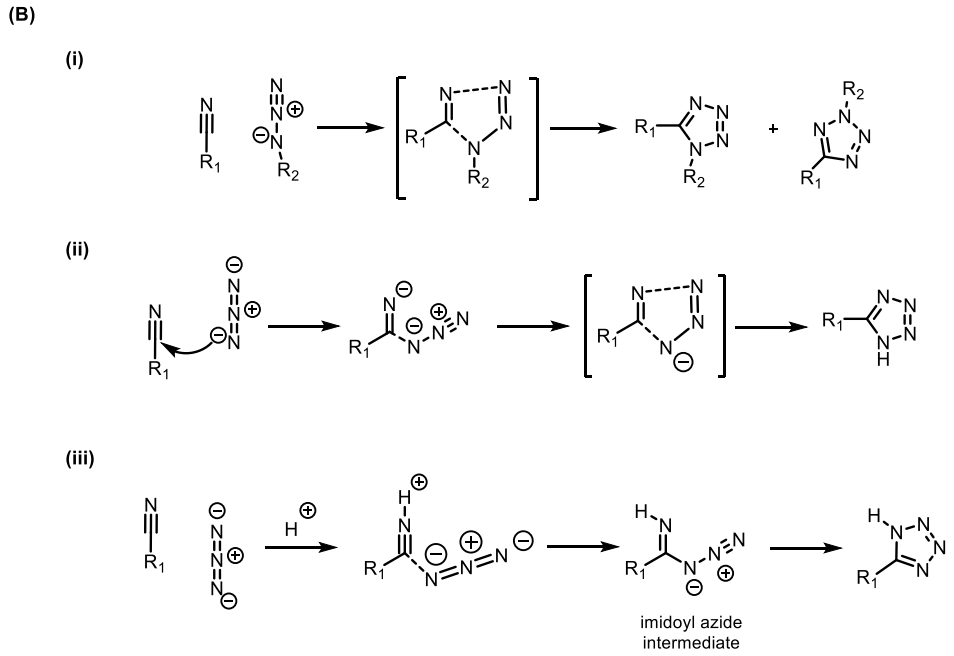

Figure 2.13: (A) Antihypertensive drug losartan and (B) possible mechanisms for tetrazole synthesis in acidic conditions – (i) concerted dipolar [2+3] cycloaddition, (ii) anionic 2 step [2+3] cycloaddition and (iii) nitrile activation by a protic source.

In case the α – aminonitriles contains a α – hydrogen, *Umpolung* reactions can also be performed: upon addition of a strong base, the acidic proton is removed, and a nucleophile specie is formed[130]. Due to its outstanding reactivity, several methodologies have been developed to insert the nitrile functionality in Lupanine and Sparteine **(Figure 2.14)**. Santamaria and co-workers developed a photooxidation protocol, using methylene blue as sensitizer and KCN as cyanide source, yielding 17-cyano-*rac*-lupanine in 88% and (-)-17-cyano-sparteine in 34% [131]. Different sensitizers like tropylium ion[132] gave (-)-17-cyanosparteine in 90% and rose bengal[133] afforded 17-cyano-*rac*-sparteine in 52% yield. A different approach for α – cyanation consists in Lupanine oxidation with DDQ, leading to 17-hydroxy-lupanine, that after treatment with $HClO_4$ gives the electrophilic iminium salt. This intermediate trapped with KCN affords 17-cyanolupanine in 74% yield [134].

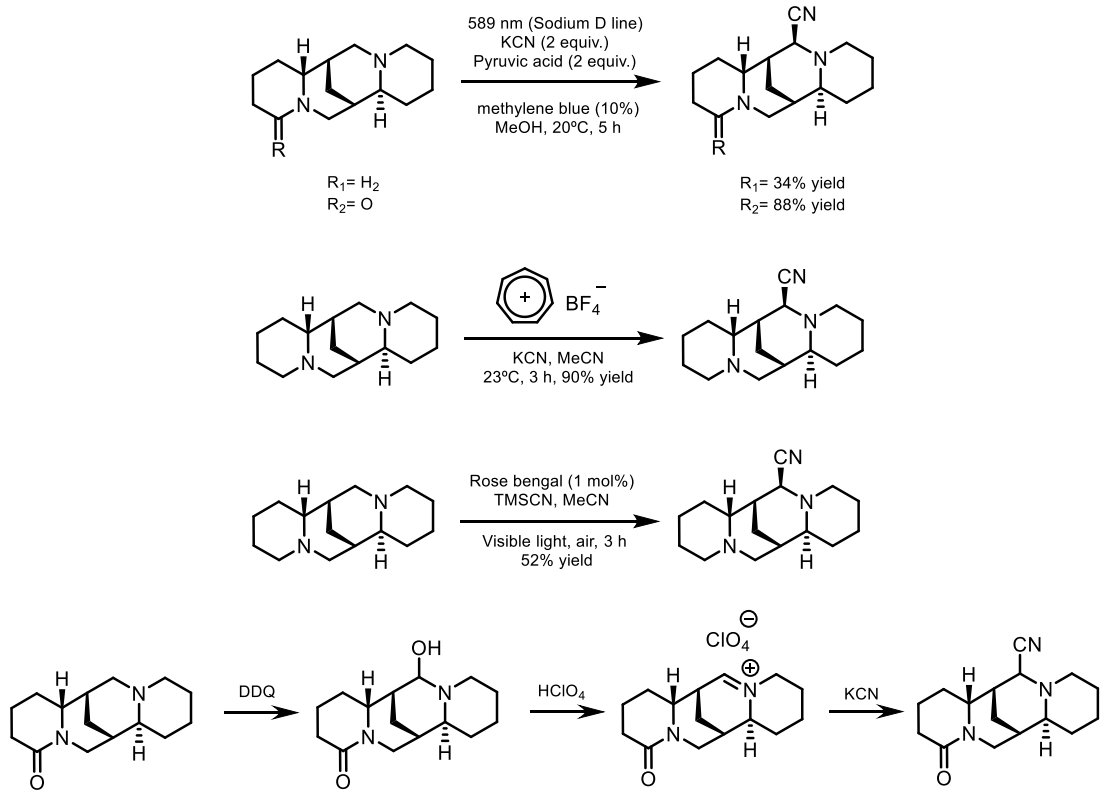

Figure 2.14: Cyanation of Sparteine and Lupanine methodologies

Functionalization of Lupanine and Sparteine using Electrochemistry has not been reported yet. Therefore, based on the uses of quinolizidine alkaloids in organic synthesis and pharmacological activity (*vide supra*), introduction of a nitrile moiety in *rac*-lupanine and *rac*-sparteine was performed using Electrochemistry. While optimizing the process, derivatizations of α – aminonitriles were executed as an attempt to develop a new series of catalysts for asymmetric reactions.

2.4 Objectives

An unreported electrochemical methodology for C-H activation of lupanine and sparteine was investigated, to instal the nitrile functionality. To achieve this goal, batch and flow electrochemistry experiments were executed. Based on the versatility of the nitrile group, derivatizations of both QA would follow, with the objective of developing a new series of catalyst for asymmetric synthesis.

Continuing with the purpose of finding new AQP modulators, biological assays were performed in three different AQPs (AQP1, AQP3 and AQP5). The inhibitory effect in orthodox AQPs (AQP1 and AQP5) was measured using light scattering stopped-flow technique, and for aquaglyceroporins (AQP3) fluorescent stopped-flow technique was used.

2.5 Results and Discussion

Protocol for the cyanation of *rac*-lupanine **(8)** and *rac*-sparteine **(9)** in batch were previously developed in our lab by MSc Andreia Fortuna **(Section 3.9/3.10.2-Procedure A)**. In this work, we will focus our attention in the electrochemical cyanation of *rac*-lupanine **(8)** and in derivatizations of both cyanated QA. Two solvents are used in this reaction: MeCN due to its wide electrochemical window and H_2O, that despite its smaller window in comparison with MeCN, it is used to dissolve NaCN salts. The cyanide salt has a dual role: besides acting as nucleophile, it also acts as supporting electrolyte. The reaction was performed at constant current, which after 6 h afforded 17-cyano-*rac*-lupanine in 80% yield. This protocol was developed based on compound **8** CV data **(Section 3.7)**.

An oxidation mechanism for *rac*-lupanine **(8)** and *rac*-sparteine **(9)** was proposed **(Figure 2.15)**. Anodic oxidation of the starting material forms a radical cation, followed by α-H radical abstraction by water. The removal of a second electron affords the iminium cation which is trapped by CN- nucleophilic attack, ultimately forming a C-C bond. The second half-reaction consists in H_2 generation.

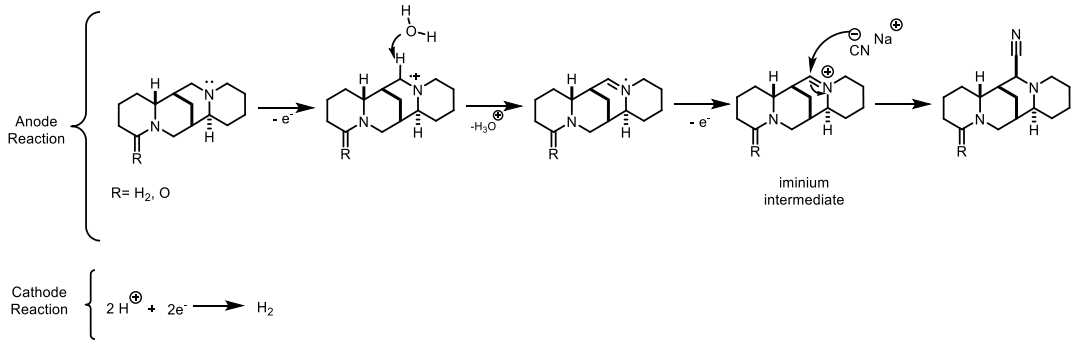

Figure 2.15: Proposed mechanism for compounds **8** and **9** cyanation

Considering the advantages of Flow Chemistry, Flow experiences were initiated with the aim of installing the nitrile functionality in *rac*-lupanine **(8)** in a lower reaction time and with full conversion.

2.5.1 Electrochemical Reactions

2.5.1.1 Flow Electrochemical Reactions

The equipment used was *ElectraSyn flow* by IKA **(Figure 2.16)** and was assembled as an undivided cell based on the protocol developed in batch.

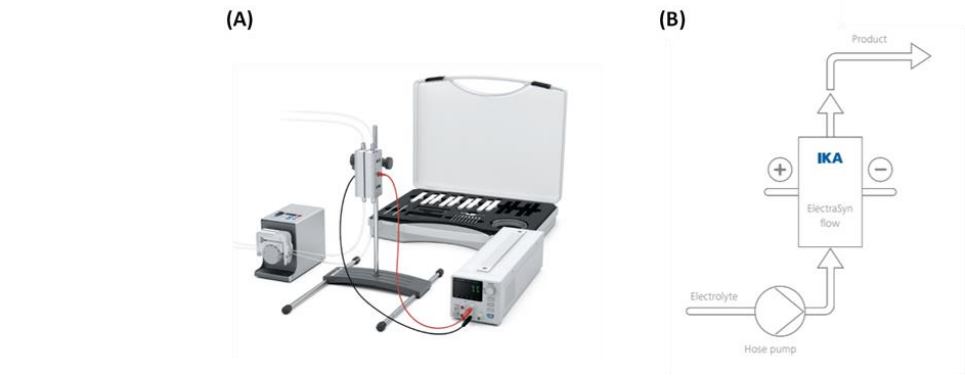

Figure 2.16: (A) ElectraSyn flow – the flow electrosynthesis equipment used in the experiences; (B) Flow system with how it works: the reaction mixture enters in the flow cell thanks to the peristaltic pump, and the departure of the product after the end of the electrochemical reaction.

Flow reaction conditions **(Section 3.10.1)** were optimized for the cyanation of **8** as summarized in **Table 2**. Reaction selectivity was calculated by ^{1}H NMR to monitor the development of each flow experiment. The use of the previously optimized batch electrochemical reaction conditions **(Table 2, Entry 0)**, at 1.0 or 0.25 ml/min resulted in no product formation **(Table 2, Entry 1 and 2).** Increasing the current to 10 mA **(Table 2, Entry 3)** resulted in product formation, however, lower selectivity was observed at 15 mA **(Table 2, Entry 4)**, indicating that high current density does not promote product formation. Thus, constant potential experiments were performed to increase reaction selectivity.

Table 2: Electrochemical reactions in Flow. Deviations from the developed protocol in batch (figure) such as current (*I*) and potential (*U*) are described in the following table.

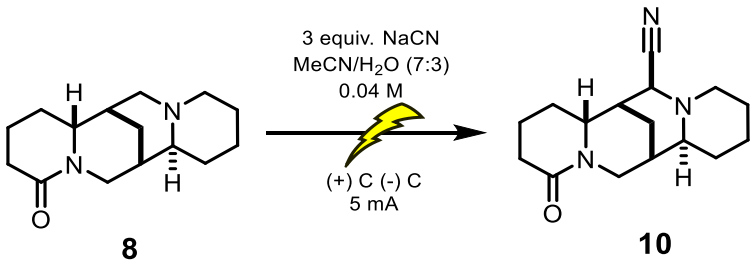

Entry	Deviation from above conditions	*I* (mA)	*U* (V)	Flow rate (ml/min)	Selectivity[a] (%)	Yield[b] (%)	Conv.[d] (%)
0	none	5	[c]	batch	ND	80	ND[f]
1	none	5	[c]	1	ND	ND	ND
2	none	5	[c]	0.25	ND	ND	ND
3	*I*	10	[c]	0.25	16	ND	ND
4	*I*	15	[c]	0.25	6	ND	ND
5	*U*	[c]	2.5	0.25	25	ND	ND
6	*U*	[c]	2.5	0.19	18	ND	ND
7	0.25 M $TBABF_4$	[c]	2.5	0.25	17	ND	ND
8	*U*	[c]	3	0.25	78	21	ND
9	*U*	[c]	3	0.13	39	ND	ND
10	*U*	[c]	3.5	0.25	ND	ND	ND
11	*U*	[c]	3.3	0.25	76	ND	ND
12	*U*	[c]	3.4	0.25	ND	ND	ND
13	0.08 M *U*	[c]	3	0.25	63	ND	ND
14	0.02 M *U*	[c]	3	0.25	67	ND	ND

15	NaCN 1.5 equiv. *U*	c	3	0.25	69	ND	ND
16	NaCN 5 equiv. *U*	c	3	0.25	74	ND	ND
17	KCN 3 equiv. *U*	c	3	0.25	82	ND	ND
18	NaOH 1 equiv. *U*	c	3	0.25	77	ND	ND
19	(+) GC (-) GC *U*	c	3	0.25	26	6	82
20	thicker membrane [e] *U*	c	3	0.25	36	20	65

a) Ratio product/starting material determined by ^{1}H NMR analysis of the crude reaction mixture.
b) No isolated yield (%). Calculated by qNMR using as calibration standard 1,3,5-trimethoxybenzene
c) Parameter not defined as constant during the experiment
d) Conversion of starting material (*rac*-lupanine) based on qNMR
e) 1 mm thickness. Apart from Entry 20, all reactions were performed with a 0.5 mm thickness membrane.
f) ND - not determined parameter

Rac-lupanine **(8)** CV experiments show 2 oxidative potentials at 1.1 V and 1.7 V, indicating the presence of 2 electrophores **(Section 3.7)**. Stabilization of the amide moiety through resonance, promote a LUMO orbital lower in energy, which indicates that amides are more challenging to oxidate ($E_{1/2}$=1.7 V). On contrary, the presence of aliphatic chains near the tertiary amine contribute to a higher electron density, leading to an easier oxidation target ($E_{1/2}$=1.1 V). Therefore, to achieve C17 *rac*-lupanine functionalization, potentials above 1.1 V need to be employed. Starting at 2.5 V **(Table 2, Entry 5)**, product was obtained in 25% selectivity. Approaches to increase selectivity such as diminishing flow rate or addition of $TBABF_4$ **(Table 2, Entry 6 and 7)**, were attempted without success. The decrease in selectivity using $TBABF_4$ **(Table 2, Entry 7)** confirmed the superfluous use of supporting electrolyte in flow.

The higher selectivity obtained was 78% under 3 V **(Table 2, Entry 8)** and decrease in flow rate **(Table 2, Entry 9)** did not increase reaction selectivity. At 3.5 V **(Table 2, Entry 10)**, an unexpected product was visible by TLC and ^{1}H NMR, which after suitable characterization and purification **(Appendix 7 - Section 5.7)**, 17-oxo-*rac*-lupanine **(11)** was obtained[135] .

The formation of this specie can be explained by the overoxidation of 17-cyano-*rac*-lupanine **(10)**. Since compound **10** has 2 oxidative potential values **(Section 3.8)** – 1.1 V and 1.9 V– working above these values, may lead to its undesirable degradation. Therefore, 2 reaction mechanisms were proposed. As a first hypothesis **(Figure 2.17– A)**, the tertiary amine lone pair of electrons eliminates the nitrile, since it is a good leaving group. The resulting iminium ion would be attacked by water molecules, which upon a SET mechanism, a diamide would be formed. The second hypothesis (**Figure 2.17– B)** is after compound **10** formation, a water molecule would attack C17, eliminating the nitrile. Afterwards, a SET mechanism would yield compound **11**.

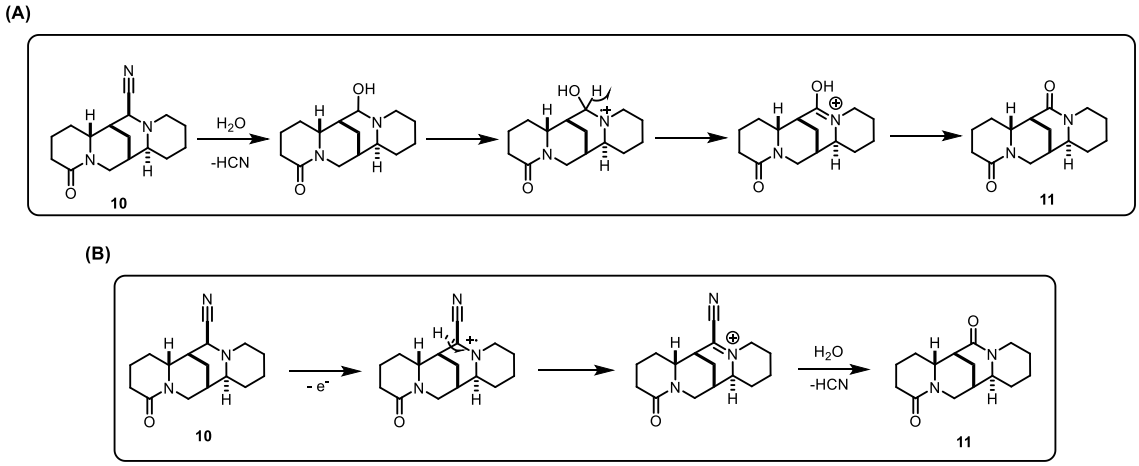

Figure 2.17: 2 mechanistic hypotheses (A and B) for the formation of the 17-oxo-*rac*-lupanine **(11)**.

The second hypothesis seems more plausible since electron transfer mechanisms predominate in electrochemical reactions[136]. Besides that, the aminal formed in **Figure 2.17-(A)** was not isolated as an intermediate for **11** formation, which promotes the second reaction mechanism as the most favourable. Even though working at constant potential is characterized by lower yields and higher selectivity, this experiment shows that selectivity issues may arise depending on the employed conditions. Experiments were conducted to see the maximum potential that could be applied in the system to eliminate selectivity issues **(Table 2, Entry 11 and 12)**, indicating that working above 3.3 V leads to 17-oxo-*rac*-lupanine **(11)** formation.

Until now, all experiments had a concentration of 0.04 M and 3 equiv. of NaCN. As an attempt to increase reaction rate, reaction concentration was increased **(Table 2, Entry 13)**, however higher selectivity was not observed. A similar result was obtained when concentration was decreased by half **(Table 2, Entry 14)**, indicating that future experiences will be conducted at 0.04 M. Regarding the quantity of salt used, **(Table 2, Entry 15,16 and 17)** an increase or decrease did not improve reaction selectivity. Using KCN as a different source of cyanide lead to a slightly higher selectivity (82%), but since the difference in selectivity is not significant, the subsequent reactions were performed with NaCN which is cheaper source of cyanide.

According to the mechanism of 17-cyano-*rac*-lupanine **(10)** formation, it was believed that NaOH was being formed, and higher values of selectivity could not be attained due to NaOH inhibition. The solution pH was approximately 10 before and after each reaction, showing no increase in basicity. To study this potential inhibitory effect, an experiment was conducted using 1 equiv. of NaOH **(Table 2, Entry 18**), which resulted in a 77% selectivity, discarding the NaOH inhibition theory.

A selectivity of 78% was the best result, however, predicting the yield of the reaction based on a ^{1}H NMR selectivity is not accurate, since signal integration can vary depending on ^{1}H NMR quality. IR spectra of *rac*-lupanine **(8)** and 17-cyano-*rac*-lupanine **(10) (Appendix 5 -Figure 5.21 and Appendix 6 -Figure 5.26)** do not present any difference between each other, despite nitrile characteristic band at 2238 cm^{-1} [134]. Therefore, quantitative NMR (qNMR) was the chosen technique to apply as quantification methodology, using as calibration standard 1,3,5-trimethoxybenzene. After using qNMR, we realized that high selectivity is not synonym for high yield. After repeating the best flow condition **(Table 2, Entry 8)**, the yield obtained was 21%, indicating that reaction conditions were non-reproducible **(Figure 2.18)**. Exchange for glassy carbon electrodes **(Table 2, Entry 19)** which are characterized by good chemical stability and wide potential range, did not improve reaction yield. Use of a thicker membrane to increase retention time **(Table 2, Entry 20)** was also an unsuccessful approach.

The low yields are not supported by TLC and ^{1}H NMR analysis, where the only species observed are 17-cyano-*rac*-lupanine **(10)** and *rac*-lupanine **(8) (Figure 2.18)**.

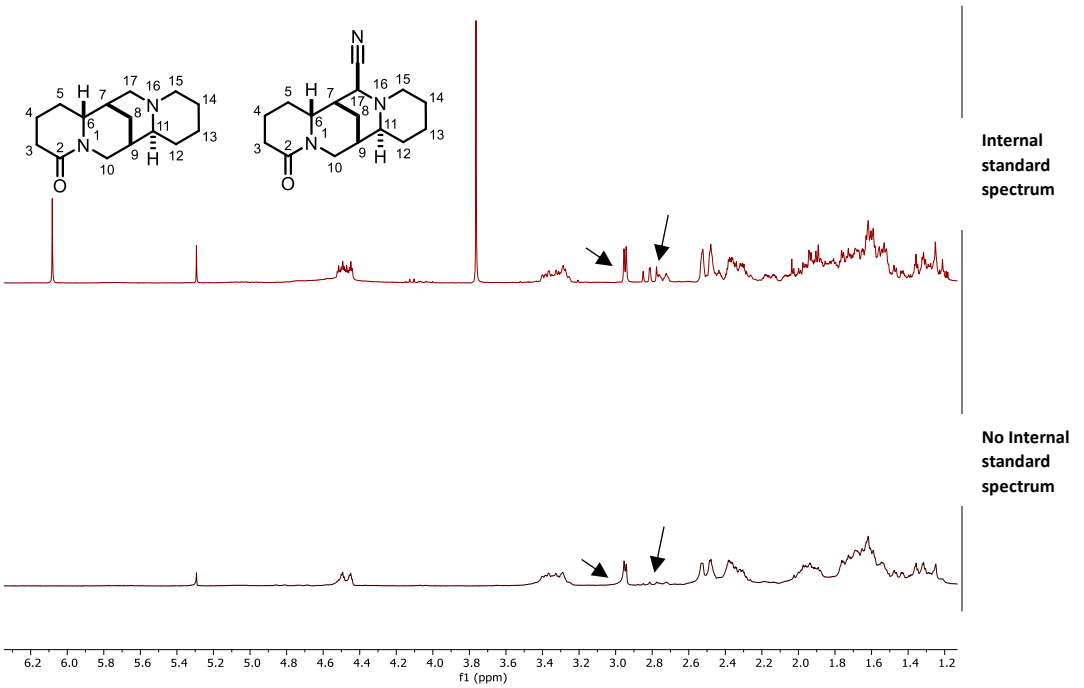

Figure 2.18 - ^{1}H NMR spectrum of **Table 2-Entry 8**, using internal standard (top spectrum) and no internal standard (bottom spectrum). Both spectra depict the presence of only 2 species (17-cyano-*rac*-lupanine characterized by H17 duplet, and *rac*-lupanine characterized by H15a/17a multiplet). The lack of reproducibility is seen on the top spectra, where a high quantity of *rac*-lupanine has not converted to 17-cyano-*rac*-lupanine.

This lack of selectivity might be indicative of product decomposition due to overoxidation. Considering that the potentials employed in all flow reactions were above 17-cyano-*rac*-lupanine **(10)** oxidative potentials (1.1 V and 1.9 V), side reactions can occur, such as amide oxidation. Through a Shono Oxidation reaction and assuming as potential nucleophiles CN- and H_2O, at least 2 side products can be formed, despite any side product isolation **(Figure 2.19)**.

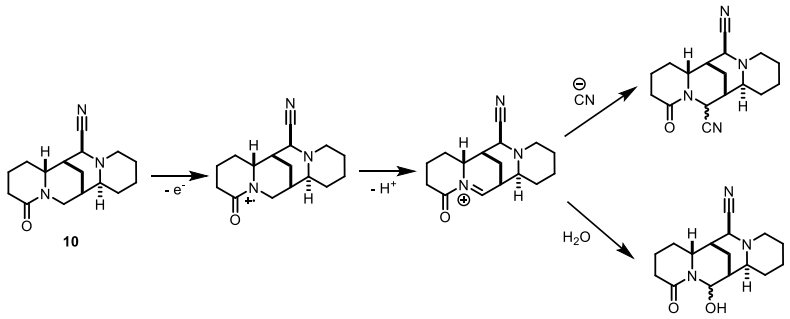

Figure 2.19: Possible overoxidation products through a Shono oxidation mechanism

The high conversion of *rac*-lupanine **(8)** and low yields depicted in **Entry 19** and **Entry 20**, can be explained by the leakages that occurred in the apparatus during flow reactions. Despite set-up cleaning prior and after each reaction, the presence of residues from previous reactions invisible to the naked eye, may be the cause behind leakages, preventing the total amount of starting material to enter in the cell and react. Therefore, the high conversion values mean that the actual amount of **8** that enters in the cell react almost in total; while the low yields are probably due to the lower quantity of starting material that enters in the cell, leading to less product exiting. These issues may be accounted for the membrane used between the electrodes, that has probably reached its lifespan. Its replacement is important to enable good performance of the equipment and consequently good reaction outcome.

However, reaction low yields indicate that a new strategy needs to be employed: application of tubes with a smaller diameter would decrease the minimal flow rate of the peristaltic pump (0.13 ml/min), allowing higher retention times. Selectivity issues can be overcome by lowering the potential to below 1.7 V since overoxidation side products are probably being formed. Since Flow is used mainly to scale-up, electrochemical reactions in batch were executed to have a deep understanding of the reaction. After optimization, flow experiments would be restarted.

2.5.1.2 Batch Electrochemical Reactions

Based on flow experiments, qNMR was used as quantitative methodology in batch experiments **(Table 3)**, since it proved to be a reliable approach.

Table 3: Electrochemical reaction performed in Batch. Deviations from the developed protocol in batch (figure) such as changes in potential (*U*), solvent proportion, electrodes and F/mol, are described in the following table. Conversion (Conv.) describes the yield of the reaction using qNMR as the quantification methodology

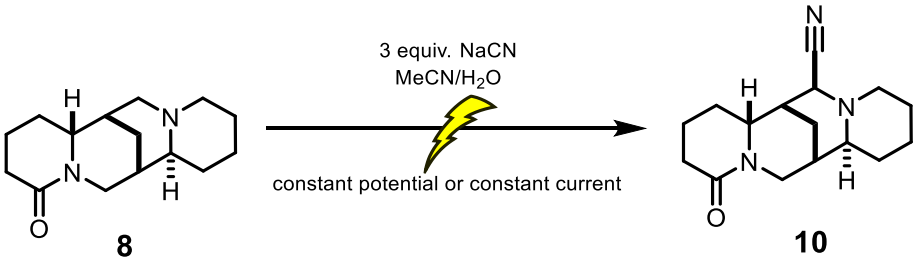

Entry	Solvent	Electrodes	rpm[a]	*I* (mA)	*U* (V)	F/mol	time (h)	Yield[b] (%)	Conv.[f] (%)
0	MeCN/H_2O (7:3)	(+) C (-) C	400	5	[d]	1.3	6	80	ND[e]
1	MeCN/H_2O (7:3)	(+) C (-) C	400	5	[d]	5.2	4	69	95
2	MeCN/H_2O (7:3)	(+) C (-) C	400	[d]	2.5	[c]	4	ND	ND
3	MeCN/H_2O (7:3)	(+) C (-) C	500	[d]	2.1	[c]	11	47	94
4	MeCN/H_2O (6:4)	(+) C (-) C	650	[d]	2.1	[c]	11	69	86
5	MeCN/H_2O (6:4)	(+) C (-) C	660	[d]	2.1	[c]	3	24	41
							6	44	54
							9	58	66
							11	69	67
							14	64	100
6	MeCN/H_2O (6:4)	(+) C (-) Pt	660	[d]	2.1	[c]	3	52	60
							5	66	79
							6	60	85
							11	34	100
7	MeCN/H_2O (6:4)	(+) Pt (-) Pt	660	[d]	2.1	[c]	2	13	33
							6	40	47
							8	56	49
							11	59	70
							14	59	79
8	MeCN/H_2O (6:4)	(+) C (-) C	650	[d]	2.1	[c]	11	21	87

9	MeCN/H_2O (6:4)	(+) C (-) C	660	[d]	2.1	[c]	11	98	97

a) rpm – magnetic stir bar rotation per minute
b) No isolated yield (%). Calculated by qNMR using as calibration standard 1,3,5-trimethoxybenzene
c) "Run Continuous" mode experiences, where the only predefined parameters were potential (*U*) and rpm
d) Parameter not defined as constant during the experiment
e) ND - not determined parameter
f) Conversion of starting material (*rac*-lupanine) based on qNMR

The batch protocol previously developed **(Section 3.10.2 - Protocol A)** was performed in ElectraSyn 2.0. The reaction had a duration of 6 h and used 1.3 F/mol **(Table 3, Entry 0)**. To decrease reaction time and increase yield, the electron equivalents were increased, while maintaining 5 mA as constant current **(Table 3, Entry 1)**. A moderate yield was obtained (69%) however the high conversion is due to the presence of secondary products on TLC. The lack of selectivity prompted us to initiate constant potential experiments under "Run Continuous" mode. This setting enables the operator to select the desired potential and rotation per minute (rpm), while current and F/mol, are not pre-defined and change throughout the progress of the reaction. Besides that, the reaction can be easily stopped and monitored by TLC. Starting with 2.5 V just as in the first constant potential experiment in flow **(Table 3, Entry 2/Table 2, Entry 5)**, after 2h of reaction, TLC showed the desired product already formed, but in low quantity. As the reaction proceeds, the desired product degrades, until almost no product is seen on TLC after 4h. Therefore, the potential was reduced to 2.1 V and rpm was increased for a higher mass transfer **(Table 3, Entry 3)**. After 11 h, a yield of 47% was obtained, and 2 phases were observed in the reaction mixture. Analysis of each phase by ^{1}H NMR and TLC, indicates a higher quantity of product in the less dense phase, which could be a consequence from a "salting-out" effect: the strong interaction of NaCN salts with water molecules, increases the polarity and viscosity of the solvent, turning 17-cyano-*rac*-lupanine less soluble in water[137]. Once again, the conversion is high, and by looking at the crude ^{1}H NMR, only starting material and product were seen. The veracity of the calibration standard was proved by isolating 17-cyano-*rac*-lupanine **(10) (Section 3.10.2 – Protocol B**) in 35% yield, proving that just as was observed in flow experiments possible side products from compound **10** overoxidation **(Figure 2.19)** can be in the reaction medium. To achieve homogeneity, a higher proportion of water was added to dissolve NaCN salts completely. Repeating the previous reaction with the new solvent mixture **(Table 3, Entry 4),** the increase to 69% yield showed the importance of homogeneity in the reaction outcome. Therefore, this proportion was applied in the following reactions.

Based on the best condition which afforded a 69% yield, a detailed analysis of the reaction was done **(Table 3, Entry 5)**: aliquots were taken to see reaction development over time. Data showed that (1) after 14h, product starts to degrade, and (2) the reaction was reproducible leading to a yield of 69% after 11h **(Figure 2.20)**. Due to the fact that H_2 is produced in our reaction, Platinum was used as cathode in an attempt to improve yields[138]. After monitoring the reaction for 11h, degradation is visible after 5h **(Figure 2.21).** The conversion value after 5h is higher than at 11h on **Entry 5**, but since Platinum electrodes are more expensive than graphite, reaction optimization was continued with graphite electrodes.

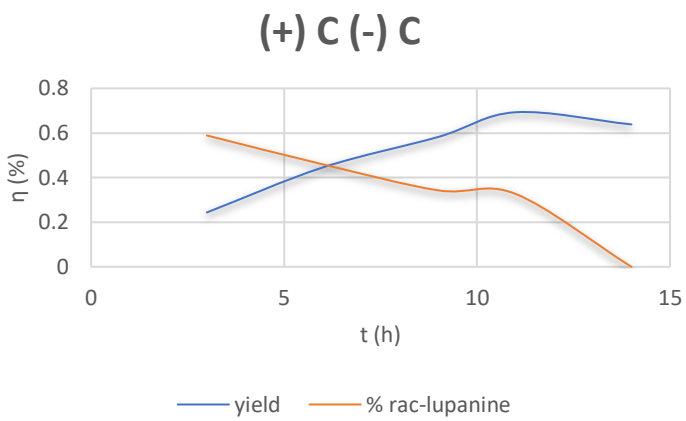

Figure 2.20: Batch reaction **(Table 3 - Entry 5)**, analysed by several aliquots: as conversion reaches 100%, and 69% yield is obtained at 11h.

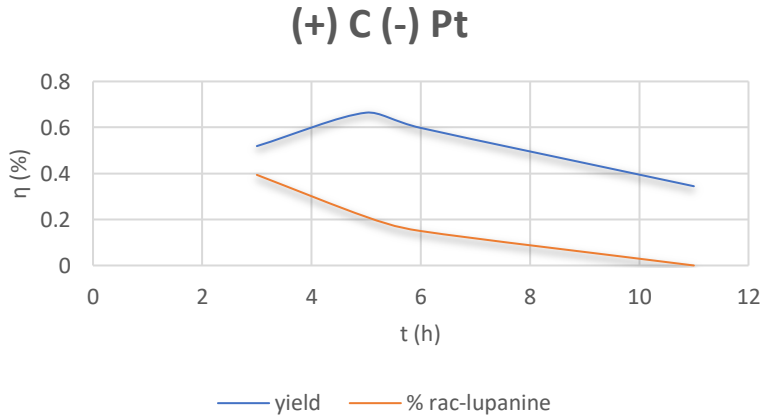

Figure 2.21: Batch reaction **(Table 3 - Entry 6)**, analysed by several aliquots: as conversion reaches 100%, and 66% yield is seen at 6h.

Shifting both electrodes to Platinum **(Table 3, Entry 7)**, conversion values increase over time, but since the yield does not increase very much as reaction proceeds, Platinum electrodes were abandoned.

However, when repeating the best condition depicted on **Entry 4**, an unexpected yield of 21% is observed **(Table 3, Entry 8).** Graphite electrodes are known for their high stability, but under highly oxidative conditions formation of graphene oxide occurs. When this product is dark grey, it is similar with graphite at naked eye[139]. This similarity prompted us to change graphite electrodes to new ones, proving that the source of low yield was due to electrode degradation: after 11h, a 98% yield was obtained, with a conversion of 97% **(Table 3, Entry 9)**. This result showed that electrode degradation occurs even though invisible to the naked eye.

Having accomplished almost full conversion, with high yields and high selectivity, the optimization of 17-cyano-*rac*-lupanine **(10)** in batch was complete. Flow experiments can be restarted to decrease reaction time and to scale-up. As a first approach, experiments should start at 2.1 V based on batch optimized protocol. Meanwhile, derivatizations of compound **10** were conducted.

2.5.2 Derivatization of 17-cyano-*rac*-lupanine and 17-cyano-*rac*-sparteine

2.5.2.1 Nitrile reduction

Nitrile reduction up to a primary amine, would yield a H-bond donor and acceptor site in both QAs. Assuming that the presence of this functionality would be a good approach for a "tridentate" ligand that could improve asymmetric catalysis, reduction experiments were initiated with 17-cyano-*rac*-lupanine **(10)**. Two different reagents were used for nitrile and amide reduction: DIBAL and $LiAlH_4$. Using DIBAL **(Section 3.11.1),** amide reduction and decyanation afforded *rac*-sparteine **(9) (Appendix 8, Figure 5.37)**, indicating that replacement of the nitrile group for a hydride is the preferable reaction path instead of primary amine formation **(Figure 2.22).** In the presence of $LiAlH_4$ **(Section 3.11.2)**, full conversion was attained, and by crude ^1H NMR analysis **(Appendix 8, Figure 5.36)** a new product was obtained. Since $LiAlH_4$ is a stronger reducing agent than DIBAL, reduction of the tertiary amide was expected, as well as decyanation which is supported by the literature. However, *rac*-sparteine was not obtained. Product identification is ongoing.

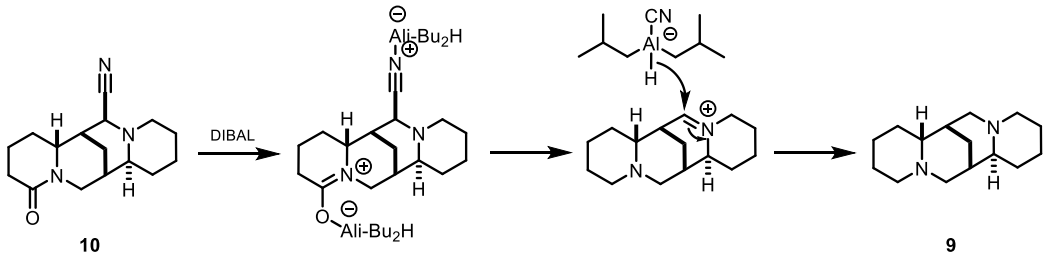

Figure 2.22: 17-cyano-*rac*-lupanine decyanation and amide reduction with DIBAL.

As a greener approach, nitrile hydrogenation was performed using 17-cyano-*rac*-lupanine **(10)** and 17-cyano-*rac*-sparteine **(12) (Section 3.11.3)**. To avoid formation of by-products, polar solvents were used in both reactions, since it has a great impact in reaction outcome. On one hand, solvent-catalyst interaction inhibits the absorption of the primary amine, avoiding therefore condensation reactions. On the other hand, solvent-product interactions promote substrate solvation, which hinders its reabsorption on the metal surface. Both types of interaction promote higher selectivity for primary amine formation[115]. Regarding compound **12**, its hydrogenation was performed using AcOH **(Section 3.11.3 – Procedure A)**. This solvent promotes tertiary amine protonation which otherwise could displace the nitrile functionality, yielding an iminium ion. However, instead of nitrile reduction, we observed once again a decyanation reaction: since nitrile is a moderate leaving group (pk_a=9.21), its displacement upon hydrogen addition yielded *rac*-sparteine **(9)** after product purification **(Appendix 8, Figure 5.38)**. 17-cyano-*rac*-lupanine **(10)** hydrogenation was performed using a catalyst based on cobalt: Co/SiO_2 **(Section 3.11.3 – Procedure B)**. Using a different but protic solvent (EtOH), the reaction took the same path: instead of reducing the nitrile to primary amine, a decyanation occurred once again **(Appendix 8, Figure 5.39)**. This result may be accounted for the non-activation of the catalyst upon heat, which was suggested in the literature[140]. These results show the inertness of the nitrile upon harsh and selective reductive conditions. Other methodologies could be tested in the future: use of other metals and supports for catalytic hydrogenation that favour primary amine synthesis; use of H-cube apparatus to achieve higher pressures in the hydrogenation reaction.

2.5.2.2 Nitrile Hydrolysis

Due to nitrile high stability, 17-cyano-*rac*-sparteine **(12)** hydrolysis was performed in harsh conditions using H_2SO_4 at rt **(Section 3.11.4 – Procedure A)**. Crude characterization by ^1H NMR, ^{13}C NMR and IR suggest the presence of an amide compound **(Figure 2.23)**: strong band at 1678 cm^{-1} in addition to a carbon peak at 179.9 ppm **(Appendix 8 – Section 5.8.2)**. 2 broad singlets at 6.88 ppm and 5.43 ppm may be attributed to the chemically inequivalent protons of the primary amine: delocalization of nitrogen lone pair of electrons into the carbonyl group, will induce a partial double bond character of the C-N bond, which will restrict free bond rotation[141]. Assuming that an amide was obtained, upon reduction with diborane[142], an alternative methodology for primary amine synthesis in 2 steps can be an accomplished. Nevertheless, due to technical issues, product further characterization and purification is ongoing.

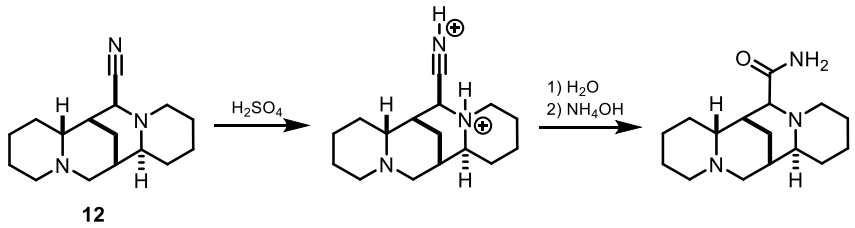

Figure 2.23: Amide formation mechanism, using H_2SO_4

Using a different mineral acid – HCl – hydrolysis compound **10** was investigated **(Section 3.11.4 – Procedure B)**. Despite the fact that HCl as a higher hydrolysis rate compared to H_2SO_4 [143] and α-aminoacids were expected to be the major reaction product, carboxylic acid group versatility could be exploited for primary amine synthesis **(Figure 2.24)**: reduction with $LiAlH_4$ would afford a primary alcohol and tertiary amide reduction; alcohol conversion to a sulfonate would then be displaced by NaN_3 nucleophilic attack; finally, azide reduction through a Staudinger reaction would yield the desired amine. However, HCl hydrolysis reaction did not afford promising results. In the future, new hydrolysis experiments under mild conditions should be experimented such as biocatalytic nitrile hydrolysis[144] .

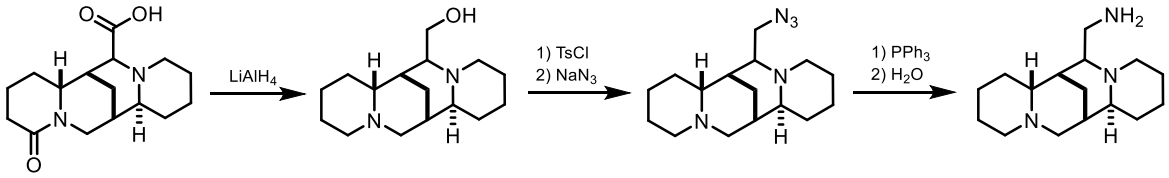

Figure 2.24: Proposed primary amine linear synthesis from α-aminoacids

2.5.2.3 Oxazole synthesis

Considering its potential in medicinal chemistry, a synthetic methodology consisting in 2 steps was followed to synthetize oxazoles from compound **10 (Section 3.12.1)**[126]: nitrile is activated with triflic acid (TfOH), which then suffers a nucleophilic attack from the alcohol, leading to an imidate intermediate. This intermediate will then undergo a double hydrogen atom transfer (HAT) and aromatization to afford the oxazole **(Figure 2.25)**.

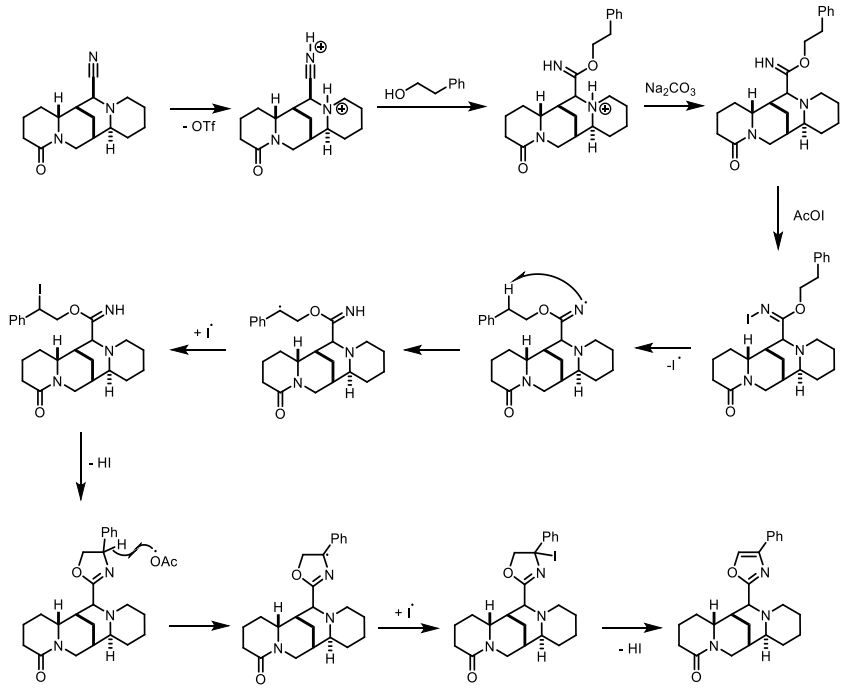

Figure 2.25: Proposed mechanism of oxazole synthesis.

Due to the high basicity of the nitrile group (pK_a = -10), TfOH was used in excess to activate the nitrile before alcohol nucleophilic attack. Crude ^{1}H NMR analysis shows that the alcohol did not react. After alcohol removal and subsequential characterization, we were upon the presence of an iminium ion with triflate as counterion: 17-dehydrolupaninium triflate **(13)**. The actual mechanism of this reaction consists in nitrile activation with TfOH which is then displaced by tertiary amine lone pair **(Figure 2.26/ Appendix 8, Section 5.8.3)**.

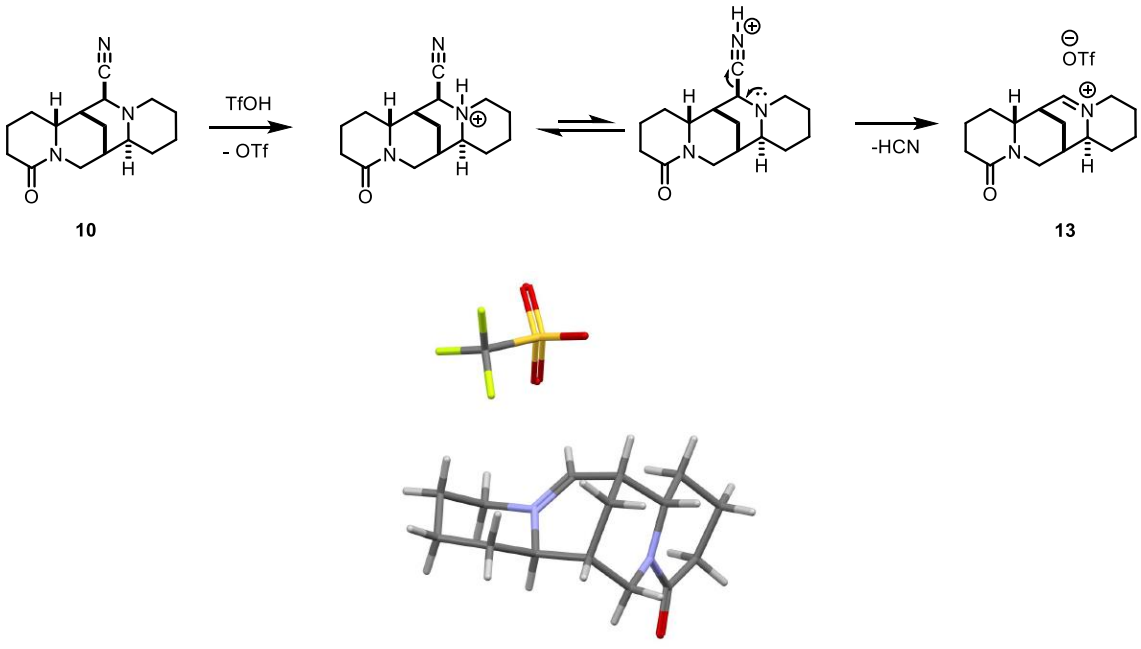

Figure 2.26: Proposed mechanism for the synthesis of compound **13** with correspondent X-ray analysis of the obtained product

Reaction screening showed that the iminium specie was formed regardless of using the alcohol as reagent, and in the presence or absence of inert atmosphere. Substituting the alcohol for water also yielded the compound. This compound can present an alternative synthetic methodology for primary amines: upon addition on nitromethane and its posterior reduction, a primary amine could be afforded, in addition to another carbon atom in the molecule.

2.5.2.4 Tetrazole synthesis

Continuing with the purpose of synthetizing N-heterocyclic compounds, tetrazole synthesis was performed **(Section 3.13 – Procedure A)**. Due to the absence of strongly electron-withdrawing groups in 17-cyano-*rac*-lupanine **(10)** and 17-cyano-*rac*-sparteine **(12)**, the nitrile was activated using acidic conditions for NaN_3 nucleophilic attack. Using as proton source NH_4Cl, a six membered ring transition state is formed, leading to an imidoyl intermediate which upon spontaneous cyclization a tetrazole ring is afforded[129] **(Figure 2.27)**.

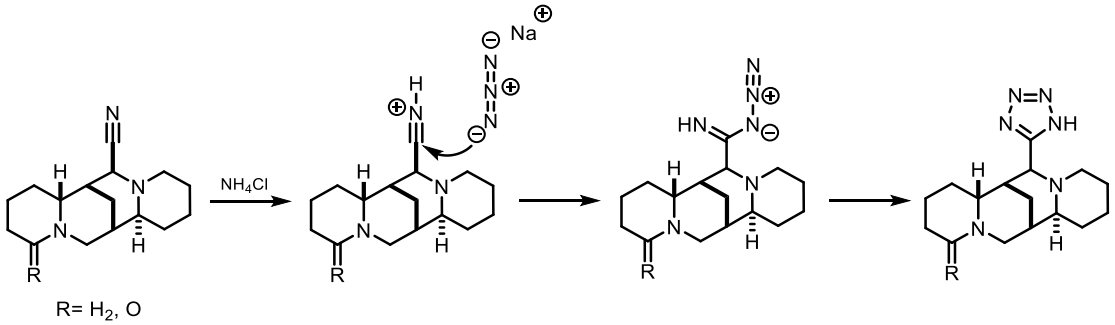

Figure 2.27: Tetrazole synthesis mechanism using NH_4Cl and NaN_3

Using compound **12** as starting material, several compounds were formed, without possible purification of the reaction mixture **(Appendix 8, Section 5.8.4)**. This lack of selectivity can be explained by the high temperature employed in the reaction (90 °C). Therefore, a reaction at room temperature was performed, using compound **10** as starting material **(Section 3.13 – Procedure B)**. After 24h no conversion of starting material was visible, indicating that temperature is crucial for reaction development, but selectivity is undermined by higher temperatures. In future attempts, reaction below 90°C should be tested, and also a different approach for nitrile activation such as Lewis acids[145].

2.5.3 Characterization analysis

Throughout this work, 3 compounds were obtained and characterized by ^{1}H NMR and ^{13}C NMR: 17-cyano-*rac*-lupanine **(10)** from the cyanation of *rac*-lupanine **(8)**; 17-oxo-*rac*-lupanine **(11)**, a side product observed during the optimization of compound **8** cyanation; and 17-dehydrolupaninium triflate **(13)** as the product from the reaction of compound **10** with TfOH. **(**

Table *4*).

Compound **10 (Table 4 – Entry 2)** is characterized by a carbon peak at 121.0 ppm correspondent to the carbon of the nitrile moiety, and a duplet at 2.91 ppm which corresponds to proton H17 **(Figure 2.28)**. In compound **10** as well as compound **8**, the presence of an amide functional group is depicted by the deshielded carbon peak at 171.4 ppm (C2). Nitrogen lone pair delocalization promotes $H10_a$ as the most deshielded proton in both molecules, depicted by peak at 4.43 ppm in compound **10**, and peak at 4.49 ppm in compound **8**. Attribution of the several diastereotopic protons in compound **10** were based upon 2D NMR analysis and reported spectral data **(Appendix 6)**[134].

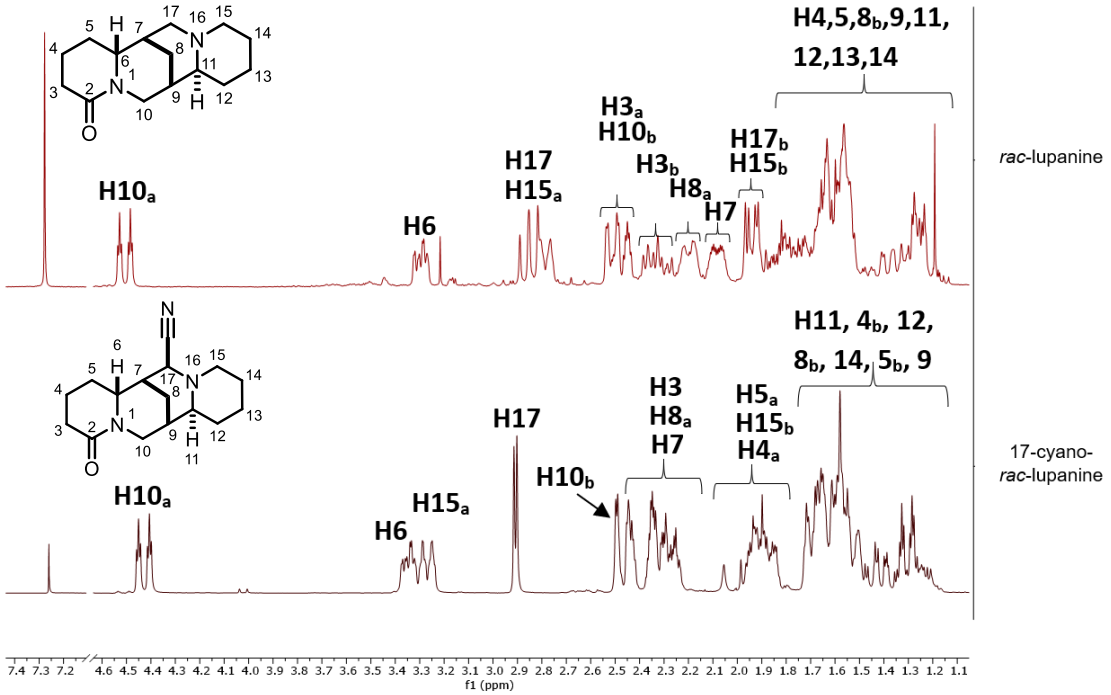

Figure 2.28: Comparison between the ^{1}H NMR of *rac*-lupanine **(8)** (top spectra) with ^{1}H NMR of 17-cyano-*rac*-lupanine **(10)** (bottom spectra).

Compound **10** overoxidation yielded compound **11 (Table 4 – Entry 1/ Appendix 7):** amide carbonyl shift depicted by peaks at 171.0 ppm (C2) and at 167.4 ppm (C17); amide α-diastereotopic protons $H10_a$ and $H15_a$ (depicted by peaks 4.82 ppm and 4.70 ppm, respectively) correspond to the most deshielded protons due to amide negative inductive effect; considering that inductive effect transmission decreases with distance, a lower shift is observed on amide β-protons (H14 and H9)[146]. Attribution of the several diastereotopic protons were based upon 2D NMR analysis and reported spectral data **(Appendix 7)**[135]**.**

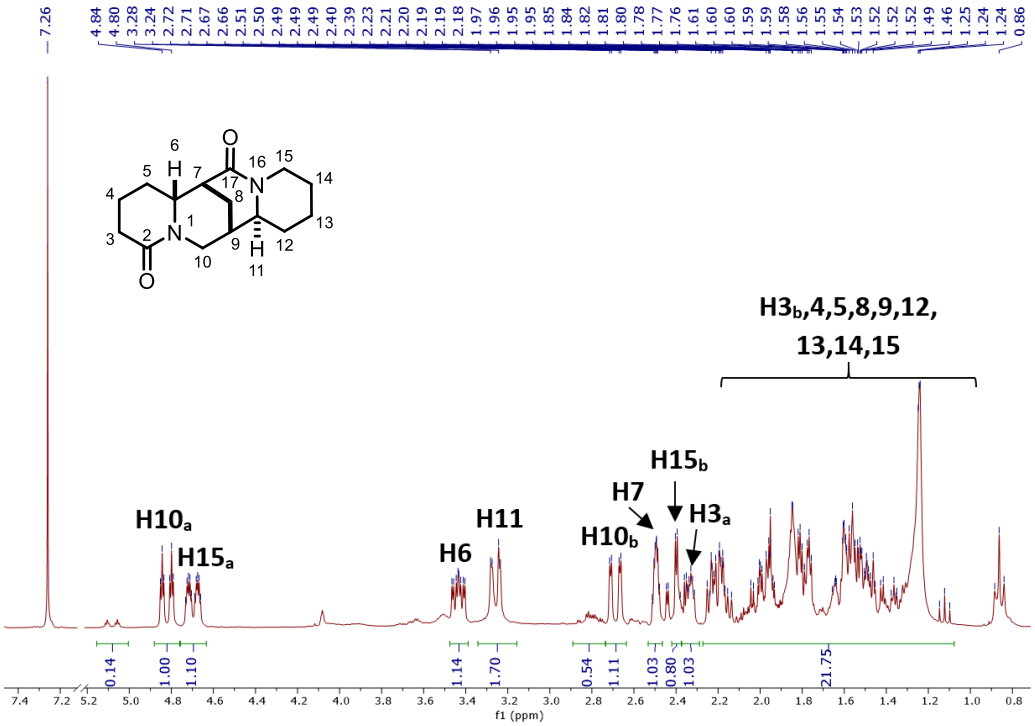

Figure 2.29: ^{1}H NMR spectrum of 17-oxo-*rac*-lupanine **(11)**

Compound **13 (Table 4 – Entry 3/ Appendix 8 – Section 5.8.3)**, the unexpected product of the reaction of 17-cyano-*rac*-lupanine with TfOH, is characterized by the deshielded iminium proton duplet at 9.02 ppm (H17), along with deshielded carbon peak at 179.2 ppm; amide carbonyl peak is depicted by peak at 171.3 ppm; presence of the triflate as counterion is supported by the quadruplet at 122.7 ppm, due to ^{13}C coupling with ^{19}F.

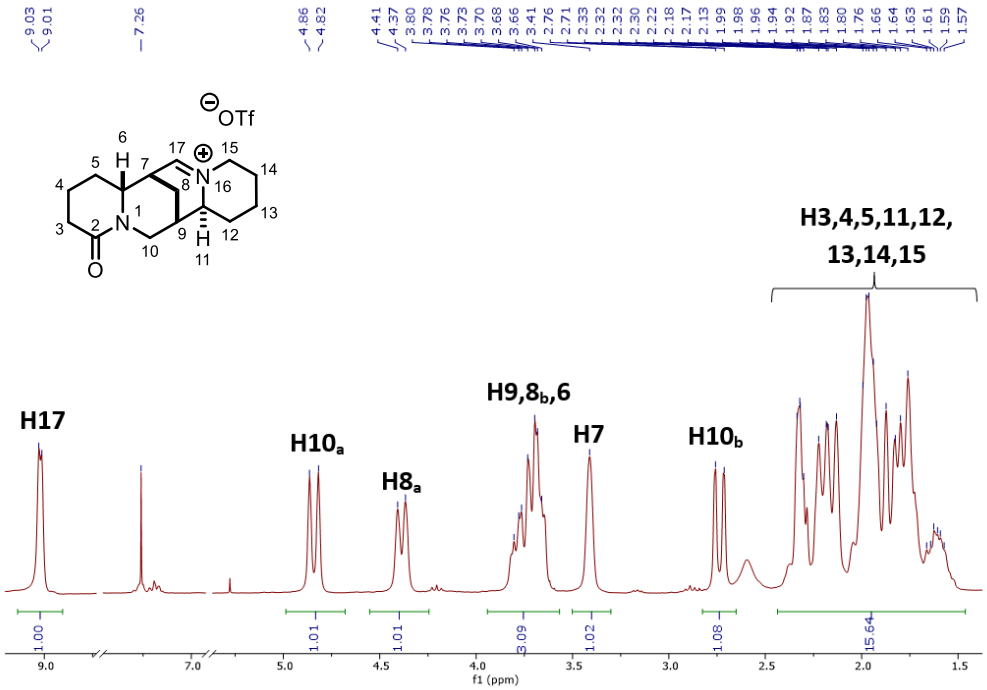

Figure 2.30: ^{1}H NMR spectrum of 17-dehydrolupaninium triflate **(13)**

Table 4: ^{1}H NMR and ^{13}C NMR characterization of the 17-oxo-*rac*-lupanine **(11)**, 17-cyano-*rac*-lupanine **(10)**, 17-dehydrolupaninium triflate **(13)** and *rac*-lupanine **(8)**, along with reported spectral data of **11**, **10** and **8**.

Entry	Compound	^{1}H NMR	^{1}H NMR reported	^{13}C NMR	^{13}C NMR reported
1	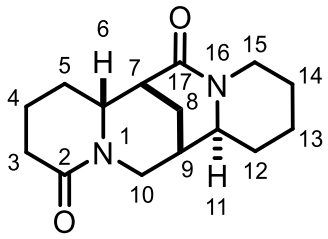 **11**	4.82 (dt, J = 13.4, 2.5 Hz, 1H, $H10_a$) 4.70 (m, 1H, $H15_a$) 3.43 (m, 1H, H6) 3.26 (dd, J = 11.7, 2.5 Hz, 1H, H11) 2.69 (dd, J = 13.4, 2.6 Hz, 1H, $H10_b$) 2.49 (m, 1H, H7) 2.40 (d, J = 2.7 Hz, 1H, $H15_b$) 2.34 (m, 1H, $H3_a$) 2.25-1.24 (m, 16H, $H3_b$,4,5,8,9,12,13,14,15).	[a] 4.84 (J = 13.4, 2.7 Hz, 1H, $H10_a$) 4.72 (J = 13.1, 4.0, 2.7 Hz, 1H, $H15_a$) 3.45 (J = 10.3, 5.8, 2.5 Hz, 1H, H6) 3.27 (J = ≈ 0, 11.9, 2.6 Hz, H11) 2.70 (J = 13.4, 2.7 Hz, $H10_b$) 2.51 (J = ≈3, 3.1, 2.5 Hz, H7) 2.41 (J = 13.1, 13.0, 2.7 Hz, $H15_b$) 2.37 (J = 17.2, 4.6, 3.1, 2.4 Hz, $H3_a$) 2.22 (J = 13.0, 3.1, 2.5 Hz, $H8_a$) 2.21 (J =17.2, 12.3, 5.5 Hz, $H3_b$) 2.04 (J = 14.0,10.3,3.6 Hz, $H5_a$)	171.0 (C2) 167.4 (C17) 61.2 (C11) 59.0 (C6) 48.1 (C10) 43.7 (C7) 43.1 (C15) 33.9 (C9) 33.5 (C12) 32.9 (C3) 27.1(C14) 25.4 (C8/C5/C13) 25.1 (C8/C5/C13) 22.8 (C8/C5/C13) 19.5 (C4)	[a] 170.82 (C2) 167.42 (C17) 60.96 (C11) 58.80 (C6) 47.88 (C10) 43.47 (C7) 42.86 (C15) 33.72 (C9) 33.37(C12) 32.72 (C3) 26.89 (C5) 26.89 (C8) 25.22 (C14) 24.96 (C13) 19.35 (C4)

			1.96 (J = 14.0, 5.8, 4.7, 3.2, 2.4 Hz, $H5_b$) 1.88 (J = 4.0 3.8, 2.7 Hz, $H13_a$) 1.87 (J = 3.1, ≈3, 2.7, 2.5, ≈0 Hz, H9) 1.81 (J = 13.0, ≈3 Hz, $H8_b$) 1.80 (J = 5.5, 4.7, 3.6, 3.1, Hz, $H4_a$) 1.64 (J = 13.2, 2.7 Hz, $H14_a$) 1.59 (J = 12.1, 2.6 Hz, $H12_a$) 1.57 (J = 13.0, 12.1, 2.7 Hz, $H13_b$) 1.56 (J = 14.0, 12.3, 3.2, 4.6 Hz, $H4_b$) 1.46 (J = 12.2, 12.1, 11.9, 3.8 Hz, $H12_b$) 1.36 (J = 13.2, 13.0, 4.0 Hz, $H14_b$)		

2	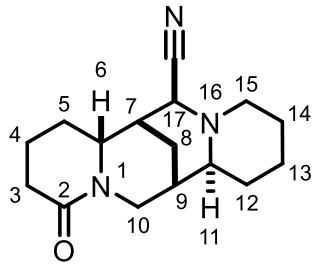 **10**	4.43 (dt, *J* = 13.3, 2.5 Hz, 1H, $H10_a$) 3.35 (m, 1H, H6) 3.27 (m, 1H, $H15_a$) 2.91 (d, *J* = 3.6 Hz, 1H, H17) 2.49 (d, *J* = 2.5 Hz, 1H, $H10_b$) 2.46 – 2.22 (m, 4H, $H3,8_a,7$) 1.90 (m, 3H, $H5_a$, 15_b, 4_a) 1.76 – 1.18 (m, 10H, $H11,4_b$, $12,8_b$, $14,5_b,9$)	[b] 4.45 (dt, *J* = 13.3, 2.4, 2.2 Hz, $H10_a$) 3.40 (dd, *J* = 10.8, 2.0 Hz, H6) 3.30 (m, $H15_a$) 2.95 (d, *J* = 3.7 Hz, H17) 2.59 (m, H3) 2.50 (dd, *J* = 13.3, 2.5 Hz, $H10_b$) 2.40 (m, H7) 2.32 (m, $H8_a$) 1.98 (m, $H15_b$) 1.96 (m, $H5_a$) 1.90 (m, $H4_a$) 1.74 (m, $H11,14_a$) 1.72 (m, $H4_b$) 1.68 (m, H9) 1.64 (m, H13) 1.62 (m, $H5_b$) 1.57 (m, H12) 1.34 (m, $H8_b$)	171.4 (C2) 121.0 (-CN) 63.0 (C11) 59.8 (C6) 54.0 (C15) 53.0 (C17) 46.4 (C10) 39.2 (C7) 34.2 (C9) 33.6 (C12) 32.9 (C3) 27.2 (C5) 25.3 (C8) 25.0 (C13) 24.4 (C14) 19.5 (C4)	[b] 171.3 (C2) 120.9 (-CN) 62.9 (C11) 59.7 (C6) 53.9 (C15) 52.9 (C17) 46.4 (C10) 39.2 (C7) 34.2 (C9) 33.5 (C12) 32.8 (C3) 27.1 (C5) 25.2 (C8) 24.9 (C13) 24.3 (C14) 19.4 (C4)

			1.30 (m, $H14_b$)		
3	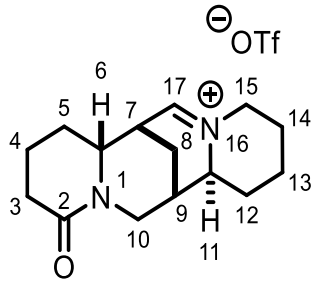 **13**	9.02 (d, J = 4.8 Hz, 1H, H17) 4.84 (d, J = 14.2 Hz, 1H, $H10_a$) 4.39 (d, J = 12.3 Hz, 1H, $H8_a$) 3.73 (m, 3H, $H9,8_b,6$) 3.41 (s, 1H, H7) 2.74 (d, J = 13.6 Hz, 1H, $H10_b$) 2.43 – 1.52 (m, 15H, H3,4,5,11,12,13,14,15)	[c]	179.2 (C17) 171.3 (C2) 122.7 (q, 323 Hz, -CF_3) 67.5 (C6) 62.1 (C8) 60.2 (C9) 47.2 (C10) 38.4 (C7) 33.0-19.8 (8C, C3,4,5,11,12,13,14).	[c]
4	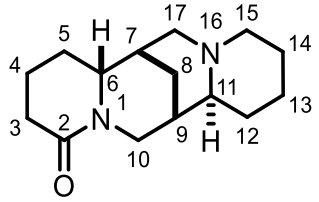 **8**	4.49 (dt, J = 13.2, 2.3 Hz, 1H, $H10_a$) 3.28 (m, 1H, H6) 2.81 (m, 2H, $H17_a$, 15_a) 2.46 (m, 2H, $H10_b,3_a$) 2.31 (m, 1H,3_b) 2.18 (m, 1H, $H8_a$) 2.07 (m, 1H, H7),	[d] 4.50 ($H10_a$) 3.29 (H6) 2.82 ($H17_a$) 2.75 ($H15_a$) 2.51 ($H10_b$) 2.47 ($H3_a$) 2.33 ($H3_b$)	171.4 (C2) 64.1 (C11) 60.8 (C6) 55.4 (C15) 52.6 (C17) 46.6 (C10) 34.6 (C9)	[e] 63.8 (C11) 61.7 (C6) 55.3 (C15) 52.8 (C17) 46.6 (C10) 32.4 (C9) 33.5 (C12)

		1.92 (m, 2H, $H17_b$, 15_b) 1.87 – 1.14 (m, 16H, $H4,5,8_b,9,11,12,13,14$)	2.16 ($H8_a$) 2.06 (H7) 1.93 ($H17_b$) 1.90 ($H15_b$) 1.83 ($H4_a$) 1.76 ($H5_a$) 1.69 ($H13_a$) 1.62 (H11,9, 4_b) 1.56 ($H14_a$) 1.55 ($H5_b$) 1.54 ($H12_a$) 1.53 ($H14_b$) 1.35 ($H12_b$) 1.26 ($H13_b$) 1.24 ($H8_b$)	33.3 (C12) 32.9 (C3) 32.0 (C7) 27.3 (C5) 26.5 (C8) 24.9 (C13) 24.2 (C14) 19.4 (C4)	33.0 (C3) 34.9 (C7) 26.7 (C5) 27.3 (C8) 24.5 (C13) 25.3 (C14) 19.6 (C4)

a. ^{1}H NMR and ^{13}C NMR reported spectra of 17-oxo-*rac*-lupanine in $CDCl_3$ (chemical shifts from TMS). ^{1}H NMR spectra was performed on a Bruker Avance 600 spectrometer at a measuring frequency of 600.31 MHz, and ^{13}C NMR on a Varian Gemini 300 spectrometer at a measuring frequency of 75.462 MHz[135].
b. ^{1}H NMR and ^{13}C NMR reported spectra of 17-cyano-*rac*-lupanine in $CDCl_3$ (chemical shifts from TMS). ^{1}H NMR and ^{13}C NMR spectra were performed on a Varian Gemini 300 spectrometer at 300 MHz[134].
c. Spectral data of 17-dehydrolupaninium triflate not available in literature
d. ^{1}H NMR reported spectra of *rac*-lupanine in $CDCl_3$ (chemical shifts from TMS). ^{1}H NMR spectra was performed on a Varian 300 Mercury spectrometer at 300.13 MHz[93].
e. ^{13}C NMR reported spectra of *rac*-lupanine in $CDCl_3$ (chemical shifts from TMS). ^{13}C NMR spectra was performed on a Varian 300 Mercury spectrometer at 300.13 MHz[147].

2.5.4 AQPs Biological assays

Similarly to LA and OA biological assays, AQP modulation was evaluated by permeability studies using the stopped-flow technique in three AQPs (AQP1,3 and 5). To see if the combination of different scaffolds could induce AQP modulation, some biological assays were done with pairs of compounds, while other experiences were performed using only 1 compound. The compounds tested include the molecules synthetized throughout this work (17-cyano-*rac*-lupanine, 17-oxo-*rac*-lupanine and 17-dehydrolupaninium triflate) along with other compounds synthetized in our group as depicted in **Figure 2.31**: **(1)** 17-cyano-*rac*-lupanine + spart rac (*rac*-sparteine); **(2)** Lup Rac (*rac*-lupanine) + AF_050719_A4-A5; **(3)** 17-cyano-*rac*-sparteine + 17-dehydrolupaninium triflate; **(4)** 17-oxo-*rac*-lupanine; **(5)** 17-cyano-*rac*-sparteine; **(6)** 17-dehydrolupaninium triflate. All assays were performed using a concentration of 25 µM.

Based on the obtained results **(Figure 2.31)**, pair **1** increases permeability in AQP1 and AQP3; pair **3** increases glycerol permeability in AQP3, and compound **4** increases AQP1-mediated water permeability. These results indicate that in regard to cancer treatment, an increase in water and glycerol permeability is not suitable for a novel therapeutic approach. Enhanced wound healing is one example of a condition that can be improved by AQP3 higher permeability[6].

The remaining pairs do not present AQP modulation, and AQP5 was not susceptible to modulation. However, when testing **5** and **6** individually in AQP1 **(Figure 2.31 – B)**, an increase in permeability is depicted, contrary to when both compounds are tested in pairs **(Figure 2.31 – pair 3)**. Further studies will be performed to understand this modulation.

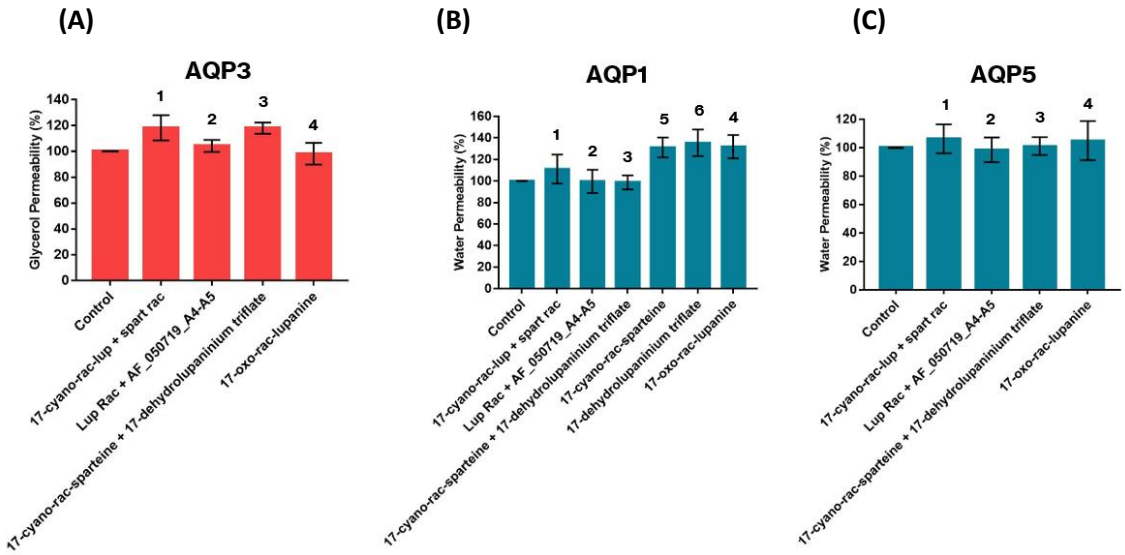

Figure 2.31: Modulation of AQP3 (A), AQP1 (B), and AQP5 (C) in the presence of the following compounds - **(1)** 17-cyano-*rac*-lupanine + spart rac (*rac*-sparteine); **(2)** Lup Rac (*rac*-lupanine) + AF_050719_A4-A5; **(3)** 17-cyano-*rac*-sparteine + 17-dehydrolupaninium triflate; **(4)** 17-oxo-*rac*-lupanine; **(5)** 17-cyano-*rac*-sparteine; **(6)** 17-dehydrolupaninium triflate

2.6 Conclusions and Future Prospects

Insertion of a nitrile moiety through an unreported C-H electrochemical functionalization approach was investigated in batch and flow, using as substrate *rac*-lupanine. In batch, optimization was complete affording 17-cyano-*rac*-lupanine in high yields and high selectivity. In the future, flow electrochemical experiences will be continued with the purpose of scaling-up and reducing batch reaction time.

As an attempt to create a new series of asymmetric catalysts, derivatizations of 17-cyano-*rac*-lupanine and 17-cyano-*rac*-sparteine were investigated, yielding so far a synthetically interesting product: 17-dehydrolupaninium triflate. As future prospects, derivatizations of 17-dehydrolupaninium triflate should be studied and more derivatives synthetized. Afterwards, an asymmetric reaction should be investigated to compare their asymmetry induction with sparteine.

Potential pharmacological activity of several compounds was investigated in three different AQPs (AQP1,3 and 5). Even though no inhibition was detected, an increase in AQP1 and AQP3 permeability was observed, which can be useful to develop a novel therapeutic approach for other diseases apart from cancer.

3. Materials and Methods

3.1 General Remarks

Plant Material: *Cistus ladaniferus* leaves were collected in Portugal in early autumn. They were stored at rt.

Reagents and Solvents: All solvents were distilled from commercial grade sources. The specific used anhydrous solvents were prepared following usual procedures. Reagents were used without any purification with >98% purity (Alfa Aesar, Fluka, Sigma Aldrich), except for Buthyl Lithium which was previously titrated.

Stationary phases: Silica gel 60A (P2050017, Carlo Erba) was used for column chromatography. Analytical TLCs were performed in silica gel 60 F254 plates (HX69787354, Merck).

HRMS: High Resolution Mass spectra were recorded in a Thermo Scientific Q Exactive hybrid quadrupole-Orbitrapmass spectrometer (Thermo ScientificTM Q ExactiveTM Plus).

Infrared Spectrometer: Performed on a spectrophotometer of Bruker, Alpha II. Bands assigned in cm^{-1}.

NMR spectroscopy: ^{1}H NMR and 13C NMR spectra were obtained using a Bruker Fourier 300 spectrometer, that operates at 300 MHz. All spectra were performed in $CDCl_3$. The chemical shifts are indicated in ppm, relative to $CDCl_3$, (δ_H= 7.26 ppm; δ_C=77,16 ppm) and the J coupling constants are indicated in Hz. Geminal protons are referred with “a” and “b” indexes. Splitting patterns are indicated as s, singlet; d, doublet; t, triplet; q, quartet; m, multiplet.

Electrochemistry Equipment: An ElectroSyn 2.0 system by IKA was used for batch reactions, and an ElectraSyn flow system by IKA was used for continuous flow reactions.

Biological assays: All the assays were performed by Dr. Catarina Pimpão in Professor Dr. Graça Soveral laboratory. 3 different AQPs were tested using 2 different techniques: light scattering stopped-flow technique for AQP1 and AQP5, and fluorescent stopped-flow technique for AQP3.

3.2 Extraction of Labdanolic Acid

Leaves of *C. ladaniferus* (*ca* 100g) were soaked in a basic ethanol solution (1 L, 20% Na_2CO_3) for 3 days at rt[49]. The leaves were removed from the solution and the solvent was removed under reduced pressure to give the crude extract as an oil. The extract was dissolved in MTBE (250 mL) and washed with aqueous 10% Na_2CO_3 solution (4 × 200 mL). The mixture was divided in 2 parts and 200 mL of MTBE was added. When phase separation was achieved, washes with aqueous 10% Na_2CO_3 solution were done (4 × 100 mL). The same procedure was made for the other half of the mixture. Then the combined basic layers were acidified (pH=1) with aqueous HCl solution (12 M). Afterwards, the solution was divided in 4 fraction and each one was extracted with MTBE (3 × 150 mL), dried over $MgSO_4$ and evaporation of the solvent to dryness gave a crude acidic fraction (52,17 g).

Basic Organic Phase

IR (ATR) ν (cm^{-1}): 3447(O-H), 2923-2853 (C-H), 1735 (C=O), 1657-1603 (C=C), 1456, 1377, 1237, 1162, 1029, 840, 699, 509.

3.3 Esterification Reaction

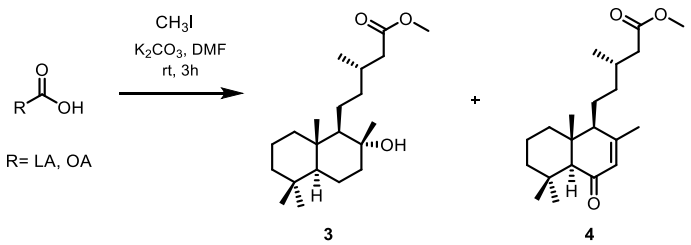

3 4

(Experiment adapted from a reported method for other substrate)[53]**:**To a solution of crude acidic fraction (500 mg, 1 equiv.) in DMF (2 mL) was added K_2CO_3 (0.75 mg, 2.7equiv.) and CH_3I (0.56 ml, 4.5 equiv.). The resulting solution was stirred at rt overnight. The reaction was followed by TLC, using as mobile phase EtOAc/Hex (20:80). After stirring for 18 h, 8 mL of MTBE was added, and the solution was washed with H_2O (2 × 15 mL) and once with brine (15 mL). The combined organic layers were dried over with $MgSO_4$ and the solvent was removed under reduced pressure. The resulting crude material was purified by column chromatography on silica gel either using an isocratic elution (EtOAc/Hex (20:80)) or a gradient elution (EtOAc/Hex (10:90) to EtOAc:Hex(15:85)), to afford LA methyl ester **(3)** in 10wt% (1 g) and OA methyl ester **(4)** in 4.2 wt% (0.42 g). TLC plates were stained with Phosphomolybdic acid (PMA).

3.4 Hydrolysis Reaction

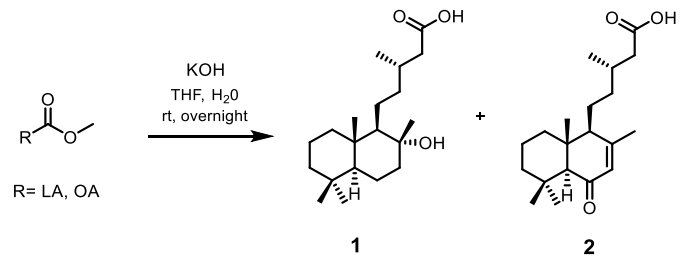

1 2

Procedure A (Experiment adapted from a reported method for other substrate)[55]:

To a round-bottomed flask charged with LA methyl ester **(3)** (20 mg, 1 equiv.), was added 1 mL of THF, 0.5 mL of H_2O and KOH (10 mg, 3 equiv.) at rt. The reaction was followed by TLC using as mobile phase EtOAc/Hex (20:80). Extra KOH (3.4 mg, 1 equiv.) was added to the reaction mixture after 24h. The resulting reaction mixture was stirred for 1h, and then was acidified with an aqueous HCl solution (2M) and extracted with MTBE (3 × 5 mL). The combined organic layers were dried over with $MgSO_4$ and the solvent was removed under reduced pressure, to afford an oil (5.5 mg) in 28% yield.

Procedure B (Optimized experiment adapted from a reported method for other substrate)[55]:
To a round-bottomed flask charged with LA methyl ester **(3)**/ OA methyl ester **(4)** (200 mg, 1 equiv.), was added 10 mL of THF, 5 mL of H_20 and KOH (132 mg, 4 equiv.) at rt. The reaction was followed by TLC using as mobile phase EtOAc/Hex (20:80). After stirring for 24h, the reaction mixture was acidified with an aqueous HCl solution (2M) and extracted with MTBE (3×30 mL). The combined organic layers were dried over with $MgSO_4$ and the solvent was removed under reduced pressure. The resulting crude material was purified by column chromatography on silica gel and the mobile phased depended on which reaction mixture we wanted to purify: (1) OA purification - EtOAc/CH_3COOH/Hex (20:1:79) and then MTBE/CH_3COOH/Hex (20:1:79) to afford OA in 0.04 wt % yield (18.7mg) ; (2) LA purification - EtOAc/CH_3COOH/Hex (30:1:69) or EtOAc/CH_3COOH/Hex (35:1:64) and then Hex/CH_3COOH/MTBE (60:1:39), to afford LA in 1.8 wt% (0.92 g). TLC plates were stained with Phosphomolybdic acid (PMA).

Labdanolic Acid (1)
Spectral data (^1H, ^{13}C NMR) similar to reported[54]

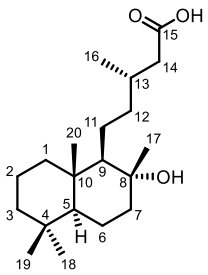

1

^{1}H NMR (300 MHz, Chloroform-d) δ (ppm) 2.29 (dd, J = 14.8, 6.0 Hz, 1H, $H14_a$), 2.11 (dd, J = 14.7, 7.8 Hz, 1H, $H14_b$),2.02 (s, 1H, H13), 1.90-1.78 (m, 2H,$H7_a$,11_a), 1.62 – 1.52 (m, 3H,$H1_a$, 2_a, 11_b), 1.44 – 1.16 (m, 11H, H3, 7_b, 2_b, 1_b, 6, 12), 1.11 (s, 3H, H17), 0.99 (m, 1H, H9), 0.93 (d, J = 6.6 Hz, 3H, H16), 0.89 (m, 1H, H5), 0.82 (s, 3H, H18), 0.74 (s, 6H, H19,20).

^{13}C NMR (75 MHz, Chloroform-d) δ (ppm) 178.2 (C15), 75.1 (C8), 62.0 (C9), 56.0 (C5), 43.8 (C7), 42.0 (C3), 41.6 (C14), 40.6 (C12), 39.7 (C1), 39.2 (C10), 33.4 (C4/18), 33.2 (C4/18), 31.2 (C13), 23.8 (C17), 23.0 (C11), 21.5 (C19), 20.5 (C6), 19.9 (C16), 18.5 (C2), 15.5 (C20).

6-Oxocativic Acid (2)

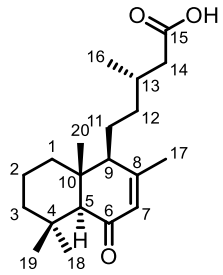

2

^{1}H NMR (300 MHz, Chloroform-d) δ (ppm) 5.76 (m, 1H, H7), 2.38 (dd, J = 15.1, 6.3 Hz, 1H, $H14_a$), 2.21 (dd, J = 15.1, 7.7 Hz, 1H, $H14_b$), 2.04 (m, 1H, H13), 2.02-1.94 (m, 2H, H11,12), 1.90 (t, J = 1.4 Hz, 3H, H17), 1.70 – 1.42 (m, 3H), 1.41 – 1.22 (m, 3H), 1.14 (d, J = 9.2 Hz, 7H, H18/19), 1.03 (d, J = 6.7 Hz, 3H, H16), 0.84 (s, 3H, H20).

^{13}C NMR (75 MHz, Chloroform-d) δ (ppm) 200.5 (C6), 178.5 (C15), 158.8 (C8), 128.7 (C7), 63.8 (C11/12), 56.9 (C11/12), 43.4, 43.3, 41.2 (C14), 39.4, 38.9, 33.6, 32.4 (C18/18), 31.0 (C13), 24.7 (C18/19), 22.1 (C17), 21.6, 19.9 (C16), 18.3, 14.8 (C20).

HRMS: Calculated for $[C_{20}H_{33}O_3]^+$ = 321.24242 m/z, found: 321.24155 m/z

3.5 Dehydration Reaction

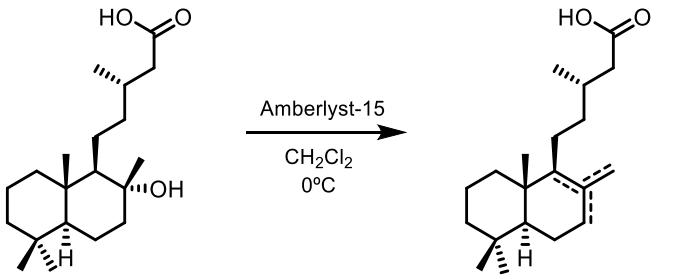

1

Tetrasubstitued olefin **- 5**
Trisubstitued olefin **- 6**
Exocyclic olefin **- 7**

(Optimized experiment adapted from a reported method for other substrate)[37]**:** To a solution of labdanolic acid (100 g, 1 equiv.) in 20 mL of DCM at 0°C, was added Amberlyst®-15(dry) (120 mg, 1.24 equiv.). The reaction was followed by TLC using as mobile phase EtOAc/Hex (25/75). After stirring for 18h at rt, Amberlyst 15-dry was removed by filtration, and the solvent was removed under reduced pressure. The residue was purified by column chromatography on silica gel (EtOAc/Hex (20:80)) to afford the mixture of olefins in 59% (56 mg) yield.

3.6 Allylic Oxidation Reactions

3.6.1 Oxidation Reaction with SeO_2

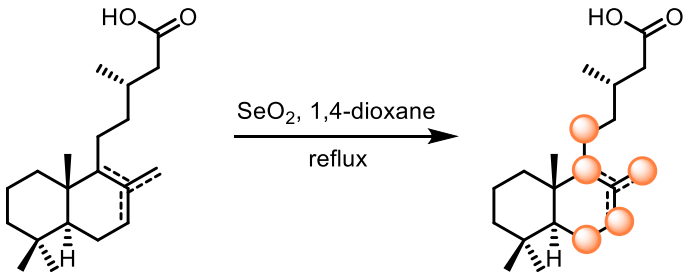

Tetrasubstitued olefin - **5**
Trisubstitued olefin - **6**
Exocyclic olefin - **7**

(Experiment adapted from a reported method for other substrate)[148]**:** To a round-bottomed flask charged with olefin mixture (36 mg, 1 equiv.), was added 0.7 mL of 1,4-dioxane and SeO_2 (40 mg, 3 equiv.). The reaction was stirred under reflux and followed by TLC using as mobile phase EtOAc/Hex (40:60). After stirring for 4h, the reaction mixture was acidified with aqueous HCl solution (2M) and extracted with MTBE (3×6 mL). The combined organic layers were dried over with $MgSO_4$ and the solvent was removed under reduced pressure. The crude product was used without further purification (94 mg).

3.6.2 Oxidation Reaction with MnO_2

(Experiment adapted from a reported method for other substrate)[149]: To a stirred solution of crude product from oxidation with SeO_2 (22.5 mg, 1equiv.), in 2 mL of DCM was added MnO_2 (0.17 g, 30 equiv.) at rt. The reaction was followed by TLC using as mobile phase EtOAc/Hex (40/60). After stirring for 2h, extra MnO_2 was added (0.11 g, 20 equiv.) due to lack of product formation. After more 3h stirring, 0.17 g of MnO_2 (30 equiv.) were added. The reaction was left overnight. After 22h stirring, the reaction was not complete, and reflux was initiated. After 3h, reaction was stopped and filtration with celite was performed, using as mobile phase DCM. Solvent was removed under reduced pressure and the crude product was not further purified (1,7 mg, 8 wt%).

3.6.3 Oxidation Reaction with TPAP and NMO

(Experiment adapted from a reported method for other substrate)[150]**:** To a round-bottomed flask charged with crude product from oxidation with SeO_2 (94 mg, 1 equiv.), was added 3 mL of DCM, 145 mg of powdered molecular sieves, NMO (51 mg, 1.5 equiv.) and TPAP (5.1 mg, 0.05 equiv.), at rt under Ar atmosphere. The reaction was followed by TLC using as mobile phase EtOAc/Hex (40:60). After 40 min stirring, extra TPAP (5.1 mg, 1equiv.) and NMO (51 mg, 1.5 equiv.) were added to the reaction mixture. After 10 min, the reaction was not complete, and reflux was initiated. After 30 min stirring, acidified water was added to the reaction mixture. The reaction mixture is then extracted with MTBE (3×5 mL), the combined organic layers were dried over with $MgSO_4$ and the solvent was removed under reduced pressure. The residue was purified by

column chromatography on silica gel (EtOAc/Hex (15:85)) affording an unidentifiable mixture (3.9 mg)

3.7 Cyclic Voltammetry of *rac*-lupanine (8)

To an undivided electrochemical cell (5 mL vial, ElectraSyn 2.0, IKA®), equipped with a working electrode (RVC), counter electrode (Pt) and a reference electrode (Ag/AgCl), was added 2 mL of MeCN, $TBABF_4$ (0.1 M) and *rac*-lupanine **(8)** (18 mM, 32 mM and 45 mM) at rt. Following IUPAC Convention, 3 cycles were performed in a potential window ranging from -2.5 V to 2.5 V, and CV analysis of *rac*-lupanine were performed in 3 different concentration.

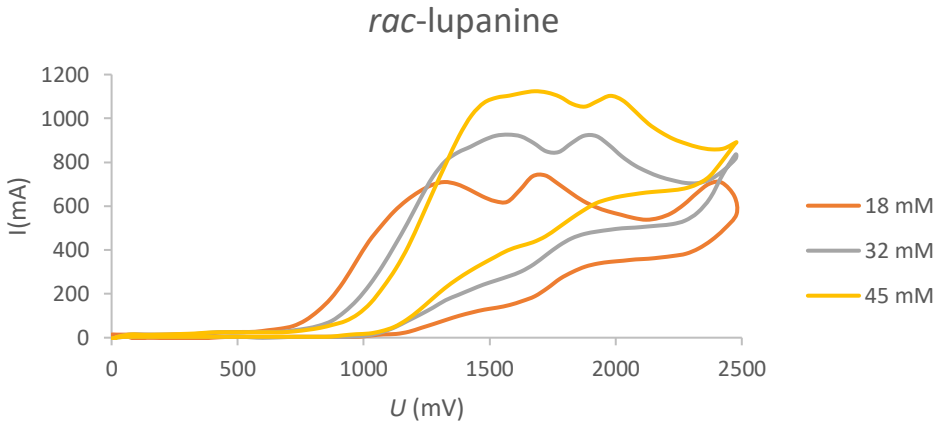

$E_{1/2}$ (tertiary amine) = + 1.1 V (Ag/AgCl)

$E_{1/2}$ (amide) = + 1.7 V (Ag/AgCl)

3.8 Cyclic Voltammetry of 17-cyano-*rac*-lupanine (10)

To an undivided electrochemical cell (5 mL vial, ElectraSyn 2.0, IKA®), equipped with a working electrode (RVC), counter electrode (Pt) and a reference electrode (Ag/AgCl), was added 2 mL of MeCN, $TBABF_4$ (0.1 M) and 17-cyano-*rac*-lupanine **(10)** (3 mM, 7mM, 9.5 mM, 13 mM and 16 mM) at rt. Following IUPAC Convention, 3 cycles were performed in a potential window ranging from -3 V to 3 V, and CV analysis of 17-cyano-*rac*-lupanine were performed in 5 different concentrations.

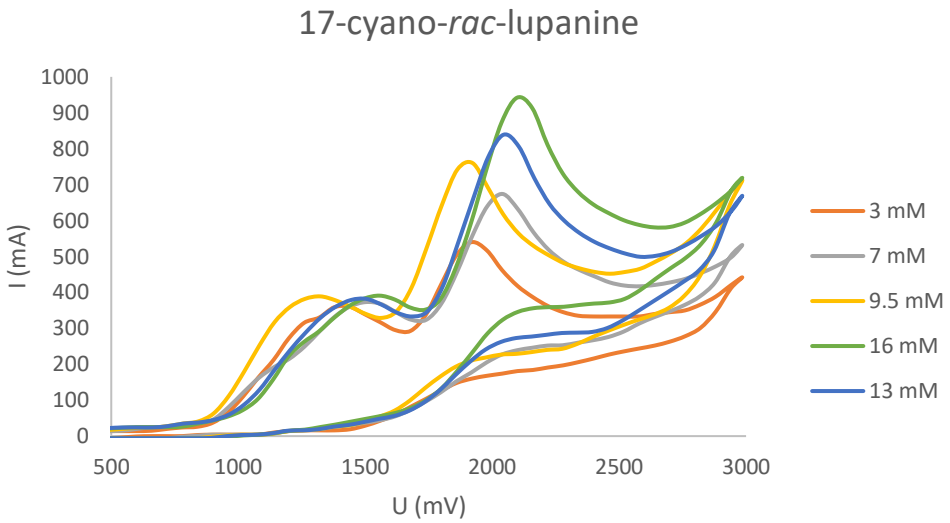

$E_{1/2}$ (tertiary amine) = + 1.1 V (Ag/AgCl)

$E_{1/2}$ (amide) = + 1.9 V (Ag/AgCl)

3.9 Batch electrochemical cyanation of *rac*-sparteine (9)

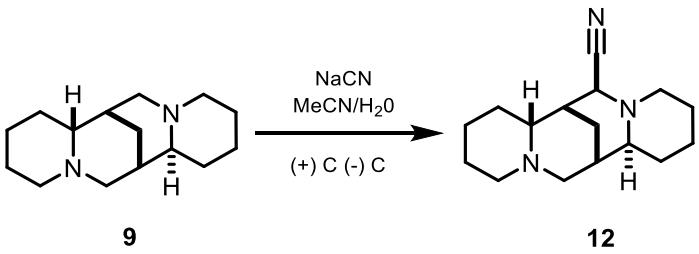

9 **12**

(previously developed protocol): In an undivided electrochemical cell (10 mL vial, ElectraSyn 2.0, IKA®), with both electrodes of graphite (0.7 x 4.0 cm^2) equipped with a magnetic stir bar, a solution of *rac*-sparteine **(9)** (300 mg, 1 equiv.), NaCN (190 mg, 3.25 equiv.) in MeCN/H_20 (7:3) was added at rt (18°C) under constant current (5mA) and 2.1 F/mol. After 16h stirring, the solvent was removed under reduced pressure. The resulting crude material was extracted with MTBE (3×30 mL) and the organic layers were combined, dried over with $MgSO_4$ and evaporated under reduced pressure. The residue was purified by column chromatography on silica gel (Hex/MTBE (10:1)) to afford 17-cyano-*rac*-sparteine **(12)** in 70% yield (233 mg).

3.10 Cyanation of *rac*-lupanine (8)

3.10.1 Flow experiments

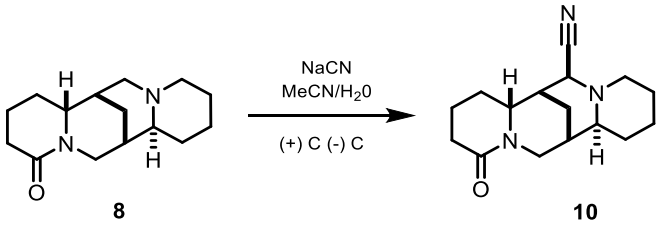

Note: Prior to any flow reaction, the whole system was filled with a mixture of MeCN/H_2O (7:3), and no leakages should occur. Reaction selectivity was calculated based on 2 signals on ^{1}H NMR spectra: signal from the desired product at 2.95 ppm (H17) and a signal from compound **8** at 2.78 ppm ($H15_a$ and $H17_a$).

Flow setup: Graphite electrodes were separated by a nafion-membrane (0.5 /1 mm thickness) and connected by 8 screws. Once assembled, the cell was connected by fluororubber tubing on each end. One of the two end was connected to a peristaltic pump that transferred the reaction mixture contained in a reservoir to the cell; the other end functioned as outlet, transferring the solution from the cell to a collecting reservoir. Two fluororubber tubes (75 cm of length and 2 mm of diameter) composed the system, corresponding to 9 mL of solution/solvent to fill the whole system.

Procedure: In an undivided electrochemical cell (ElectraSyn flow, IKA®), with both electrodes of graphite separated by a membrane of 0.5 mm, a solution of *rac*-lupanine **(8)** (100 mg, 1 equiv.), NaCN (59 mg, 3 equiv.) in MeCN/$H_2$0 (6:4) was introduced in the system using a peristaltic pump at rt (18°C) under constant potential/current. After reaction completion, solvent was removed under reduced pressure, and the resulting crude was washed (4×10mL) with DCM:isopropanol (30:10). The residue was purified by column chromatography on silica gel (NEt_3/EtOAc (5:95)) to afford 17-cyano-*rac*-lupanine **(10)** from 6-21% yield by qNMR to 30% isolated yields on average.

3.10.2 Batch experiments

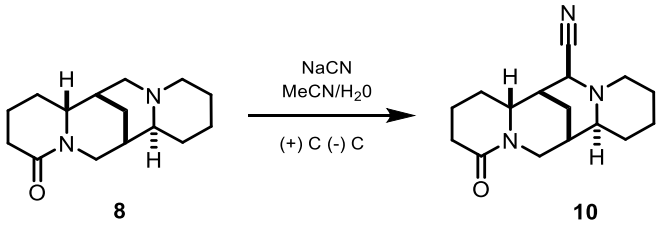

Procedure A (previously developed protocol): In an undivided electrochemical cell (10 mL vial, ElectraSyn 2.0, IKA®), with both electrodes of graphite (0.7 x 4.0 cm^2) equipped with a magnetic stir bar, a solution of *rac*-lupanine **(8)** (100 mg, 1 equiv.), NaCN (59 mg, 3 equiv.) in MeCN/$H_2$0 (7:3) was added at rt (18°C) under constant current (5mA) and 1.3 F/mol. After 6h stirring, the solvent was removed under reduced pressure. The resulting crude material was extracted with MTBE (3×30 mL). The crystals obtained were dissolved in hexane at 80 °C and submitted to a solid-liquid separation, to afford 17-cyano-*rac*-lupanine **(10)** in 80% yield (87 mg).

Procedure B: In an undivided electrochemical cell (10 mL vial, ElectraSyn 2.0, IKA®), with both electrodes of graphite (0.7 x 4.0 cm^2) equipped with a magnetic stir bar, a solution of *rac*-lupanine **(8)** (100 mg, 1 equiv.), NaCN (59 mg, 3 equiv.) in MeCN/$H_2$0 (6:4) was added at rt (18°C) under "Run Continuous" mode constant potential (2.1 V) and 660 rpm. After 11h stirring, solvent was removed under reduced pressure, and the resulting crude was washed (4×10 mL) with DCM:isopropanol (30:10). The residue was purified by column chromatography on silica gel (NEt_3/EtOAc (5:95)) to afford 17-cyano-*rac*-lupanine **(10)** in a range of 69-98% yield by qNMR, to 30% isolated yield on average.

17-cyano-rac-lupanine (10)

Spectral data (^{1}H, ^{13}C NMR) similar to reported[134]

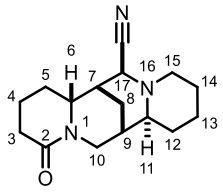

^{1}H NMR (300 MHz, $CDCl_3$) δ (ppm) 4.43 (dt, *J* = 13.3, 2.5 Hz, 1H, $H10_a$), 3.35 (m, 1H, H6), 3.27 (m, 1H, $H15_a$), 2.91 (d, *J* = 3.6 Hz, 1H, H17), 2.49 (d, *J* = 2.5 Hz, 1H, $H10_b$), 2.46 – 2.22 (m, 4H, $H3,8_a,7$), 1.90 (m, 3H, $H5_a$, 15_b, 4_a), 1.76 – 1.18 (m, 10H, $H11,4_b$, $12,8_b$, $14,5_b,9$).

^{13}C NMR (75 MHz, $CDCl_3$) δ (ppm) 171.4 (C2), 121.0(-CN), 63.0 (C11), 59.8 (C6), 54.0 (C15), 53.0 (C17), 46.4 (C10), 39.2 (C7), 34.2 (C9), 33.6 (C12), 32.9 (C3), 27.2 (C5), 25.3 (C8), 25.0 (C13), 24.4 (C14), 19.5 (C4).

IR (ATR) ν̃ (cm^{-1}): 3429 (N-H), 2929-2854 (C-H), 1631 (C=O), 1440, 1418, 1327, 1312, 1256, 1167, 1114, 1097, 1073, 1019, 975, 917, 843, 656, 495, 467, 440.

17-oxo-rac-lupanine (11)

Spectral data (^{1}H, ^{13}C NMR) similar to reported[135]

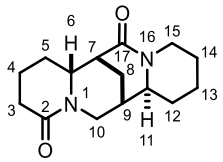

^{1}H NMR (300 MHz, $CDCl_3$) δ (ppm) 4.82 (dt, J = 13.4, 2.5 Hz, 1H, $H10_a$), 4.70 (m, 1H, $H15_a$), 3.43 (m, 1H, H6), 3.26 (dd, J = 11.7, 2.5 Hz, 1H, H11), 2.69 (dd, J = 13.4, 2.6 Hz, 1H, $H10_b$), 2.49 (m, 1H, H7), 2.40 (d, J = 2.7 Hz, 1H, $H15_b$), 2.34 (m, 1H, $H3_a$), 2.25-1.24 (m, 16H, $H3_b$,4,5,8,9,12,13,14,15).

^{13}C NMR (75 MHz, $CDCl_3$) δ (ppm) 171.0 (C2), 167.4 (C17), 61.2 (C11), 59.0 (C6), 48.1 (C10), 43.7 (C7), 43.1 (C15), 33.9 (C9), 33.5 (C12), 32.9 (C3), 27.1 (C14), 25.4 (C8/C5/C13), 25.1 (C8/C5/C13), 22.8 (C8/C5/C13), 19.5 (C4).

3.11 Nitrile reduction

3.11.1 DIBAL Reduction

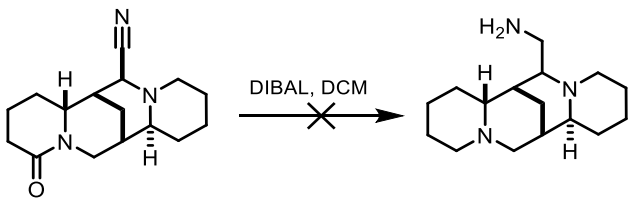

10

(Experiment adapted from a reported method for other substrate)[120]**:** To a round-bottomed flask charged with 17-cyano-rac-lupanine **(10)** (20 mg, 1 equiv.), 1 mL of dry DCM was added at rt under Ar atmosphere. Subsequently the reaction was cooled to 0ºC, and after stirring for 15 min, DIBAL (0.35 mL, 6 equiv.) was added, then allowing the reaction to slowly warm up to rt. After 2h30min the reaction was quenched with MeOH (150 µL, 6 equiv.) followed by addition of sodium potassium tartrate (Rochelle´s salt) until 2 phases were visible. Then the reaction was basified with saturated aqueous solution Na_2CO_3 solution and extracted with DCM (3 × 10 mL). The combined organic layers were dried over anhydrous $MgSO_4$ and the solvent was removed under reduced pressure. The residue was purified by column chromatography on silica gel (NEt_3/EtOH/EtOAc (5:5:90)) to afford *rac*-sparteine **(9)** in 36 % yield (5.9 mg).

3.11.2 $LiAlH_4$ Reduction

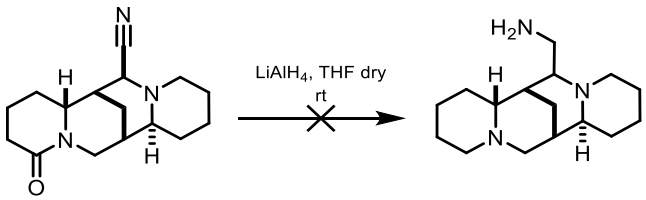

10

To a flame dried flask was added 20 mg of 17-cyano-*rac*-lupanine **(10)** (1 equiv.) and 1.1 mL of dried THF, and 15 mg (5.7 equiv.) of $LiAlH_4$. The reaction was stirred at rt under Argon atmosphere. After 20h stirring, water (5 mL) was added to quench the reaction, followed by 2 ml of saturated Na_2CO_3 aqueous solution. The reaction mixture is then extracted with AcOEt (3 × 7 ml), the combined organic layers were dried over with $MgSO_4$ and the solvent was removed under reduced pressure, affording 11.5 mg. Product identification is ongoing.

3.11.3 Catalytic Hydrogenation

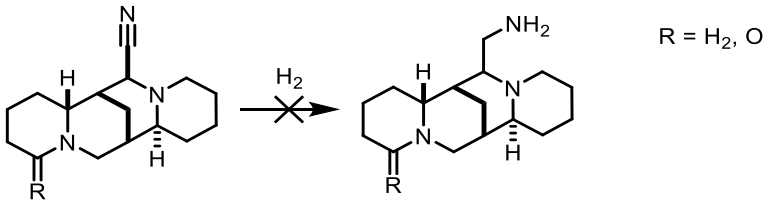

Procedure A (experiment adapted from a reported method for other substrate)[151]**:** In an appropriated vial with 17-cyano-*rac*-sparteine **(12)** (106 mg, 1 equiv.) and 4.2 mL of AcOH, was added 16 mg of Pd/C (0.15 equiv.) as catalyst. The reaction was placed in a high-pressure reactor for hydrogenation. After several purges with N_2, H_2 was introduced in the reaction mixture. The reaction was at 7 bar and stirred for 5h at 40°C and at rt overnight. The reaction was followed by TLC using as mobile phase NEt_3/AcOEt (5:95). After 48 h, filtration through celite was performed using as mobile phase DCM. Solvent was removed under reduced pressure followed by basification of the reaction crude at 0°C with NaOH 5% aqueous solution (pH=12), and extractions with MTBE (3×5 mL). The organic layers were combined, dried over with $MgSO_4$ and evaporated under reduced pressure. The residue was purified by column chromatography on silica gel (NEt_3/AcOEt (4:96)) to afford *rac*-sparteine **(9)** in 54% yield (50.7 mg).

Procedure B (experiment adapted from a reported method for other substrate)[140]**:** In an appropriated vial with *rac*-17-cyanolupanine **(10)** (20 mg, 1 equiv.) and 2.5 mL of EtOH, was added 2 mg of Co/SiO_2 (0.2 equiv.) as catalyst. The reaction was placed in a high-pressure reactor for hydrogenation. After several purges with N_2, H_2 was introduced in the reaction mixture. The

reaction was at 7 bar and stirred for 20h at 70°C. The reaction was followed by TLC using as mobile phase NEt_3/AcOEt (5:95). After reaction completion, filtration through celite was performed using as mobile phase DCM. Solvent was removed under reduced pressure, affording 17-cyano-*rac*-lupanine **(10)** in 87% yield (16.6 mg).

***rac*-lupanine (8)**

Spectral data (^{1}H, ^{13}C NMR) similar to reported[93,147]

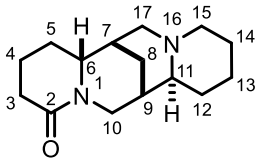

^{1}H NMR (300 MHz, $CDCl_3$) δ (ppm) 4.49 (dt, J = 13.2, 2.3 Hz, 1H, $H10_a$), 3.28 (m, 1H, H6), 2.81 (m, 2H, $H17_a$, 15_a), 2.46 (m, 2H, $H10_b$,3_a), 2.31 (m, 1H,3_b), 2.18 (m, 1H, $H8_a$), 2.07 (m, 1H, H7), 1.92 (m, 2H, $H17_b$, 15_b), 1.87 – 1.14 (m, 16H,H4,5,8b,9,11,12,13,14).

^{13}C NMR (75 MHz, $CDCl_3$) δ (ppm) 171.4 (C2), 64.1 (C11), 60.8 (C6), 55.4 (C15), 52.6 (C17), 46.6 (C10), 34.6 (C9), 33.3 (C12), 32.9 (C3), 32.0 (C7), 27.3 (C5), 26.5 (C8), 24.9 (C13), 24.2 (C14), 19.4 (C4).

IR (ATR) ν̃ (cm^{-1}): 2914-2855 (C-H), 1631 (C=O), 1585, 1439, 1394, 1333, 1309, 1277, 1248, 1185, 1163, 1134, 1115, 1097, 1071, 1026, 1012, 967, 844, 784, 696, 669, 489, 462, 441.

3.11.4 Nitrile hydrolysis

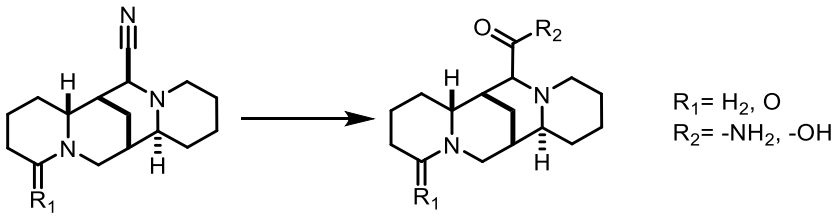

Procedure A: To a round-bottomed flask charged with 17-cyano-*rac*-sparteine (30 mg, 1 equiv.) was added 0.75 mL of H_2SO_4 (97% w/w). After stirring for 18h at rt, the reaction mixture was basified with NH_4OH at 0°C, until a pH of 12 was reached. Then, the reaction mixture was extracted with DCM (3 × 5 mL). The organic layers were combined, dried over with $MgSO_4$ and evaporated under reduced pressure. The residue was purified by column chromatography on silica gel (NEt_3/Hex/AcOEt (1:25:74)), affording 3.6 mg. Product characterization is ongoing.

Procedure B: To a round-bottomed flask charged with 17-cyano-*rac*-lupanine (21 mg, 1 equiv.) was added 0.8 mL of HCl conc. After stirring for 4h at rt, the reaction mixture was evaporated under reduced pressure, affording a complex mixture (20 mg).

3.12 Oxazole synthesis

3.12.1 Imidate synthesis

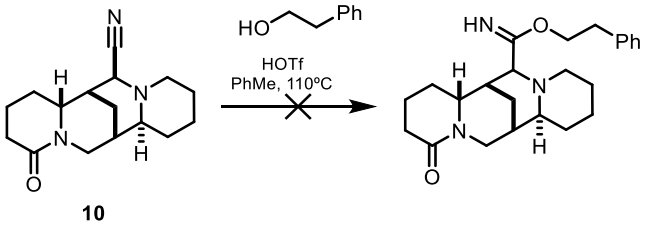

10

Procedure A (experiment adapted from a reported method for other substrate)[126]**:** To a round-bottomed flask charged with 17-cyano-*rac*-lupanine **(10)** (68.5 mg, 1 equiv.) in toluene (0.5 mL), was added TfOH (48 µL, 2.18 equiv.). The solution was heated to 110 °C and stirred for 3 h. Then, 260 mg of Na_2CO_3 (10 equiv.) and 2ml of toluene were added to the reaction mixture and after stirring for 20 min, the toluene was removed by filtration. This step was repeated with DCM (3 × 2 mL). The combined organic layers were evaporated under reduced pressure, affording 17-dehydrolupaninium triflate **(13)** in 34% yield (33.2 mg).

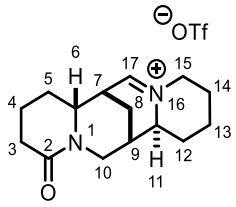

^{1}H NMR (300 MHz, $CDCl_3$) δ 9.02 (d, J = 4.8 Hz, 1H, H17), 4.84 (d, J = 14.2 Hz, 1H, $H10_a$), 4.39 (d, J = 12.3 Hz, 1H, $H8_a$), 3.73 (m, 3H, $H9,8_b,6$), 3.41 (s, 1H, H7), 2.74 (d, J = 13.6 Hz, 1H, $H10_b$), 2.43 – 1.52 (m, 15H, H3,4,5,11,12,13,14,15).

^{13}C NMR (75 MHz, $CDCl_3$) δ 179.2 (C17), 171.3 (C2), 122.73 (q, 323 Hz, $-CF_3$), 67.5 (C6), 62.1 (C8), 60.2 (C9), 47.2 (C10), 38.4 (C7), 33.0-19.8 (8C, C3,4,5,11,12,13,14).

3.13 Tetrazole synthesis

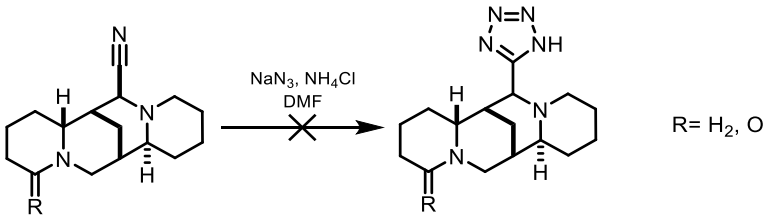

Procedure A (experiment adapted from a reported method for other substrate): To a solution of 17-cyano-*rac*-sparteine **(12)** (22 mg, 1equiv.) in DMF (1 mL), was added NaN_3 (60 mg, 10 equiv.) and NH_4Cl (50 mg, 10 equiv.). After 6h stirring at 90 °C, the solvent was removed under reduced pressure. Then, saturated aqueous Na_2CO_3 solution was added to the reaction crude and extracted with DCM (4 × 5 mL). The combined organic phases were dried over with $MgSO_4$ and the solvent was removed under reduced pressure, affording a complex mixture (11.7 mg)

Procedure B (experiment adapted from a reported method for other substrate): To a solution of 17-cyano-*rac*-lupanine **(10)** (20 mg, 1 equiv.) in DMF (1.1 mL), was added NaN_3 (46 mg, 10 equiv.) and NH_4Cl (37 mg, 10 equiv.). After 24h stirring at rt, the reaction mixture was basified

with saturated aqueous Na_2CO_3 solution and extracted with Et_2O (1 × 7 mL). The organic layer was then washed with H_20 (3 × 7 mL), dried over anhydrous MgSO4, and the solvent was removed under reduced pressure, yielding 17-cyano-*rac*-lupanine **(10)** in 8.9% yield (1.7 mg).

4. References

1. Stewart, B. & Wild International Agency for Research on Cancer, WHO, C. P. (eds. . World Cancer Report 2014. *Nat. Rev. Cancer* **17**, 20–37 (2014).
2. De Ieso, M. L. & Yool, A. J. Mechanisms of aquaporin-facilitated cancer invasion and metastasis. *Front. Chem.* **6**, 1–20 (2018).
3. L. Patrick, G. *An Introduction to Medicinal Chemistry*. **53**, (2013).
4. Hughes, J. P., Rees, S. S., Kalindjian, S. B. & Philpott, K. L. Principles of early drug discovery. *Br. J. Pharmacol.* **162**, 1239–1249 (2011).
5. da Silva, I. V., Rodrigues, J. S., Rebelo, I., Miranda, J. P. G. & Soveral, G. Revisiting the metabolic syndrome: the emerging role of aquaglyceroporins. *Cell. Mol. Life Sci.* **75**, 1973–1988 (2018).
6. Verkman, A. S., Anderson, M. O. & Papadopoulos, M. C. Aquaporins: Important but elusive drug targets. *Nat. Rev. Drug Discov.* **13**, 259–277 (2014).
7. Ribatti, D., Ranieri, G., Annese, T. & Nico, B. Aquaporins in cancer. *Biochim. Biophys. Acta - Gen. Subj.* **1840**, 1550–1553 (2014).
8. Abir-Awan, M. *et al.* Inhibitors of mammalian aquaporin water channels. *Int. J. Mol. Sci.* **20**, (2019).
9. Phillips, M. *et al.* Binding of a small molecule water channel inhibitor to aquaporin Z examined by solid-state MAS NMR. *J. Biomol. NMR* **71**, 91–100 (2018).
10. Zelenina, M. Regulation of brain aquaporins. *Neurochem. Int.* **57**, 468–488 (2010).
11. Burghardt, B. *et al.* Distribution of aquaporin water channels AQP1 and AQP5 in the ductal system of the human pancreas. *Gut* **52**, 1008–1016 (2003).
12. Saadoun, S., Papadopoulos, M. C., Hara-Chikuma, M. & Verkman, A. S. Impairment of angiogenesis and cell migration by targeted aquaporin-1 gene disruption. *Nature* **434**, 786–792 (2005).
13. Papadopoulos, M. C., Saadoun, S. & Verkman, A. S. Aquaporins and cell migration. *Pflugers Arch. Eur. J. Physiol.* **456**, 693–700 (2008).
14. Jung, H. J., Park, J. Y., Jeon, H. S. & Kwon, T. H. Aquaporin-5: A marker protein for proliferation and migration of human breast cancer cells. *PLoS One* **6**, (2011).
15. Niu, D. *et al.* Expression of Aquaporin3 in human neoplastic tissues. *Histopathology* **61**, 543–551 (2012).
16. Verkman, A. S., Hara-Chikuma, M. & Papadopoulos, M. C. Aquaporins - New players in cancer biology. *J. Mol. Med.* **86**, 523–529 (2008).
17. Direito, I., Paulino, J., Vigia, E., Brito, M. A. & Soveral, G. Differential expression of aquaporin-3 and aquaporin-5 in pancreatic ductal adenocarcinoma. *J. Surg. Oncol.* **115**, 980–996 (2017).
18. Doi, Y. Glycerol metabolism and its regulation in lactic acid bacteria. *Appl. Microbiol. Biotechnol.* **103**, 5079–5093 (2019).
19. Zhang, Z. *et al.* Expression of aquaporin 5 increases proliferation and metastasis potential of lung cancer. *J. Pathol.* **221**, 210–220 (2010).
20. Soveral, G. & Casini, A. Aquaporin modulators: a patent review (2010–2015). *Expert Opin. Ther. Pat.* **27**, 49–62 (2017).
21. Preston, G. M., Jin Sup Jung, Guggino, W. B. & Agre, P. The mercury-sensitive residue

at cysteine 189 in the CHIP28 water channel. *J. Biol. Chem.* **268**, 17–20 (1993).

22. Martins, A. P. *et al.* Targeting aquaporin function: Potent inhibition of aquaglyceroporin-3 by a gold-based compound. *PLoS One* **7**, (2012).

23. Tesse, A. *et al.* Aquaporins as targets of dietary bioactive phytocompounds. *Front. Mol. Biosci.* **5**, 1–13 (2018).

24. Stivala, L. A. *et al.* Specific Structural Determinants Are Responsible for the Antioxidant Activity and the Cell Cycle Effects of Resveratrol. *J. Biol. Chem.* **276**, 22586–22594 (2001).

25. Yeo, T. P. Demographics, epidemiology, and inheritance of pancreatic ductal adenocarcinoma. *Semin. Oncol.* **42**, 8–18 (2015).

26. Bazdi, B., Dahdouh, A., Lamarti, A. & Mansour, A. I. Composition of the essential oils of cistus ladaniferus and C. Monspeliensis from Morocco. *J. Essent. Oil Res.* **17**, 553–555 (2005).

27. Dewick, P. M. *Medicinal Natural Products: A Biosynthetic Approach: Third Edition*. *Medicinal Natural Products: A Biosynthetic Approach: Third Edition* **5**, (2009).

28. Singh, M., Pal, M. & Sharma, R. P. Biological activity of the labdane diterpenes. *Planta Med.* **65**, 2–8 (1999).

29. Ikeshiro, Y. *et al.* Iridoid glucosides from the fruits of Lonicera morrowii [2]. *Planta Med.* **58**, 109 (1992).

30. Girón, N. *et al.* Evaluation of labdane derivatives as potential anti-inflammatory agents. *Eur. J. Med. Chem.* **45**, 3155–3161 (2010).

31. Frija, L. M. T. *et al.* Short synthesis of the natural product 3β-hydroxy-labd-8(17)-en-15-oic acid via microbial transformation of labdanolic acid. *Phytochem. Lett.* **6**, 165–169 (2013).

32. Yang, S. *et al.* One-pot synthesis of (-)-Ambrox. *Sci. Rep.* **6**, 1–6 (2016).

33. M. Moyle, T. G. H. The Chemistry of Gum Labdanum: The Structure of a New Diterpene Acid, Part IV. *J. Chem. Soc.* 1324–1332 (1960).

34. Martin, J. C. & Arhart, R. J. Sulfuranes. III. A Reagent for the Dehydration of Alcohols. *J. Am. Chem. Soc.* **93**, 4327–4329 (1971).

35. Khapli, S., Mal, D., Dey, S. Burgess reagent in organic synthesis †. *Indian Inst. Sci.* **2**, 461–476 (2001).

36. Boz, N., Degirmenbasi, N. & Kalyon, D. M. Esterification and transesterification of waste cooking oil over Amberlyst 15 and modified Amberlyst 15 catalysts. *Appl. Catal. B Environ.* **165**, 723–730 (2015).

37. Frija, L. M. T. & Afonso, C. A. M. Amberlyst ®-15: A reusable heterogeneous catalyst for the dehydration of tertiary alcohols. *Tetrahedron* **68**, 7414–7421 (2012).

38. Anslyn, E. V & Dougherty, D. A. *Modern Physical Organic Chemistry*.

39. Catino, A. J., Forslund, R. E. & Doyle, M. P. Dirhodium(II) caprolactamate: An exceptional catalyst for allylic oxidation. *J. Am. Chem. Soc.* **126**, 13622–13623 (2004).

40. Nakamura, A. & Nakada, M. *Allylic oxidations in natural product synthesis*. *Synthesis (Germany)* **45**, (2013).

41. Sharpless, K. B. & Lauer, R. F. Selenium Dioxide Oxidation of Olefins. Evidence for the Intermediacy of Allylseleninic Acids. *J. Am. Chem. Soc.* **94**, 7154–7155 (1972).

42. Rabjohn, N. *Organic Reactions*. (1976).

43. Yamamoto, H. *et al. Oxidation of Alcohols to Aldehydes and Ketones*. (2004).

44. Miao, L., Wang, J. & Zhang, P. Review on manganese dioxide for catalytic oxidation of airborne formaldehyde. *Appl. Surf. Sci.* **466**, 441–453 (2019).

45. R.M. Evans. Oxidations by Manganese Dioxide in Neutral Media. *Quaterly Rev. Chem. Soc.* 61–70 (1948).

46. Bailey, A. J., Griffith, W. P., Mostafa, S. I. & Sherwood, P. A. Studies on Transition-Metal Oxo and Nitrido Complexes. 13. Perruthenate and Ruthenate Anions as Catalytic Organic Oxidants. *Inorg. Chem.* **32**, 268–271 (1993).

47. Langer, P. Tetra-n-propyl Ammonium Perruthenate (TPAP) - An Efficient and Selective Reagent for Oxidation Reactions in Solution and on the Solid Phase. *ChemInform* **31**, no-no (2010).

48. V.Ley,Steven; Norman, Joanne; P.Griffith, William; P.Marsden, S. Tetrapropylammonium Perruthenate, TPAP: A Catalytic Oxidant for Organic Synthesis. *Synthesis (Stuttg).*

49. Martins, A. N. C. *et al.* Isolation, analytical quantification and seasonal variation of labdanolic acid from the Portuguese-grown Cistus ladaniferus. *Ind. Crops Prod.* **60**, 226–232 (2014).

50. Perez, J. M. *et al.* Funneling aromatic products of chemically depolymerized lignin into 2-pyrone-4-6-dicarboxylic acid with: Novosphingobium aromaticivorans. *Green Chem.* **21**, 1340–1350 (2019).

51. Ishihara, K., Nakagawa, S. & Sakakura, A. Bulky diarylammonium arenesulfonates as selective esterification catalysts. *J. Am. Chem. Soc.* **127**, 4168–4169 (2005).

52. Neises, B. & Steglich, W. Simple Method for the Esterification of Carboxylic Acids. *Angew. Chemie Int. Ed. English* **17**, 522–524 (1978).

53. Jogalekar, A., Won, W., Koltun, E.S., Gill, A., Mellen, K., Aay, N., Buckl, A., Semko, C., Kiss, G. 2,5-Disubstituted 3-methyl pyrazines and 2,5,6-trisubstituted 3-methyl pyrazines as allosteric SHP2 inhibitors. (2018).

54. García-Sánchez, E. *et al.* Absolute configuration of (13 R)- and (13 S)-labdane diterpenes coexisting in ageratina jocotepecana. *J. Nat. Prod.* **77**, 1005–1012 (2014).

55. Bartra, M. & Vilarrasa, J. Cyclization of 9-Substituted Decanoic Acid Derivatives to 9-Decanolide and 9-Decanelactam. *J. Org. Chem.* **56**, 5132–5138 (1991).

56. Henrick, C.A.; Jeffries, P. . The Chemistry of the Euphorbiaceae-XI. **21**, (1964).

57. Lawrence, B. M. The use of silver nitrate impregnated silica gel layers in the separation of monoterpene hydrocarbons. *J. Chromatogr. A* **38**, 535–537 (1968).

58. Hirano, M., Yakabe, S., Chikamori, H., Clark, J. H. & Morimoto, T. Oxidation by Chemical Manganese Dioxide. Part 3.1 Oxidation of Benzylic and Allylic Alcohols, Hydroxyarenes and Aminoarenes. *J. Chem. Res. - Part S* 770–771 (1998).

59. Lam, V. W. Y. *et al.* Climate change, tropical fisheries and prospects for sustainable development. *Nat. Rev. Earth Environ.* **1**, 440–454 (2020).

60. Sheldon, R. A. Fundamentals of green chemistry: Efficiency in reaction design. *Chem. Soc. Rev.* **41**, 1437–1451 (2012).

61. Yan, M., Kawamata, Y. & Baran, P. S. Synthetic Organic Electrochemical Methods since 2000: On the Verge of a Renaissance. *Chem. Rev.* **117**, 13230–13319 (2017).

62. Yan, M., Kawamata, Y. & Baran, P. S. Synthetic Organic Electrochemistry: Calling All Engineers. *Angew. Chemie - Int. Ed.* **57**, 4149–4155 (2018).

63. Dimerization, T. K. Encyclopedia of Applied Electrochemistry. *Encycl. Appl. Electrochem.* (2014).

64. Danly, D. E. Development and Commercialization of the Monsanto Electrochemical

Adiponitrile Process. *J. Electrochem. Soc.* **131**, 435C-442C (1984).

65. Shono, T., Hamaguchi, H. & Matsumura, Y. Electroorganic Chemistry. XX. Anodic Oxidation of Carbamates. *J. Am. Chem. Soc.* **97**, 4264–4268 (1975).

66. Folgueiras-Amador, A. A., Philipps, K., Guilbaud, S., Poelakker, J. & Wirth, T. An Easy-to-Machine Electrochemical Flow Microreactor: Efficient Synthesis of Isoindolinone and Flow Functionalization. *Angew. Chemie - Int. Ed.* **56**, 15446–15450 (2017).

67. Roth, H. G., Romero, N. A. & Nicewicz, D. A. Experimental and Calculated Electrochemical Potentials of Common Organic Molecules for Applications to Single-Electron Redox Chemistry. *Synlett* **27**, 714–723 (2016).

68. Frontana-Uribe, B. A., Little, R. D., Ibanez, J. G., Palma, A. & Vasquez-Medrano, R. Organic electrosynthesis: A promising green methodology in organic chemistry. *Green Chem.* **12**, 2099–2119 (2010).

69. Wills, A. G., Poole, D. L., Alder, C. M. & Reid, M. A Mechanistic and Cautionary Case Study on the Use of Alternating Potential in Electrochemical Reactions. *ChemElectroChem* **7**, 2771–2776 (2020).

70. Couper, A. M., Pletcher, D. & Walsh, F. C. Electrode Materials for Electrosynthesis. *Chem. Rev.* **90**, 837–865 (1990).

71. Kingston, C. *et al.* A Survival Guide for the 'electro-curious'. *Acc. Chem. Res.* **53**, 72–83 (2020).

72. Gütz, C., Klöckner, B. & Waldvogel, S. R. Electrochemical Screening for Electroorganic Synthesis. *Org. Process Res. Dev.* **20**, 26–32 (2016).

73. Alfonso-Súarez, P., Kolliopoulos, A. V., Smith, J. P., Banks, C. E. & Jones, A. M. An experimentalist's guide to electrosynthesis: The Shono oxidation. *Tetrahedron Lett.* **56**, 6863–6867 (2015).

74. Faulkner, L. R. Understanding electrochemistry: Some distinctive concepts. *J. Chem. Educ.* **60**, 262–264 (1983).

75. Elgrishi, N. *et al.* A Practical Beginner's Guide to Cyclic Voltammetry. *J. Chem. Educ.* **95**, 197–206 (2018).

76. Schulz, L. & Waldvogel, S. R. Solvent Control in Electro-Organic Synthesis. *Synlett* **30**, 275–285 (2019).

77. Schotten, C. *et al.* Making electrochemistry easily accessible to the synthetic chemist. *Green Chem.* **22**, 3358–3375 (2020).

78. Noël, T., Cao, Y. & Laudadio, G. The Fundamentals behind the Use of Flow Reactors in Electrochemistry. *Acc. Chem. Res.* **52**, 2858–2869 (2019).

79. Pletcher, D., Green, R. A. & Brown, R. C. D. Flow Electrolysis Cells for the Synthetic Organic Chemistry Laboratory. *Chem. Rev.* **118**, 4573–4591 (2018).

80. Tsierkezos, N. G. Cyclic voltammetric studies of ferrocene in nonaqueous solvents in the temperature range from 248.15 to 298.15 K. *J. Solution Chem.* **36**, 289–302 (2007).

81. Hilt, G. Basic Strategies and Types of Applications in Organic Electrochemistry. *ChemElectroChem* **7**, 395–405 (2020).

82. Little, R. D. A Perspective on Organic Electrochemistry. *J. Org. Chem.* (2020).

83. Plutschack, M. B., Pieber, B., Gilmore, K. & Seeberger, P. H. The Hitchhiker's Guide to Flow Chemistry. *Chem. Rev.* **117**, 11796–11893 (2017).

84. Chen, L. *et al.* Electrochemical Cyclobutane Synthesis in Flow: Scale-Up of a Promising Melt-Castable Energetic Intermediate. *Org. Process Res. Dev.* (2020).

85. Maljuric, S., Jud, W., Kappe, C. O. & Cantillo, D. Translating batch electrochemistry to

single-pass continuous flow conditions: an organic chemist's guide. *J. Flow Chem.* **10**, 181–190 (2020).

86. Hardwick, T., Cicala, R. & Ahmed, N. Room Temperature Flow Electrochemistry as a Means of Retaining the "Memory of Chirality" via Hofer Moest Type Reaction. (2020).

87. Robertson, J. C., Coote, M. L. & Bissember, A. C. Synthetic applications of light, electricity, mechanical force and flow. *Nat. Rev. Chem.* **3**, 290–304 (2019).

88. Movsisyan, M. *et al.* Taming hazardous chemistry by continuous flow technology. *Chem. Soc. Rev.* **45**, 4892–4928 (2016).

89. Pastre, J. C., Browne, D. L. & Ley, S. V. Flow chemistry syntheses of natural products. *Chem. Soc. Rev.* **42**, 8849–8869 (2013).

90. Frick, K. M., Kamphuis, L. G., Siddique, K. H. M., Singh, K. B. & Foley, R. C. Quinolizidine alkaloid biosynthesis in lupins and prospects for grain quality improvement. *Front. Plant Sci.* **8**, 1–12 (2017).

91. Bunsupa, S., Yamazaki, M. & Saito, K. Quinolizidine alkaloid biosynthesis: Recent advances and future prospects. *Front. Plant Sci.* **3**, 1–7 (2012).

92. Aniszewski, T. Alkaloid chemistry. *Alkaloids* 99–193 (2015).

93. Kolanoś, R., Wysocka, W. & Brukwicki, T. A comparative study of NMR chemical shifts of sparteine thiolactams and lactams. *Tetrahedron* **59**, 5531–5537 (2003).

94. Erbas, M. The effects of different debittering methods on the production of lupin bean snack from bitter Lupinus albus L. seeds. *J. Food Qual.* **33**, 742–757 (2010).

95. Villalpando-Vargas, F. & Medina-Ceja, L. Sparteine as an anticonvulsant drug: Evidence and possible mechanism of action. *Seizure* **39**, 49–55 (2016).

96. Carmalia, S., Alves, V. D., Coelhoso, I. M., Ferreira, L. M. & Lourenço, A. M. Recovery of lupanine from Lupinus albus L. leaching waters. *Sep. Purif. Technol.* **74**, 38–43 (2010).

97. Huang, P. Q., Guo, Z. Q. & Ruan, Y. P. A versatile approach for the asymmetric syntheses of (1R,9aR)-epiquinamide and (1R,9aR)-homopumiliotoxin 223G. *Org. Lett.* **8**, 1435–1438 (2006).

98. Boczoń, W. & Jasiewicz, B. Synthesis and conformational analysis of disubstituted sparteine derivatives. *Collect. Czechoslov. Chem. Commun.* **68**, 696–710 (2003).

99. García López, P. M. *et al.* Quinolizidine alkaloids isolated from Lupinus species enhance insulin secretion. *Eur. J. Pharmacol.* **504**, 139–142 (2004).

100. Kurek, J., Jasiewicz, B., Wyrzykiewicz, E. & Boczoń, W. New 2-oxosparteine derivatives: Synthesis and spectroscopic characterization. *J. Mol. Struct.* **1003**, 10–20 (2011).

101. Parmaki, S. *et al. Bioconversion of alkaloids to high-value chemicals: Comparative analysis of newly isolated lupanine degrading strains*. *Chemosphere* **193**, (Elsevier B.V., 2018).

102. Maulide, N., Peng, B., Afonso, C., Frade, R. Process for converting Lupanine into Sparteine. (2016).

103. Pugsley, M. K., Saint, D. A., Hayes, E., Berlin, K. D. & Walker, M. J. A. The cardiac electrophysiological effects of sparteine and its analogue BRB-I-28 in the rat. *Eur. J. Pharmacol.* **294**, 319–327 (1995).

104. Ahrens, H., Paetow M., Hoppe, D. Stereoselective Generation of 1,3- and 1,4-Dioxy-Substituted Carbanions by Sparteine-Assisted Deprotonation of Chiral Precursors: Substrate or Reagent Control in the Synthesis of alpha,beta- and alpha-gama-Diols. **3**, 5327–5330 (1992).

105. Hoppe, D. *et al.* Enantioselective synthesis via sparteine induced asymmetric

deprotonation. *Pure Appl. Chem.* **66**, 1479–1486 (1994).

106. Faibish, N. C., Park, Y. S., Lee, S. & Beak, P. A mechanistic and structural investigation of the (-)-sparteine mediated asymmetric benzylic lithiation substitution reactions of N-Boc-N-(p-methoxyphenyl)benzylamine. *J. Am. Chem. Soc.* **119**, 11561–11570 (1997).

107. Gallagher, D. J., Du, H., Long, S. A. & Beak, P. Chiral organolithium complexes: The structure of β-lithiated β-phenylcarboxamides and the mechanism of asymmetric substitution in the presence of (-)-sparteine. *J. Am. Chem. Soc.* **118**, 11391–11398 (1996).

108. Beak, P., Du, H. Asymmetric Substitution: Highly Enantioselective Substitutions Induced at the Carbanion of a Racemic Organolithium Substrate by (-)-Sparteine. *J. Am. Chem. Soc* 2516–2518 (1993).

109. Trost, B. M. Asymmetric catalysis: An enabling science. *Proc. Natl. Acad. Sci. U. S. A.* **101**, 5348–5355 (2004).

110. Gallagher, D. J., Wu, S., Nikolic, N. A. & Beak, P. Chiral Organolithium Complexes: The Effect of Ligand Structure on the Enantioselective Deprotonation of Boc-Pyrrolidine. *J. Org. Chem.* **60**, 8148–8154 (1995).

111. Saint-Denis, T. G., Zhu, R. Y., Chen, G., Wu, Q. F. & Yu, J. Q. Enantioselective c(sp 3)–H bond activation by chiral transition metal catalysts. *Science (80-.).* **359**, (2018).

112. Shi, L. & Xia, W. Photoredox functionalization of C–H bonds adjacent to a nitrogen atom. *Chem. Soc. Rev.* **41**, 7687–7697 (2012).

113. Strecker, A. Ueber die künstliche Bildung der Milchsäure und einen neuen, dem Glycocoll homologen Körper; *Justus Liebigs Ann. Chem.* **75**, 27–45 (1850).

114. Opatz, T. The chemistry of deprotonated α-aminonitriles. *Synthesis (Stuttg).* 1941–1959 (2009).

115. Segobia, D. J., Trasarti, A. F. & Apesteguía, C. R. Synthesis of n-butylamine from butyronitrile on Ni/SiO2: Effect of solvent. *J. Braz. Chem. Soc.* **25**, 2272–2279 (2014).

116. Volf, J. & Pašek, J. Hydrogenation of Nitriles. *Stud. Surf. Sci. Catal.* **27**, 105–144 (1986).

117. Zhu, J., Quirion, J. C. & Husson, H. P. Asymmetric Synthesis. 29. Preparation of 1,8-Diazaspiro[5.5]undecane Derivatives. *J. Org. Chem.* **58**, 6451–6456 (1993).

118. Mattalia, J. M. R. The reductive decyanation reaction: An overview and recent developments. *Beilstein J. Org. Chem.* **13**, 267–284 (2017).

119. Cacciarini, M. *et al.* Towards solar energy storage in the photochromic dihydroazulene-vinylheptafulvene system. *Chem. - A Eur. J.* **21**, 7454–7461 (2015).

120. Lowe, J. T. *et al.* Synthesis and Profiling of a Diverse Collection of Azetidine-Based Scaffolds for the Development of CNS-Focused Lead-like Libraries. (2012).

121. Morciano, G. *et al.* Discovery of Novel 1,3,8-Triazaspiro[4.5]decane Derivatives That Target the c Subunit of F1/FO-Adenosine Triphosphate (ATP) Synthase for the Treatment of Reperfusion Damage in Myocardial Infarction. *J. Med. Chem.* **61**, 7131–7143 (2018).

122. Dhanasekaran, S., Suneja, A., Bisai, V. & Singh, V. K. Approach to Isoindolinones, Isoquinolinones, and THIQs via Lewis Acid-Catalyzed Domino Strecker-Lactamization/Alkylations. *Org. Lett.* **18**, 634–637 (2016).

123. Cadierno, V. Synthetic applications of the Parkins nitrile hydration catalyst [PtH{(PMe2O)2H}(PMe2OH)]: A review. *Appl. Sci.* **5**, 380–401 (2015).

124. Taylor, A. R. D., Maccoss, M. & Lawson, A. D. G. Rings in Drugs. *J. Med. Chem.* **57**, 5845–5859 (2014).

125. Kakkar, S. & Narasimhan, B. A comprehensive review on biological activities of oxazole derivatives. *BMC Chem.* **13**, 1–24 (2019).

126. Chen, A. D. *et al.* Radical cascade synthesis of azoles: via tandem hydrogen atom transfer. *Chem. Sci.* **11**, 2479–2486 (2020).

127. Mittal, R. & Awasthi, S. K. Recent Advances in the Synthesis of 5-Substituted 1 H-Tetrazoles: A Complete Survey (2013-2018). *Synth.* **51**, 3765–3783 (2019).

128. Roh, J., Vávrová, K. & Hrabálek, A. Synthesis and functionalization of 5-substituted tetrazoles. *European J. Org. Chem.* 6101–6118 (2012).

129. Himo, F., Demko, Z. P., Noodleman, L. & Sharpless, K. B. Mechanisms of tetrazole formation by addition of azide to nitriles. *J. Am. Chem. Soc.* **124**, 12210–12216 (2002).

130. Enders, D. & Shilvock, J. P. Some recent applications of α-amino nitrile chemistry. *Chem. Soc. Rev.* **29**, 359–373 (2000).

131. Herlem, D. & Khuong-Huu, F. Oxydation photochimique d'amines tertiaires et d'alcaloïdes—X. *Tetrahedron* **35**, 633–639 (1979).

132. Allen, J. M. & Lambert, T. H. Tropylium ion mediated α-cyanation of amines. *J. Am. Chem. Soc.* **133**, 1260–1262 (2011).

133. Orejarena Pacheco, J. C. *et al.* A Highly Active System for the Metal-Free Aerobic Photocyanation of Tertiary Amines with Visible Light: Application to the Synthesis of Tetraponerines and Crispine A. *Chem. - A Eur. J.* **22**, 5409–5415 (2016).

134. Jasiewicz, B., Boczoń, W. & Kurek, J. Synthesis and conformational analysis of new 17-alkyl derivatives of lupanine and their perchlorate salts. *Collect. Czechoslov. Chem. Commun.* **69**, 2068–2080 (2004).

135. Kolanós, R., Wysocka, W., Borowiak, T., Dutkiewicz, G., Brukwicki, T. V. Thioanalogues of sparteine lactams. (+)-2-Thiono-17-oxosparteine and (+)-2,17-dithionosparteine. *J. Mol. Struct.*

136. Yoshida, J. I., Kataoka, K., Horcajada, R. & Nagaki, A. Modern strategies in electroorganic synthesis. *Chem. Rev.* **108**, 2265–2299 (2008).

137. Endo, S., Pfennigsdorff, A. & Goss, K. U. Salting-out effect in aqueous NaCl solutions: Trends with size and polarity of solute molecules. *Environ. Sci. Technol.* **46**, 1496–1503 (2012).

138. Kawamata, Y. Electroorganic Chemistry: Choice of Electrodes. (2016).

139. Srivastava, S. K. & Pionteck, J. Recent advances in preparation, structure, properties and applications of graphite oxide. *J. Nanosci. Nanotechnol.* **15**, 1984–2000 (2015).

140. Segobia, D. J., Trasarti, A. F. & Apesteguía, C. R. Hydrogenation of nitriles to primary amines on metal-supported catalysts: Highly selective conversion of butyronitrile to n-butylamine. *Appl. Catal. A Gen.* **445**–**446**, 69–75 (2012).

141. Jonathan Clayden, N. G. and S. W. *Organic Chemistry*. (2012).

142. Brown, H. C. & Heim, P. Selective Reductions. XVIII. The Fast Reaction of Primary, Secondary, and Tertiary Amides with Diborane. A Simple, Convenient Procedure for the Conversion of Amides to the Corresponding Amines. *J. Org. Chem.* **38**, 912–916 (1973).

143. Krieble, V. K. & Noll, C. I. The Hydrolysis of Nitriles with Acids. *J. Am. Chem. Soc.* **61**, 560–563 (1939).

144. Debabov, V. G. & Yanenko, A. S. Biocatalytic hydrolysis of nitriles. *Rev. J. Chem.* **1**, 385–402 (2011).

145. Demko, Z. P. & Sharpless, K. B. Preparation of 5-substituted 1H-tetrazoles from nitriles in water. *J. Org. Chem.* **66**, 7945–7950 (2001).

146. Hasan, M. U. 13C NMR spectra of some amides and imides. Effect of inductive and mesomeric interactions, cyclization and hydrogen bonding on 13C NMR chemical shifts. *Org. Magn. Reson.* **14**, 447–450 (1980).

147. Bohlmann, F. & Zeisberg, R. Lupinen-Alkaloide, XLI. 13C-NMR-Spektren von Lupinen-Alkaloiden. *Chem. Ber.* **108**, 1043–1051 (1975).

148. Meng, D. & Danishefsky, S. J. Stereospecific Sulfur-Mediated Cleavage of a Spirocyclobutanone: Synthesis of a Fully Functional Precursor to the CP Compounds. *Angew. Chemie Int. Ed.* **38**, 1485–1488 (1999).

149. Schmidt, J. P. *et al.* The first synthesis of the ABC-ring system of ’upenamide. *Org. Lett.* **9**, 4041–4044 (2007).

150. V.Ley, S., Norman, J., Griffith W., Marsden, S. Tetrapropylammonium Perruthenate, PrN+RuO4-, TPAP: A Catalytic Oxidant for Organic Synthesis. *Synthesis (Stuttg).* (1994).

151. Yoshimura, M. *et al.* Selective Synthesis of Primary Amines from Nitriles under Hydrogenation Conditions. *Adv. Synth. Catal.* **360**, 1726–1732 (2018).

5. Attatchments

5.1 Appendix 1 - Basic Organic Phase Characterization

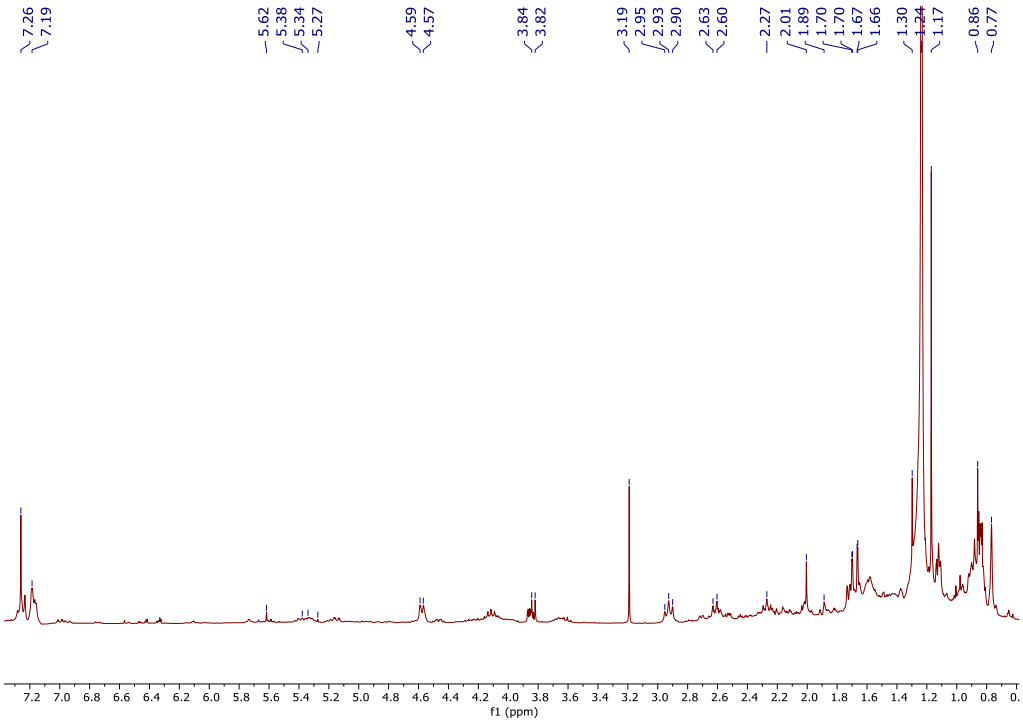

Figure 5.1: ^{1}H NMR spectrum of organic phase obtained from the extraction methodology.

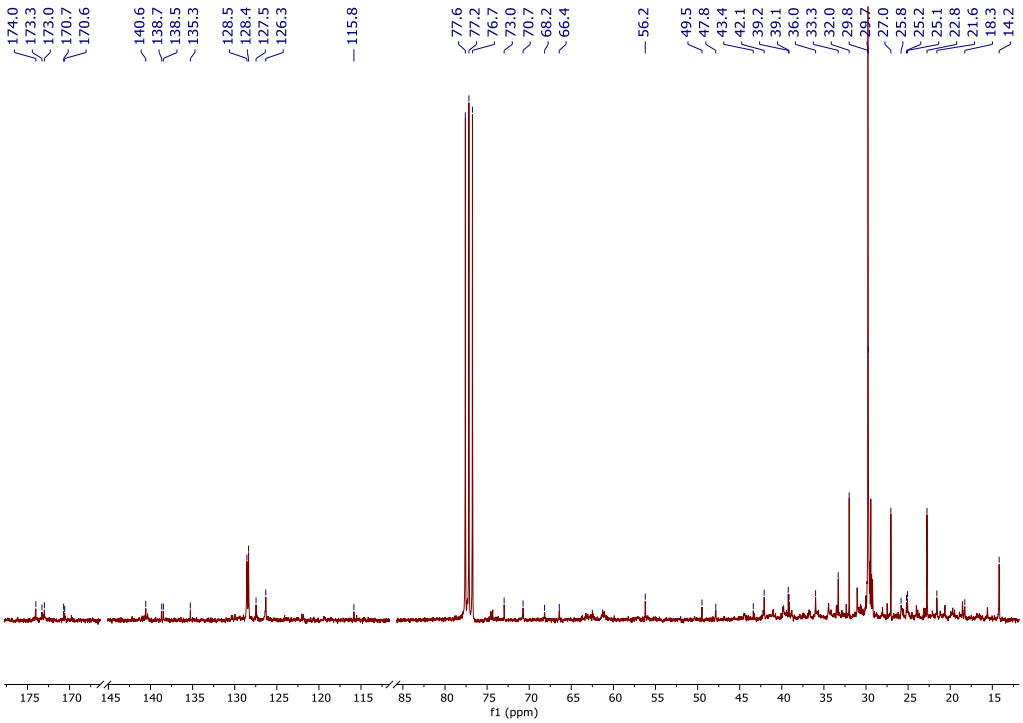

Figure 5.2: ^{13}C NMR spectrum of organic phase obtained from the extraction methodology.

5.2 Appendix 2 - ^{1}H NMR from Esterification Reaction

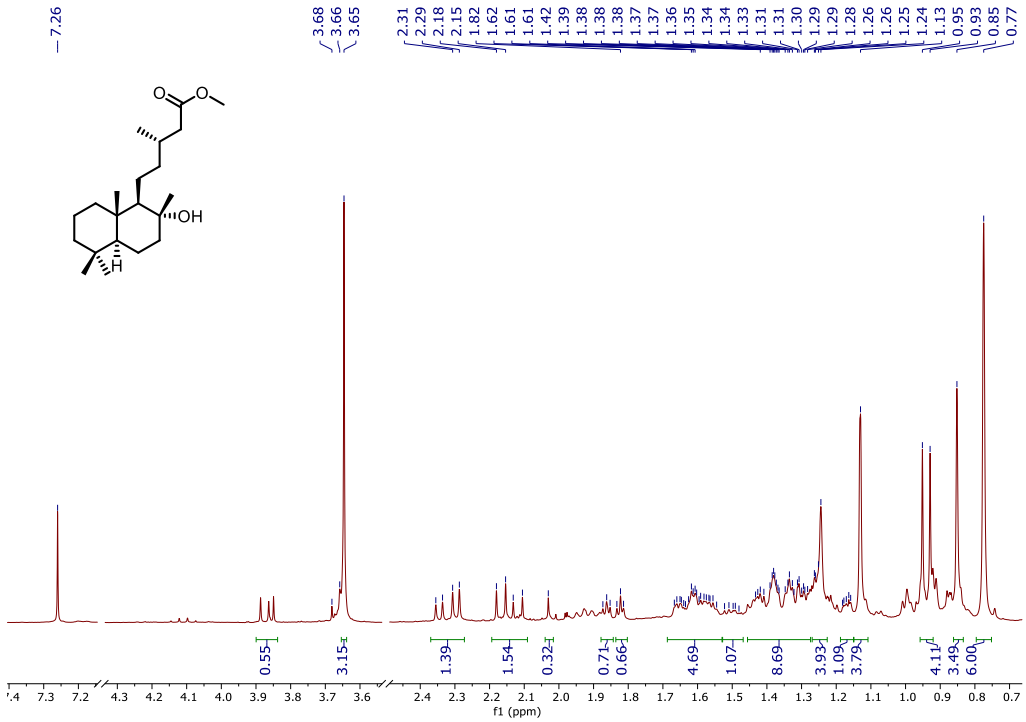

Figure 5.3: ^{1}H NMR spectrum from the fraction containing LA methyl ester, later described as LA methyl ester – 1

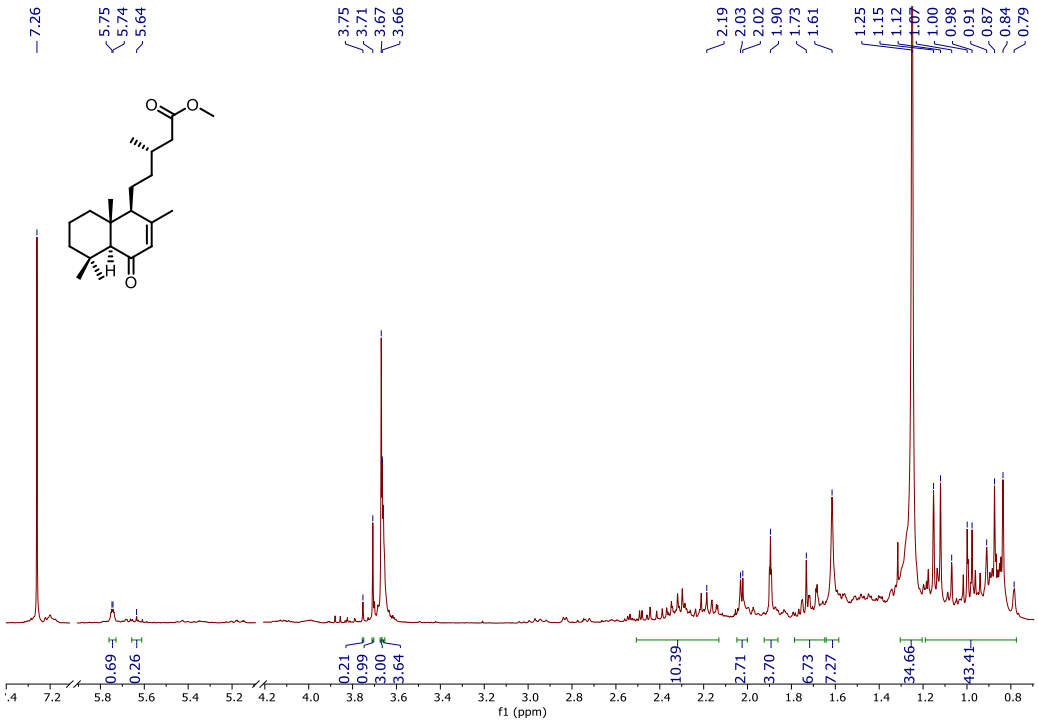

Figure 5.4: ^{1}H NMR spectrum from a fraction containing OA methyl ester, later described as OA methyl ester – 1

5.3 Appendix 3 - ^{1}H NMR from Upscaled Esterification Reactions

5.3.1 6-Oxocativic Acid Isolation (2)

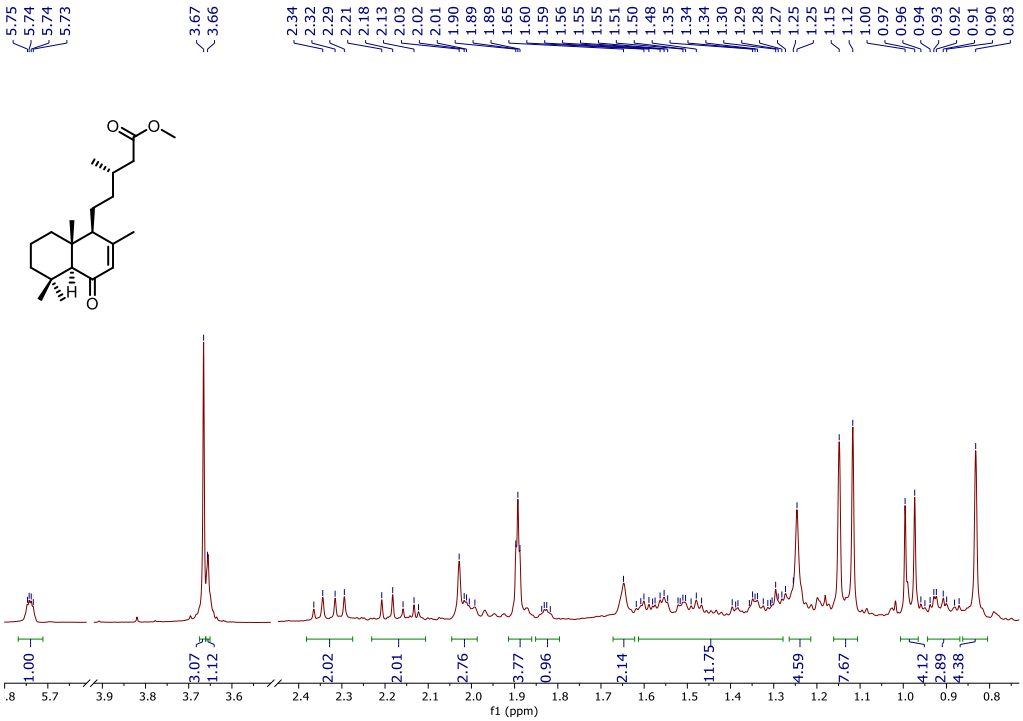

Figure 5.5: ^{1}H NMR spectrum of OA methyl ester-2

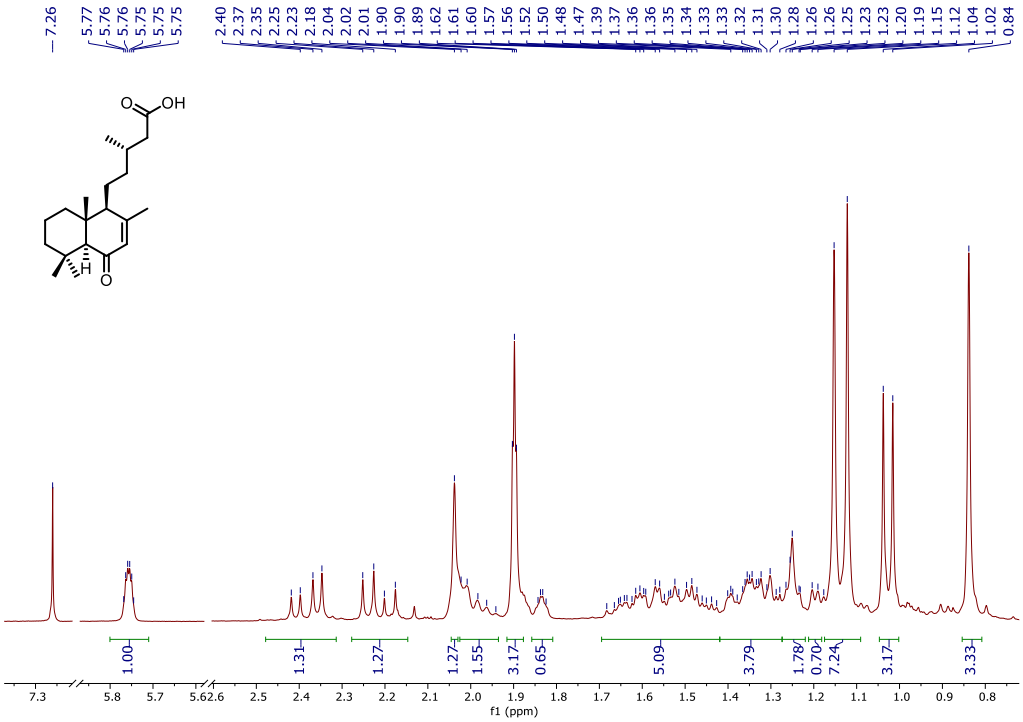

Figure 5.6: ^{1}H NMR spectrum of OA (2)

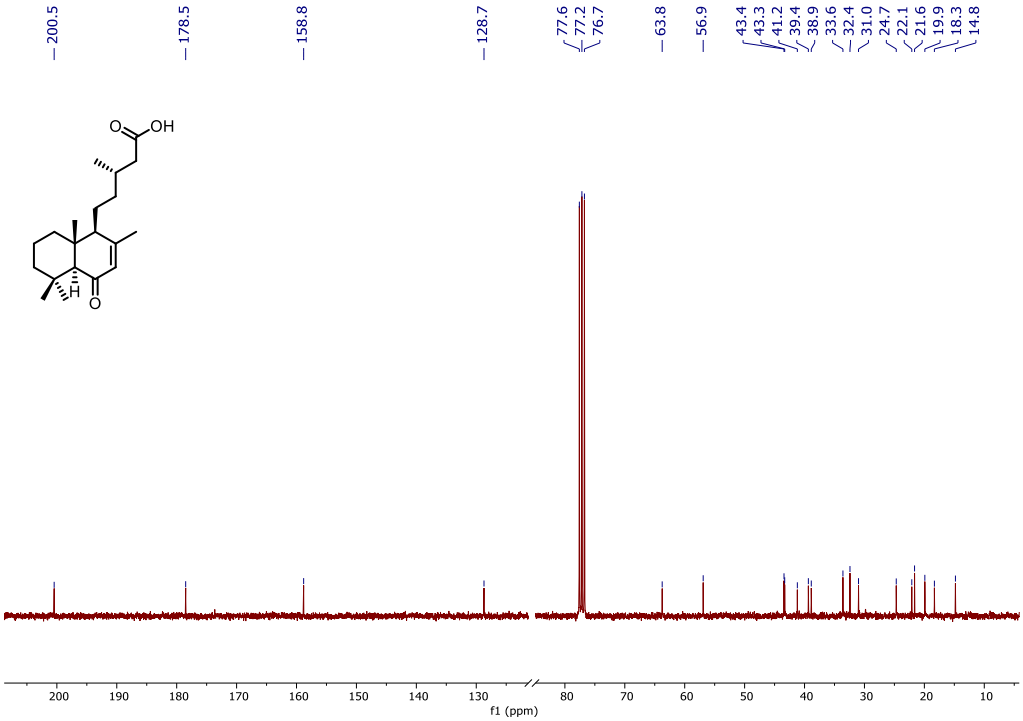

Figure 5.7: ^{13}C NMR spectrum of OA (2)

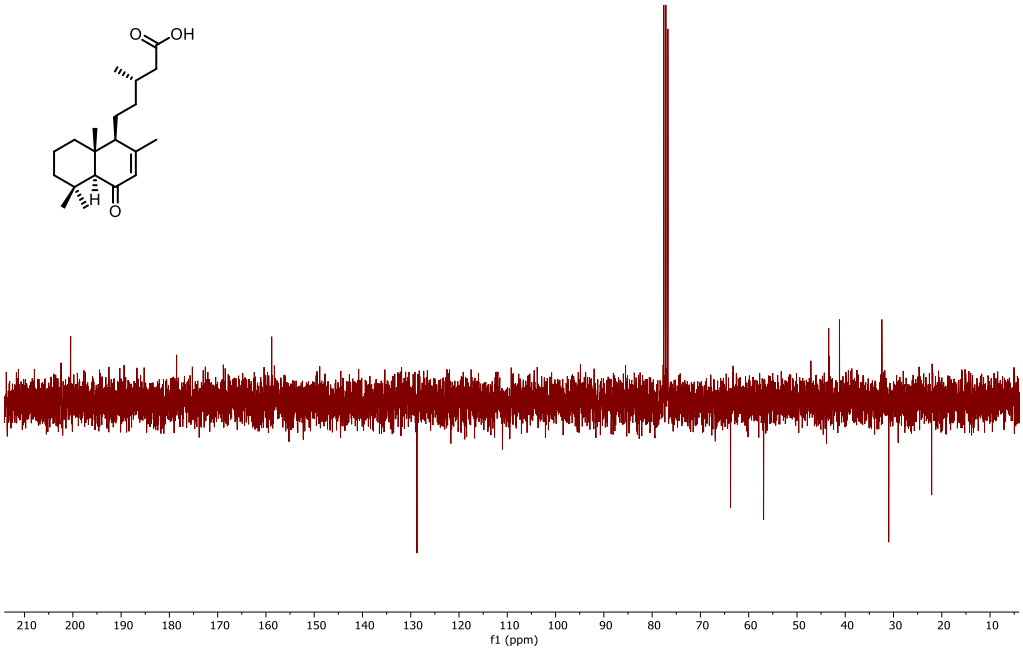

Figure 5.8: APT DEPT spectrum of OA (2)

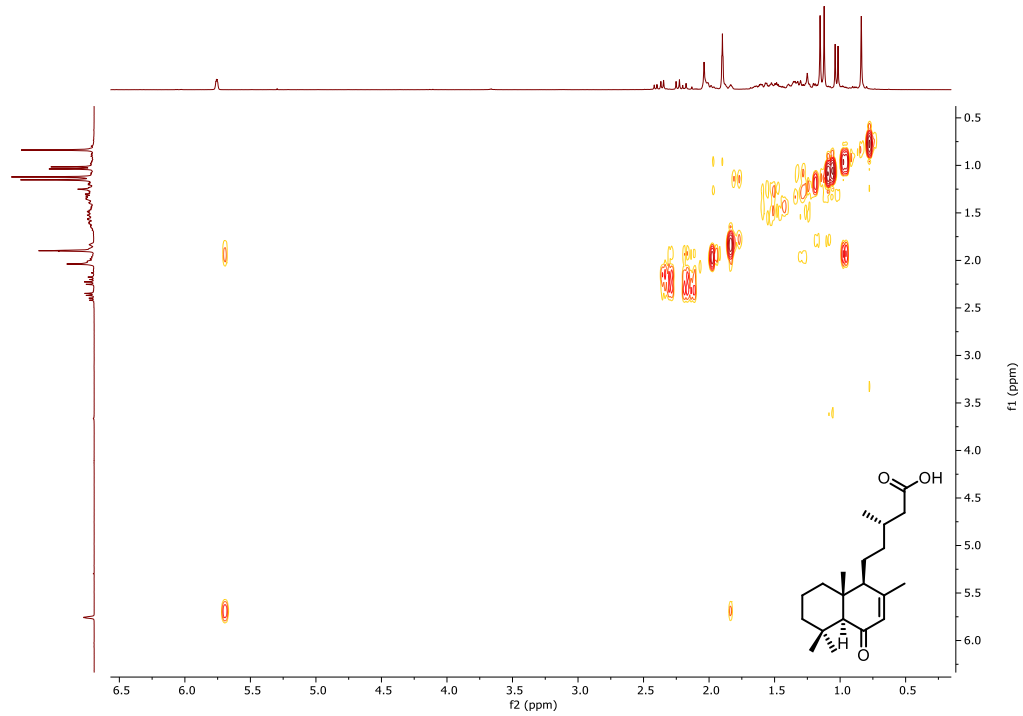

Figure 5.9: COSY spectrum of OA (2)

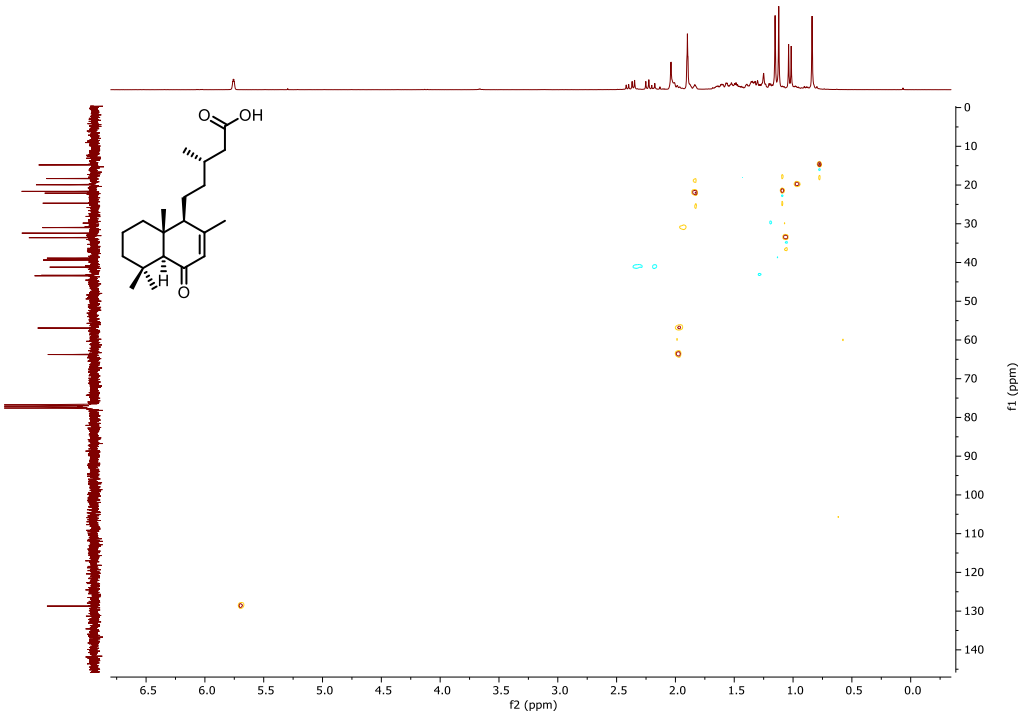

Figure 5.10: HSQC spectrum of OA (2)

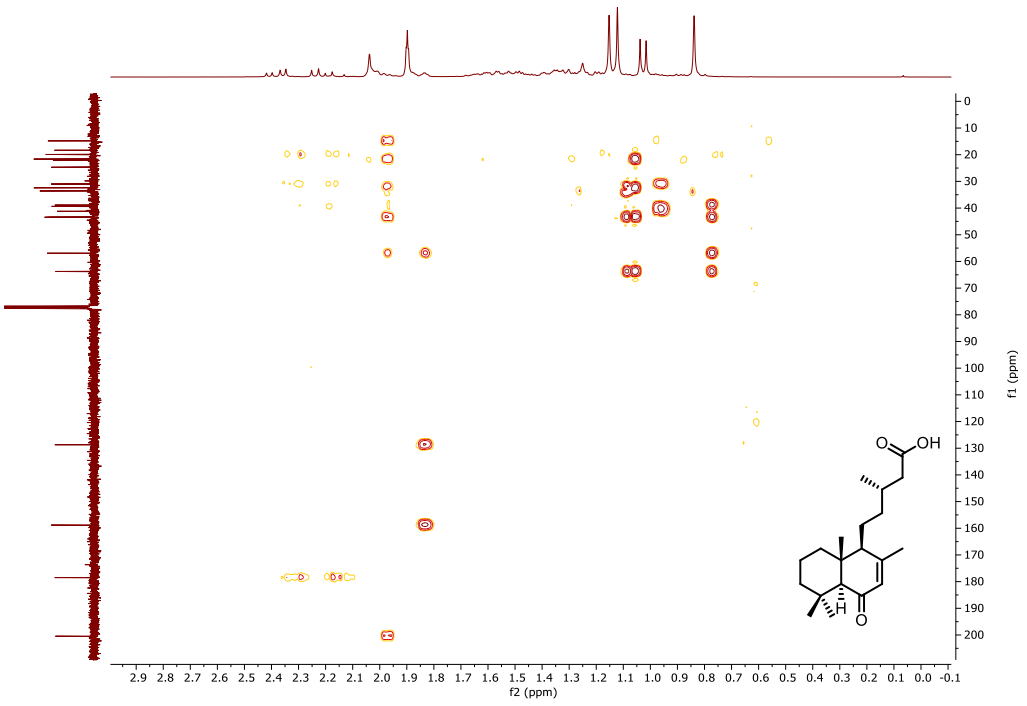

Figure 5.11: HMBC spectrum of OA (2)

5.3.2 Labdanolic Acid Isolation (1)

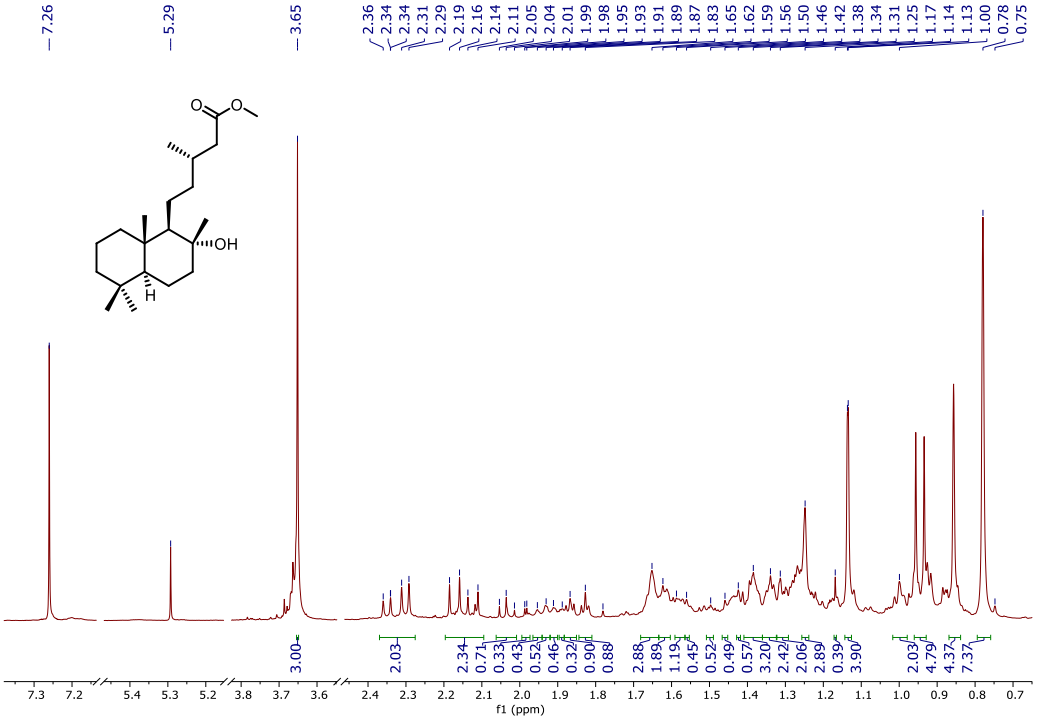

Figure 5.12: ^{1}H NMR of a fraction containing LA methyl ester, from an upscaled esterification reaction.

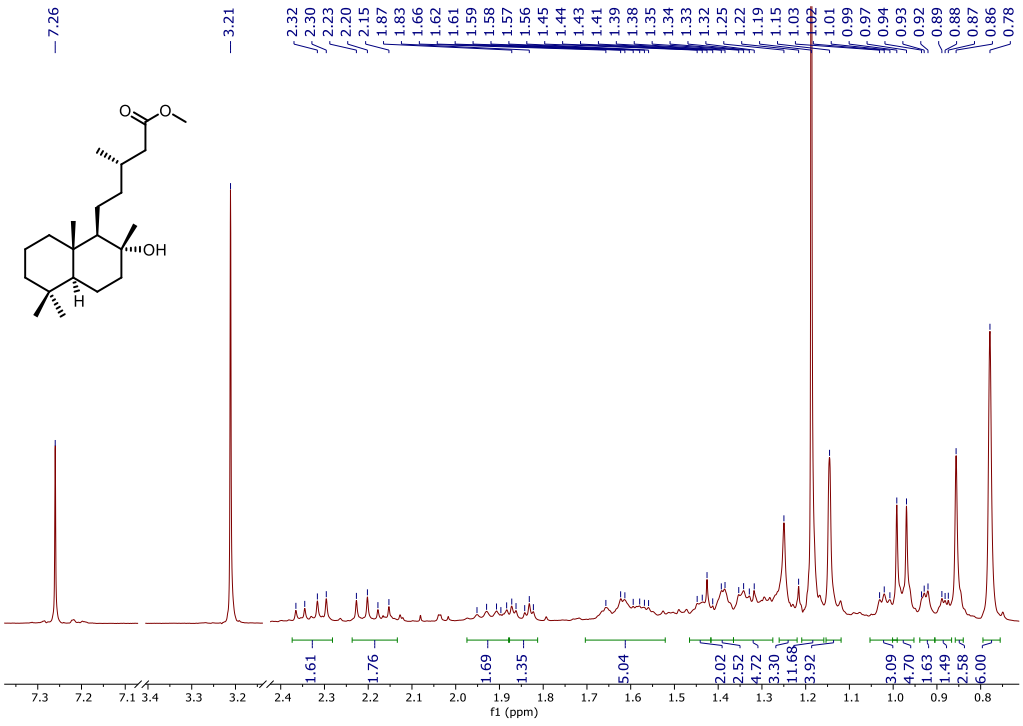

Figure 5.13: ^{1}H NMR of LA methyl ester hydrolysis before purification

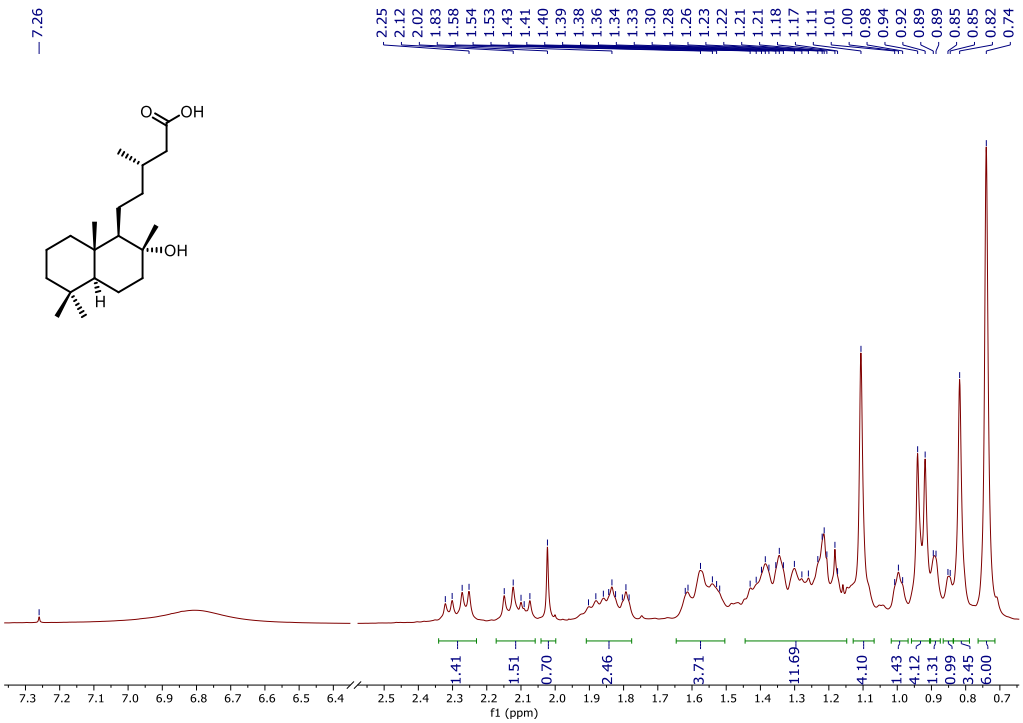

Figure 5.14: ^{1}H NMR spectrum of LA (1)

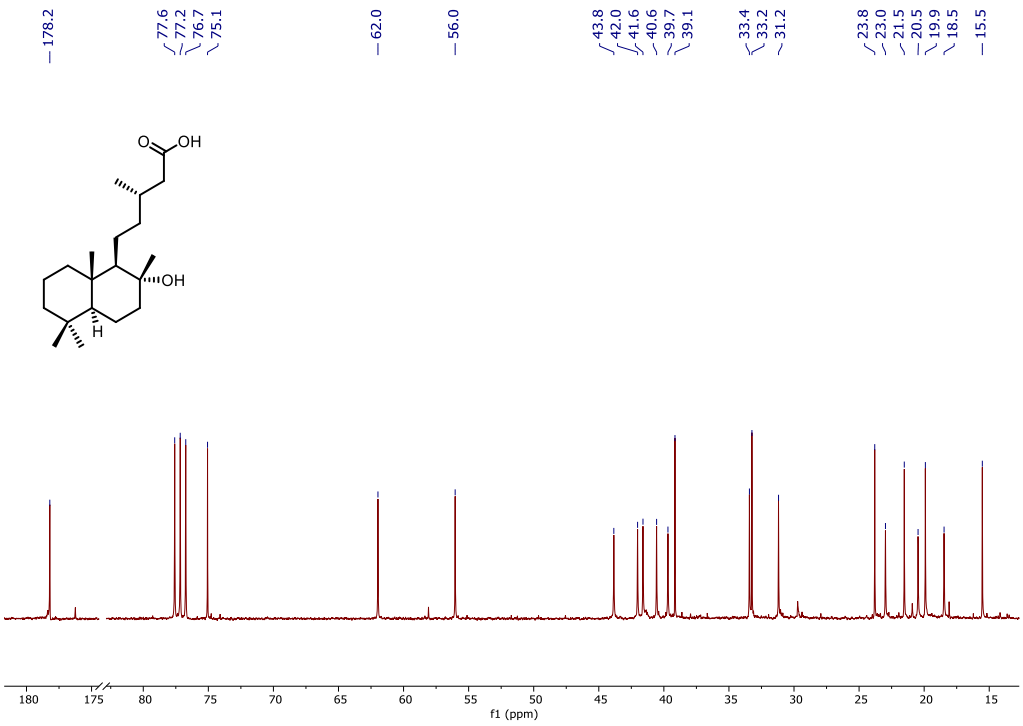

Figure 5.15: ^{13}C NMR spectrum of LA (1)

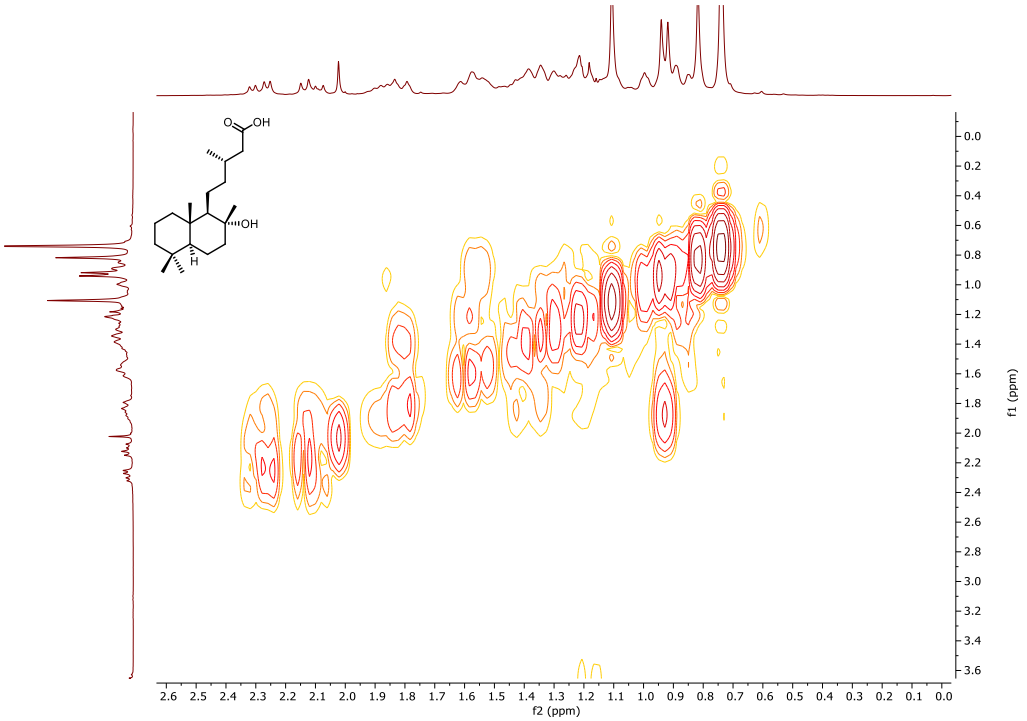

Figure 5.16: COSY spectrum of LA (1)

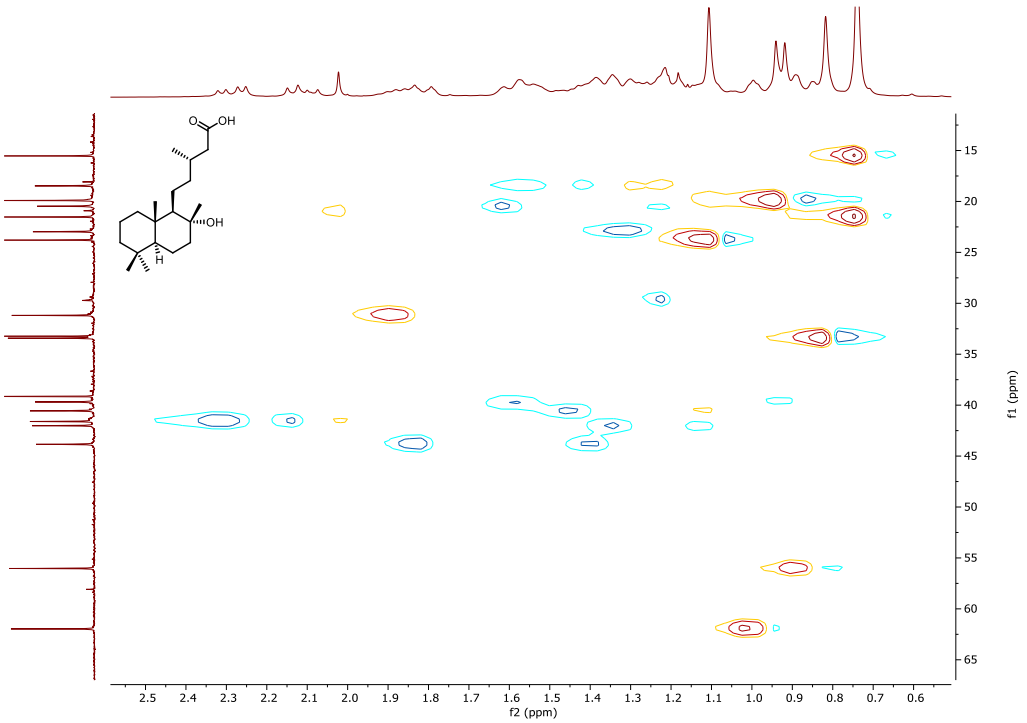

Figure 5.17: HSQC spectrum of LA (1)

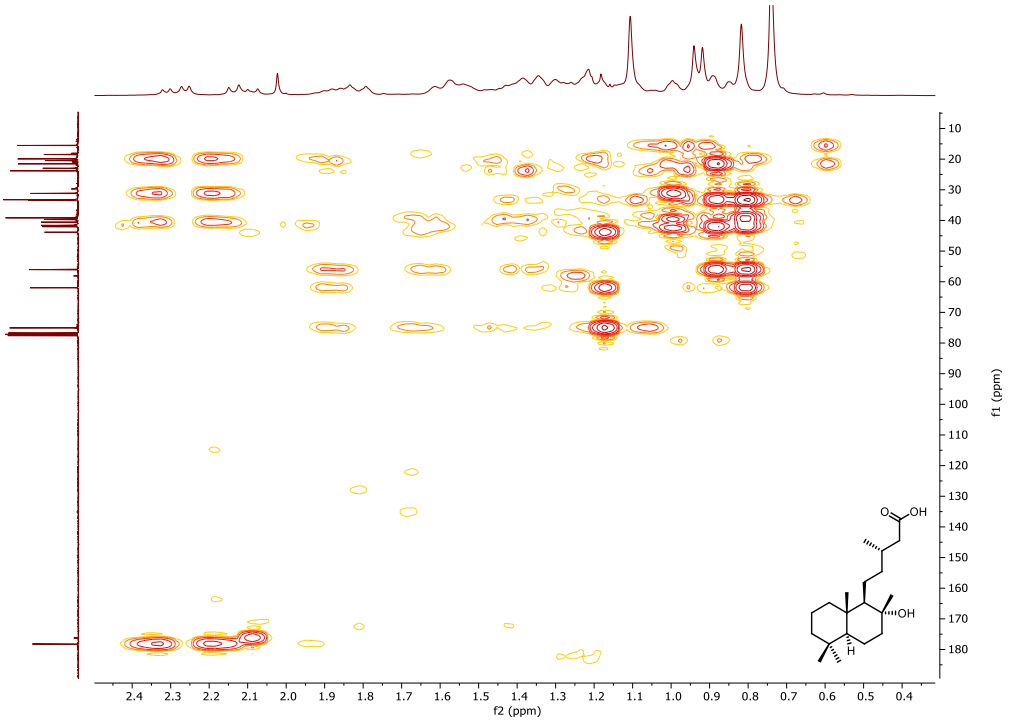

Figure 5.18: HMBC spectrum of LA (1)

5.4 Appendix 4 - ^{1}H NMR from Allylic Oxidations

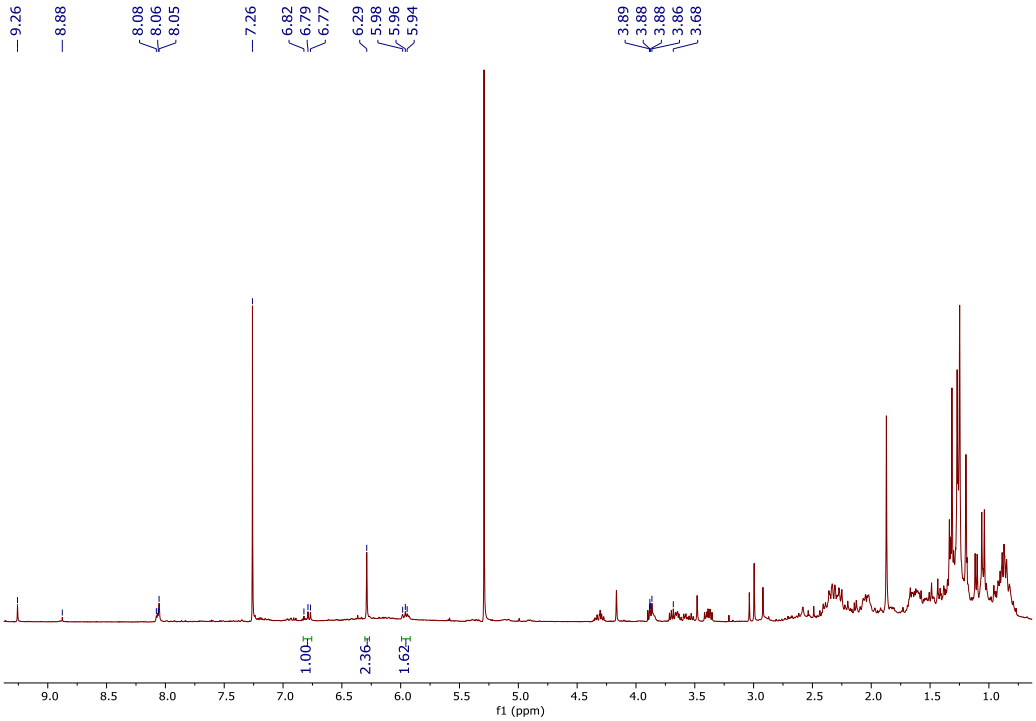

Figure 5.19: ^{1}H NMR of the crude from the allylic oxidation with TPAP.

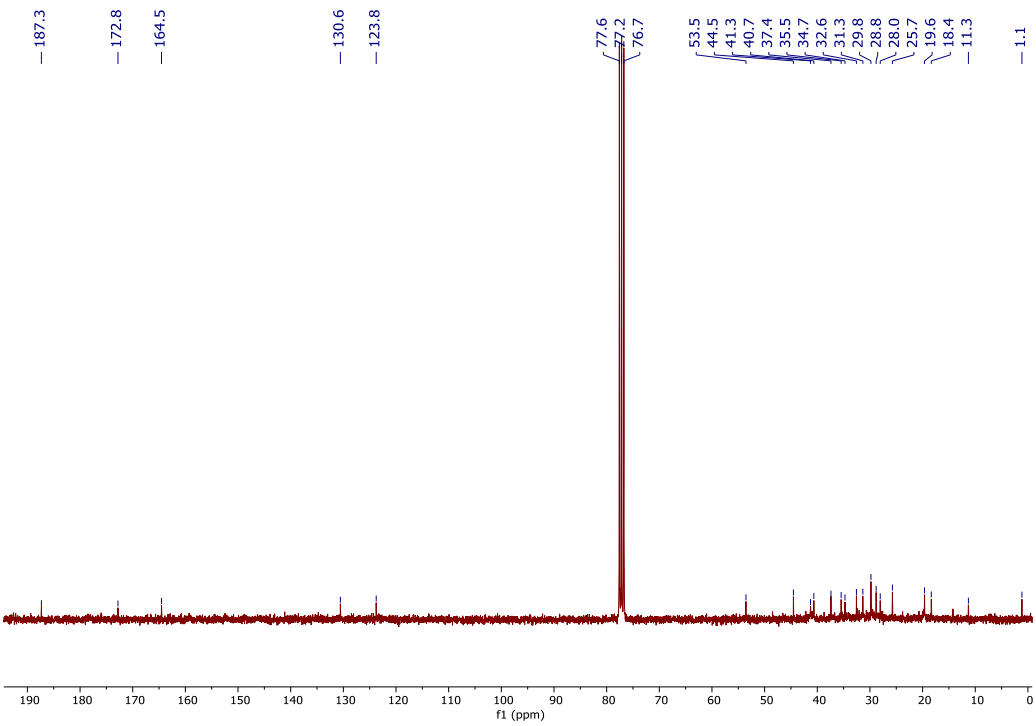

Figure 5.20: ^{13}C NMR of the crude from the allylic oxidation with TPAP.

5.5 Appendix 5: rac-lupanine (8) Characterization

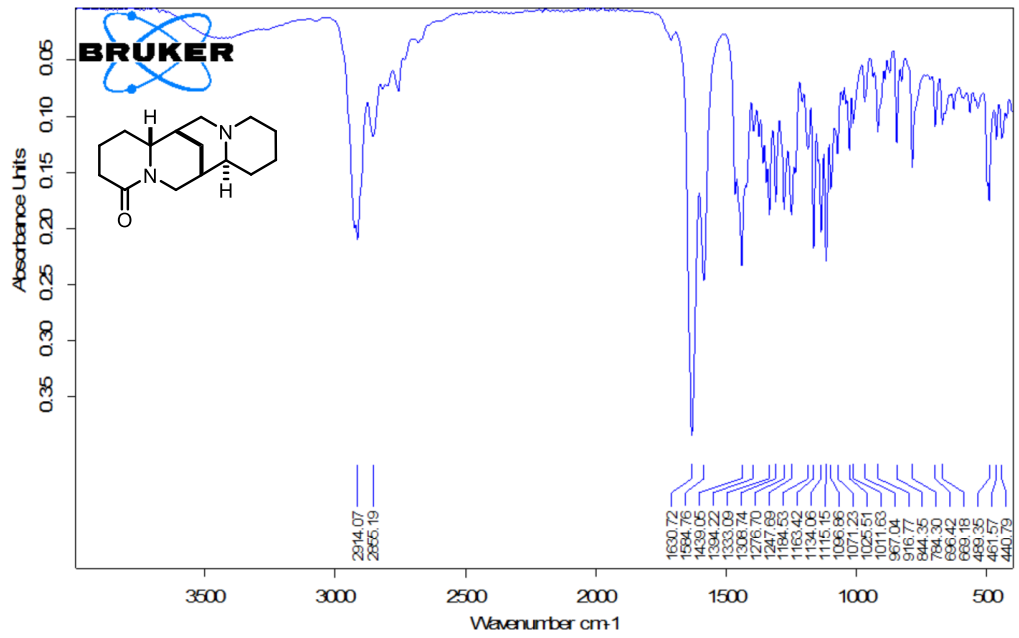

Figure 5.21: IR spectrum of *rac*-lupanine (8)

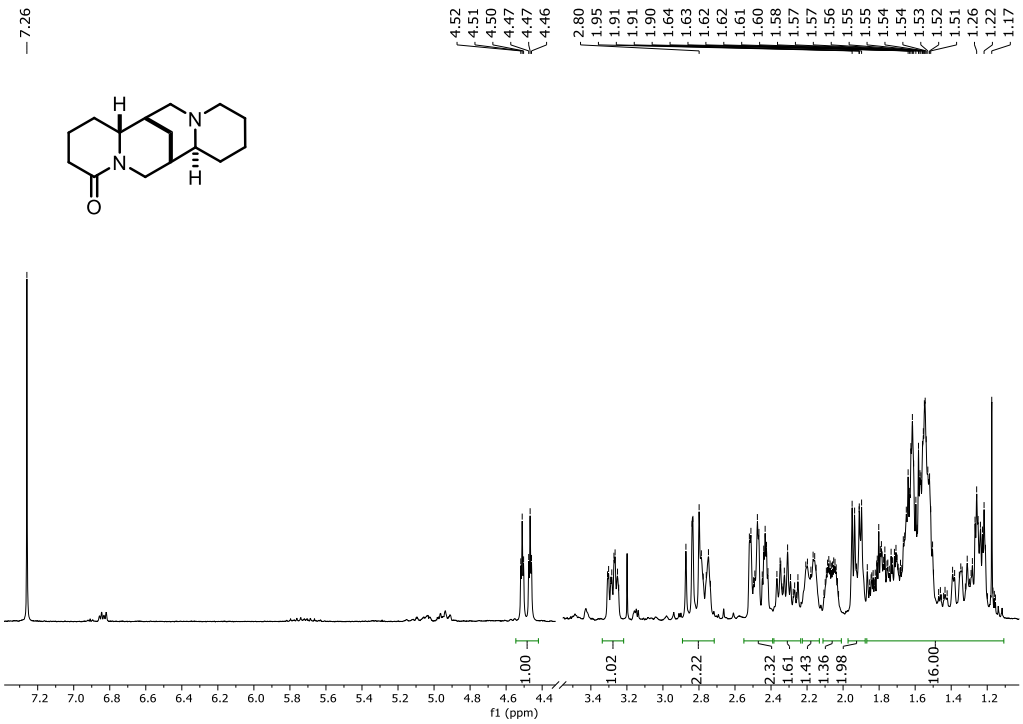

Figure 5.22: ^{1}H NMR spectrum of *rac*-lupanine (8)

Figure 5.23: ^{13}C NMR spectrum of *rac*-lupanine (8)

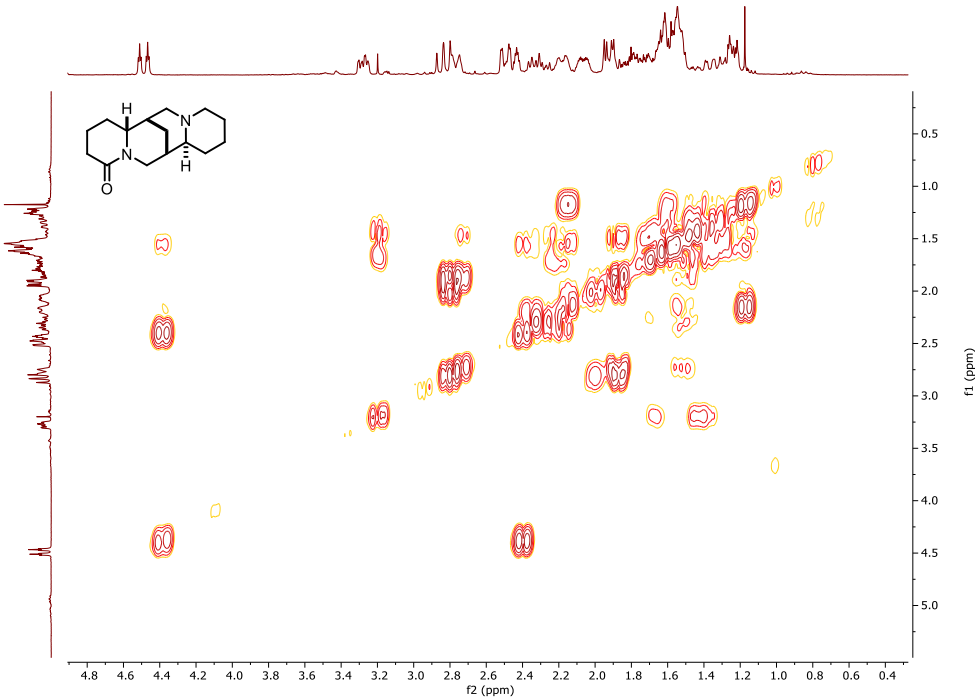

Figure 5.24: COSY spectrum of *rac*-lupanine (8)

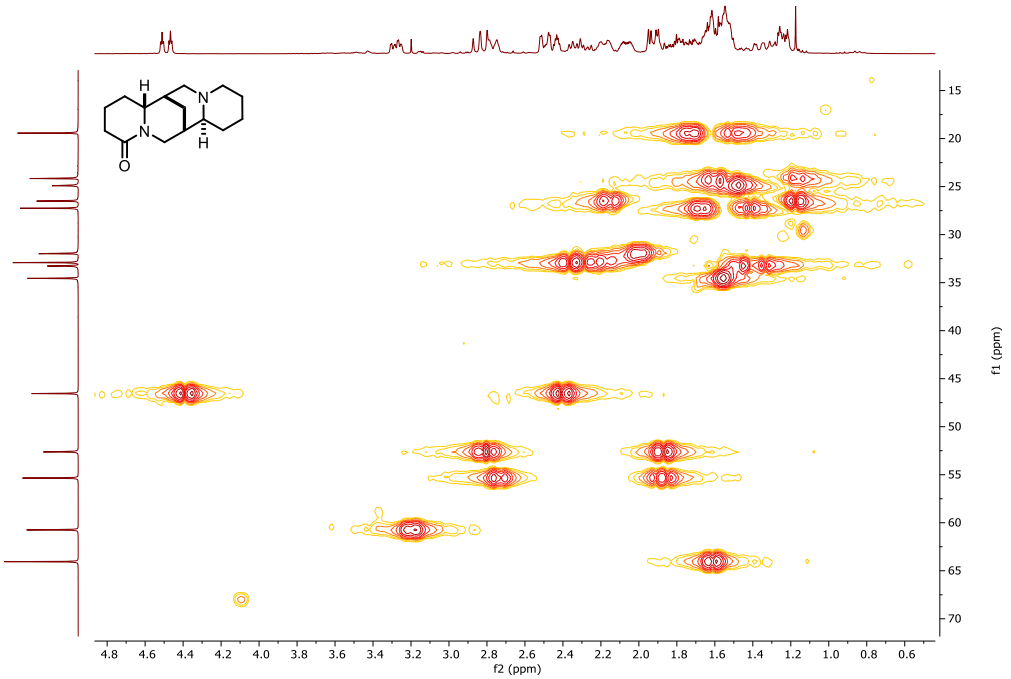

Figure 5.25: HSQC spectrum of *rac*-lupanine (8)

5.6 Appendix 6: 17-cyano-*rac*-lupanine (10) Characterization

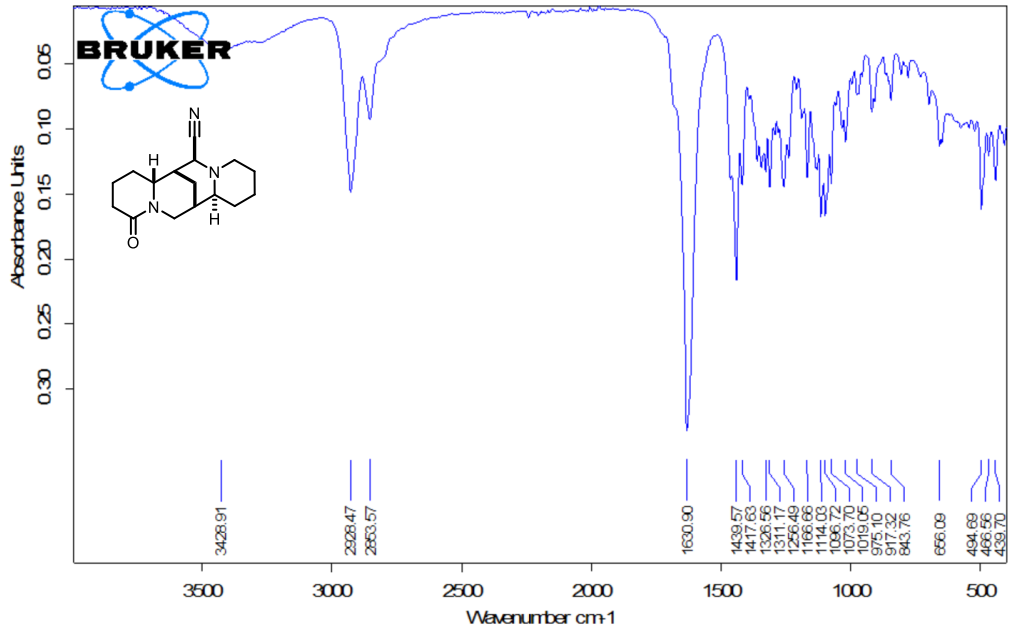

Figure 5.26: IR spectrum of 17-cyano-*rac*-lupanine (10)

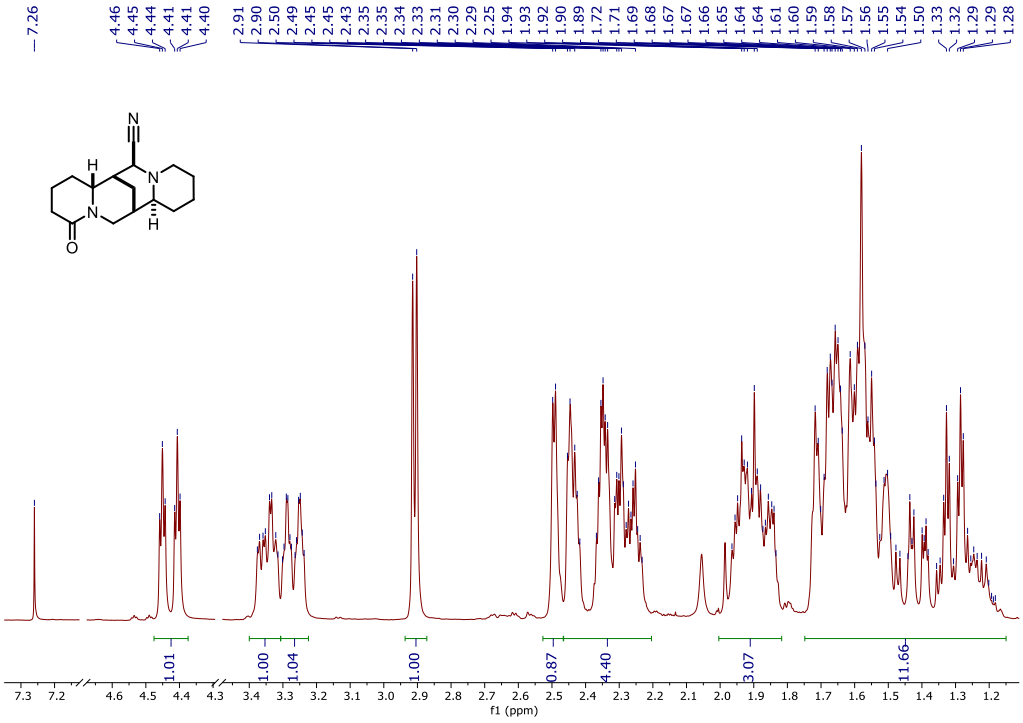

Figure 5.27: ^{1}H NMR spectrum of 17-cyano-*rac*-lupanine (10)

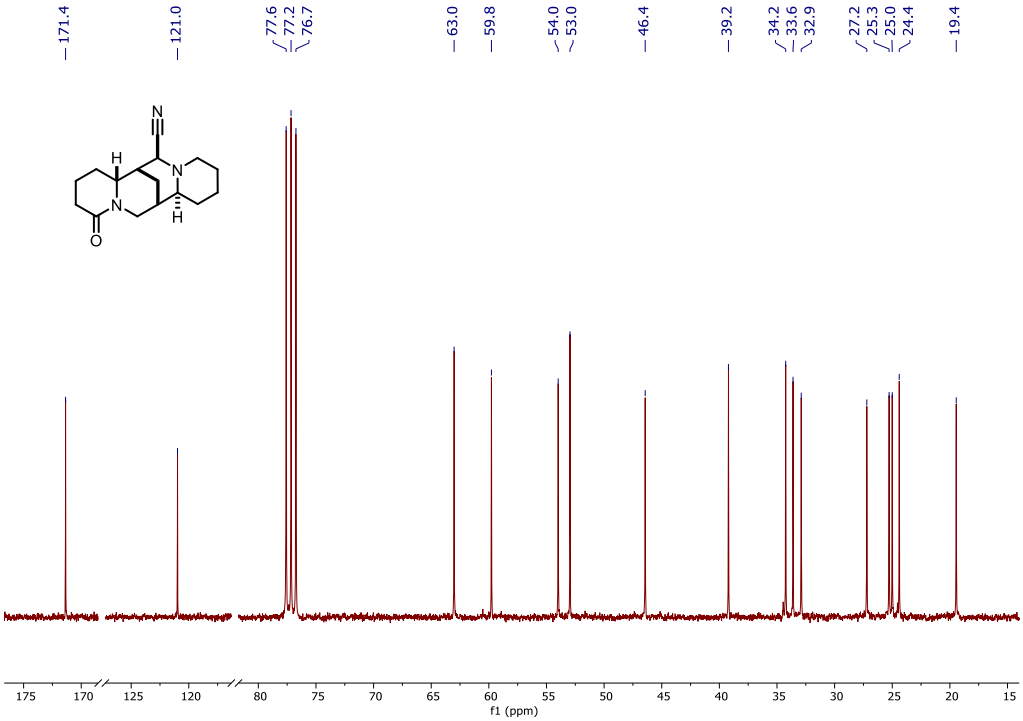

Figure 5.28: ^{13}C NMR spectrum of 17-cyano-*rac*-lupanine (10)

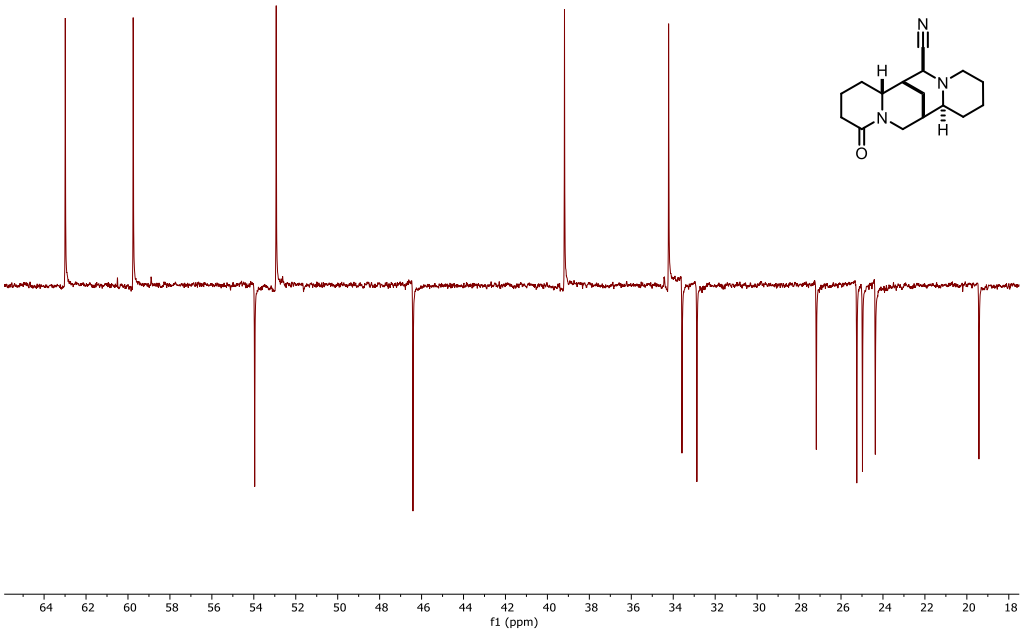

Figure 5.29: APT DEPT of 17-cyano-*rac*-lupanine (10)

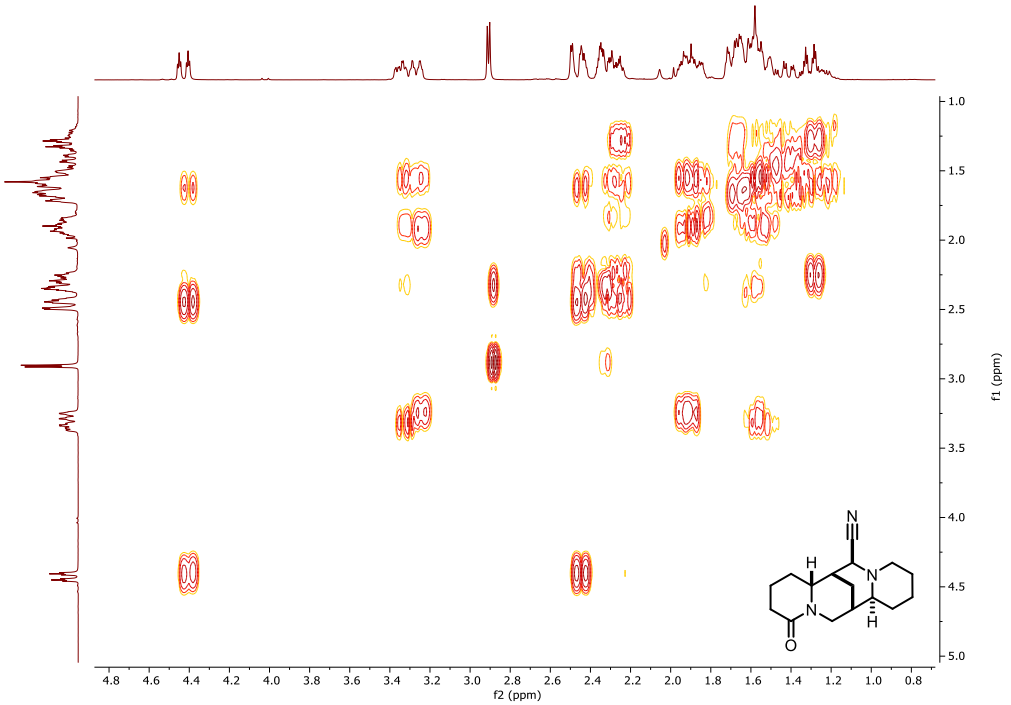

Figure 5.30: COSY spectrum of 17-cyano-*rac*-lupanine (10)

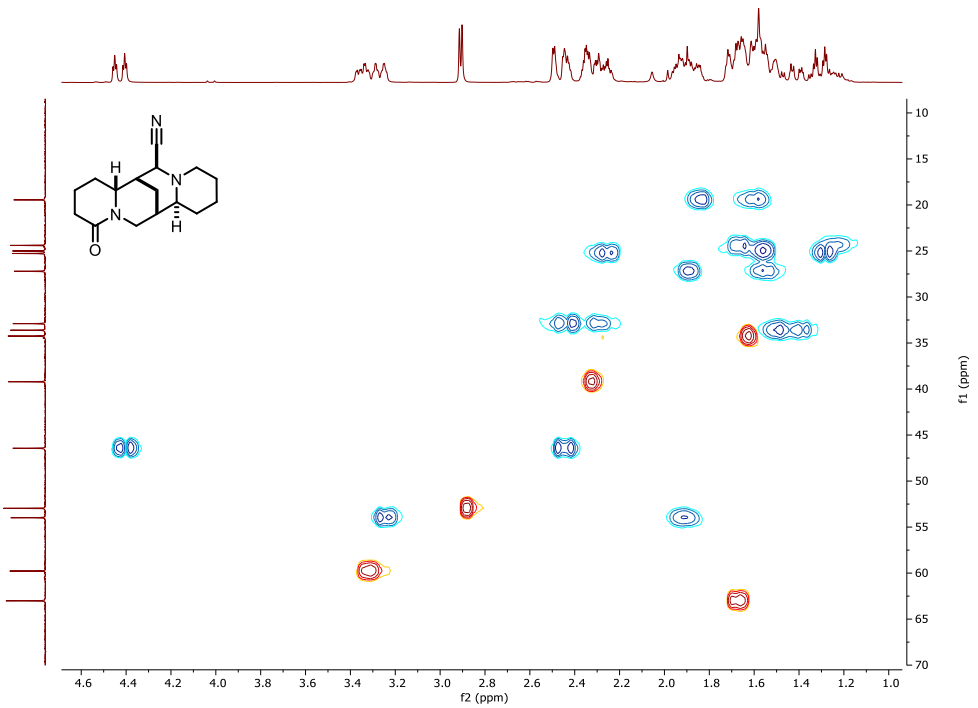

Figure 5.31: HSQC spectrum of 17-cyano-*rac*-lupanine (10)

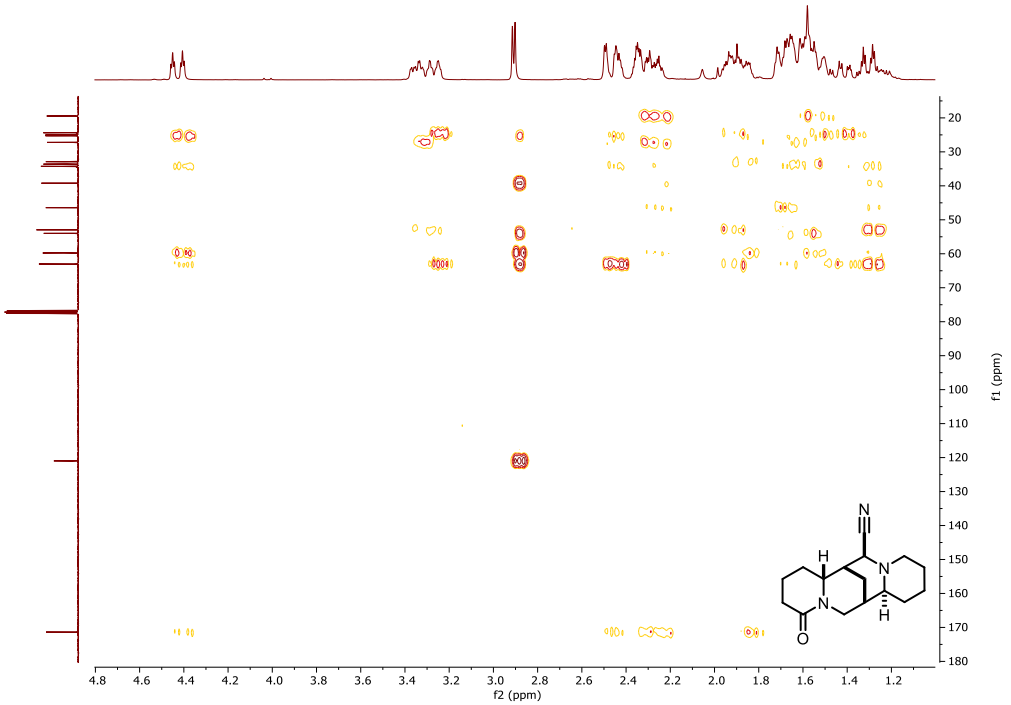

Figure 5.32: HMBC spectrum of 17-cyano-*rac*-lupanine (10)

5.7 Appendix 7: 17-oxo-*rac*-lupanine (11) Characterization

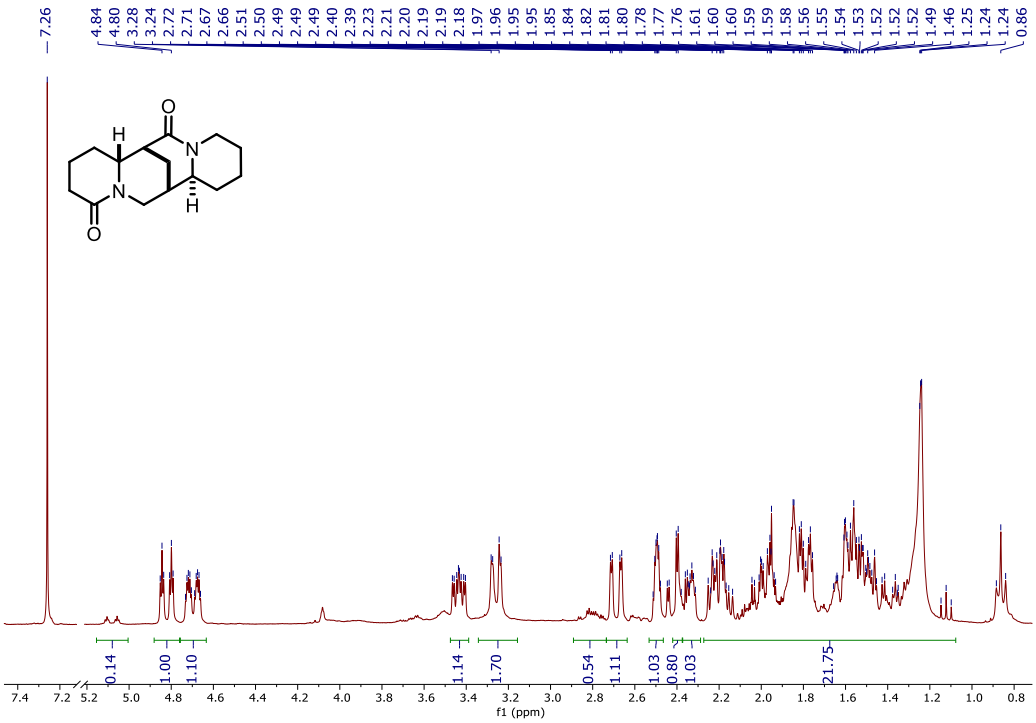

Figure 5.33: ^{1}H NMR spectrum of 17-oxo-*rac*-lupanine (11)

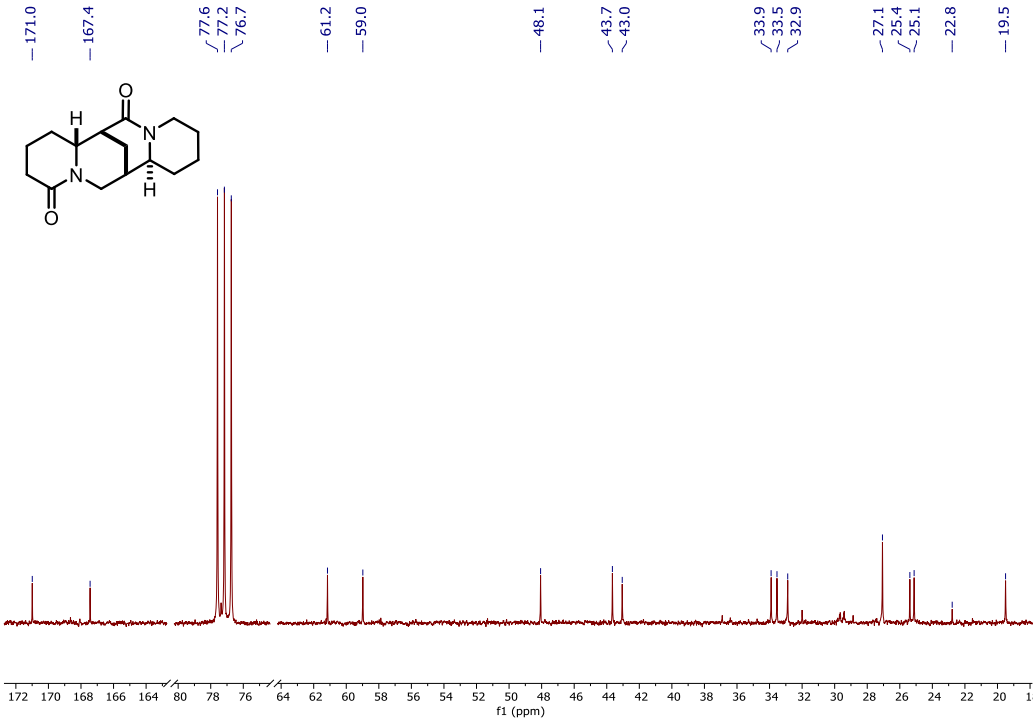

Figure 5.34: ^{13}C NMR spectrum of 17-oxo-*rac*-lupanine (11)

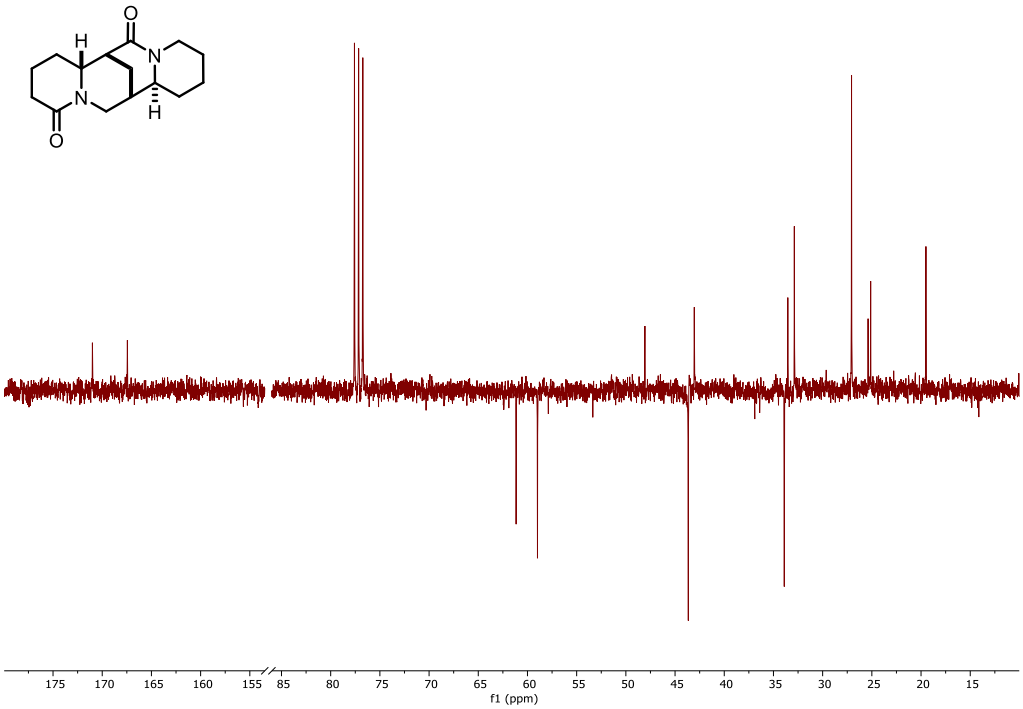

Figure 5.35: APT DEPT spectrum of 17-oxo-*rac*-lupanine (11)

5.8 Appendix 8: Derivatization of 17-cyano-*rac*-lupanine and 17-cyano-*rac*-sparteine

5.8.1 Nitrile reduction

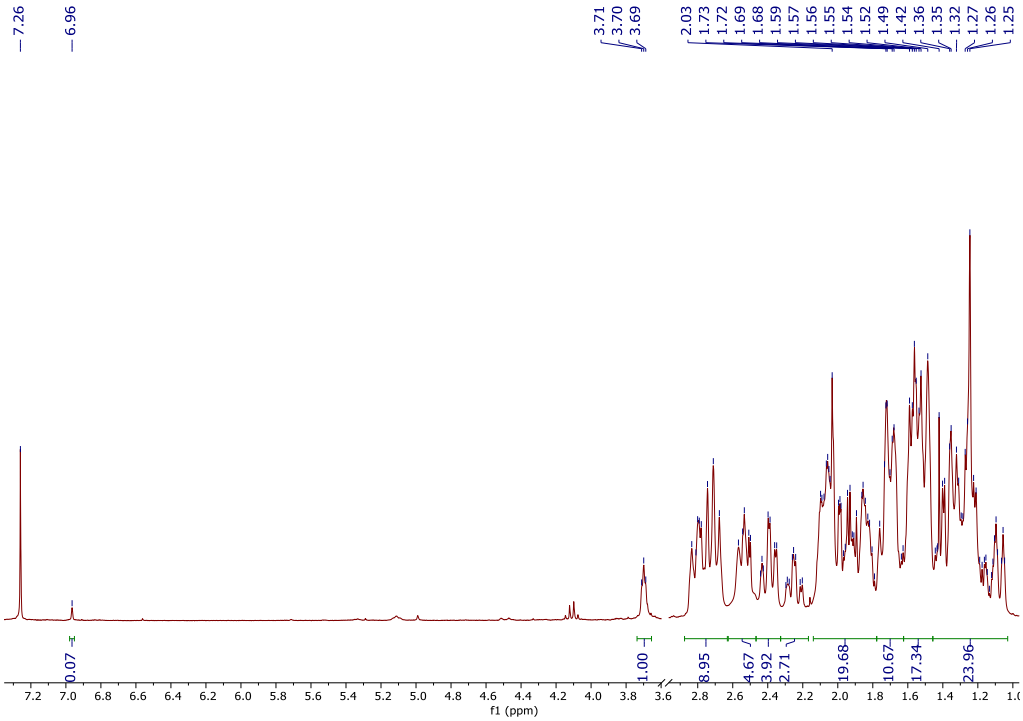

Figure 5.36: ^{1}H NMR crude of 17-cyano-*rac*-lupanine reduction with $LiAlH_4$.

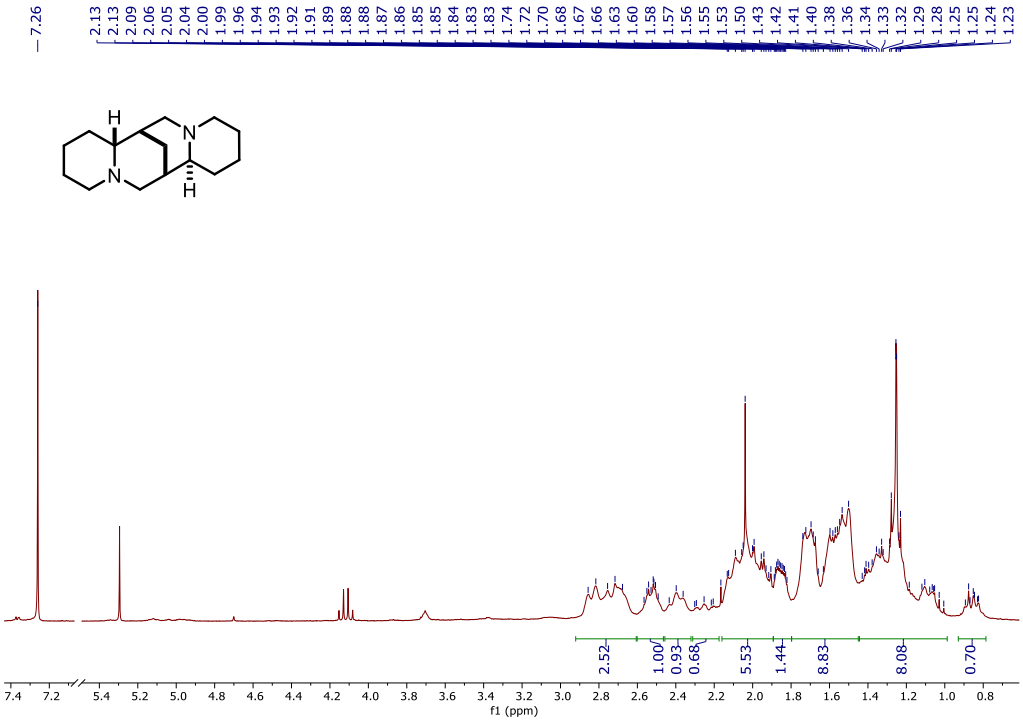

Figure 5.37: ^{1}H NMR spectrum of *rac*-sparteine (9) from 17-cyano-*rac*-lupanine reduction with DIBAL

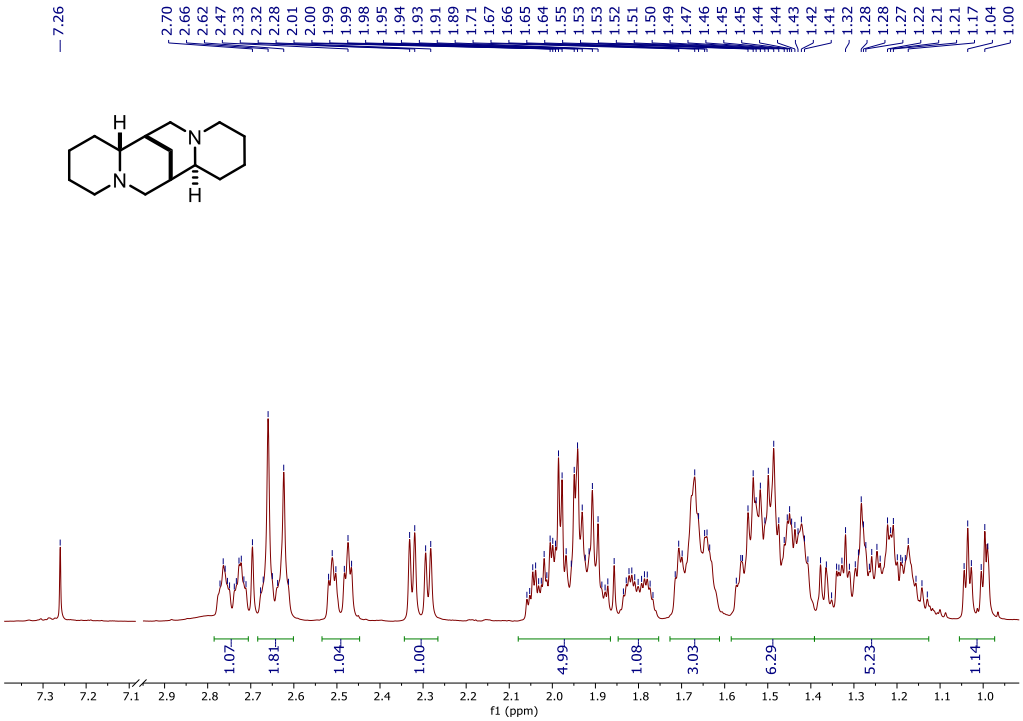

Figure 5.38*:* ^{1}H NMR spectrum of *rac*-sparteine (9) from 17-cyano-*rac*-sparteine catalytic hydrogenation

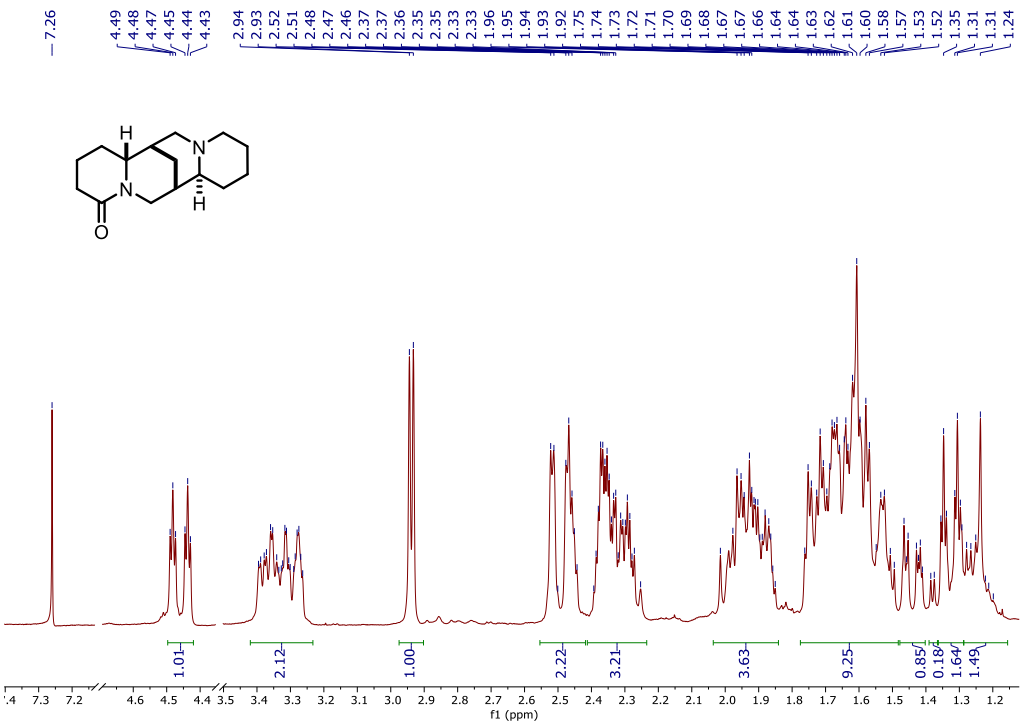

Figure 5.39*:* ^{1}H NMR spectrum of *rac*-lupanine (8) from 17-cyano-*rac*-lupanine catalytic hydrogenation

5.8.2 Nitrile Hydrolysis

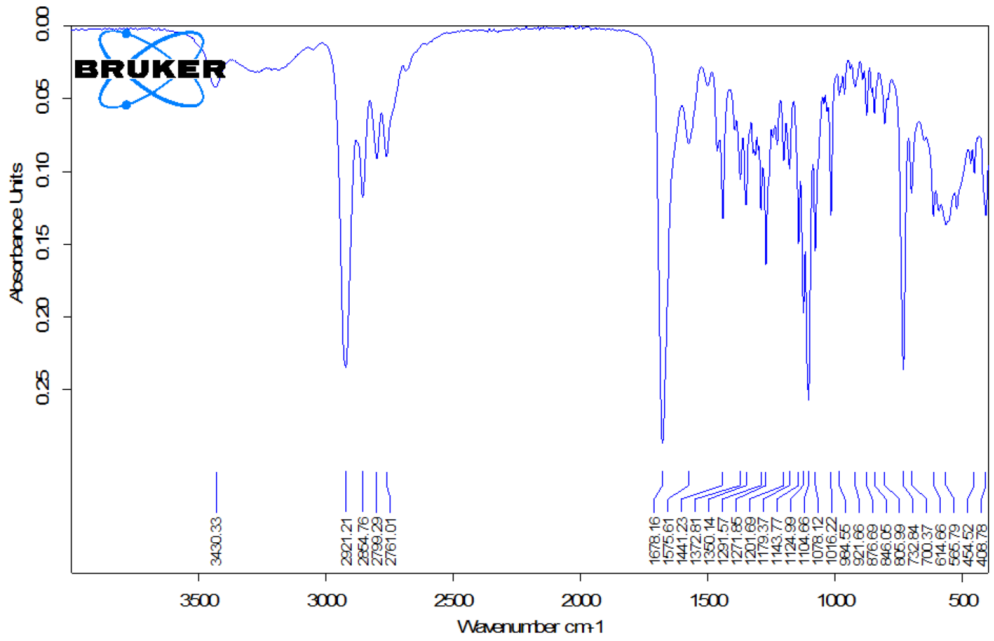

Figure 5.40: IR spectrum from crude of 17-cyano-rac-sparteine hydrolysis

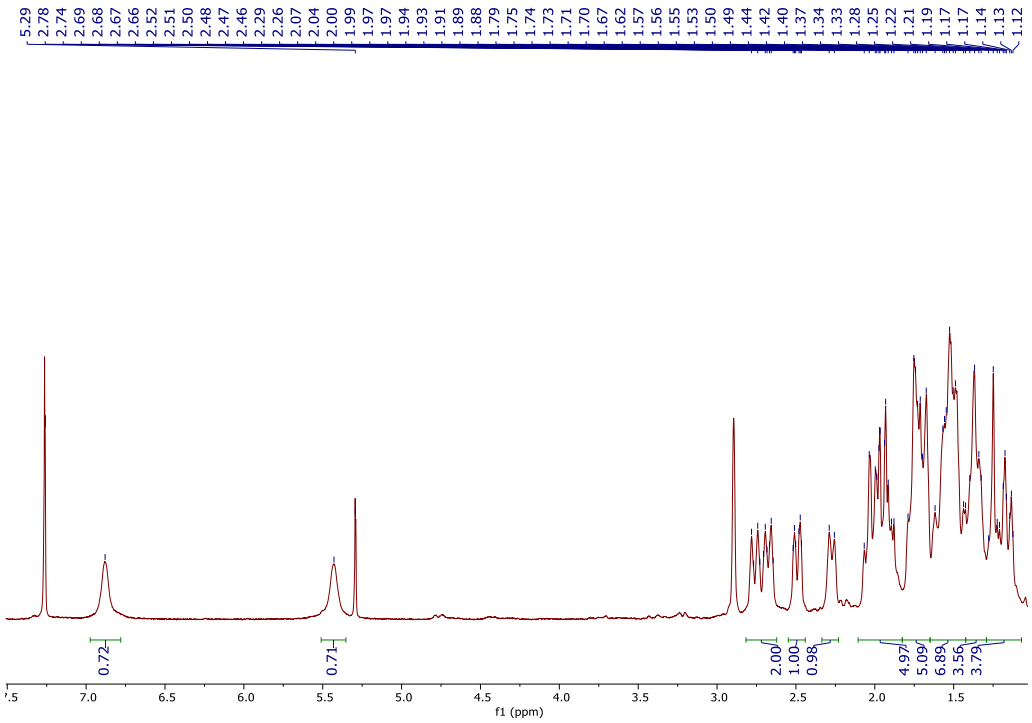

Figure 5.41: ^{1}H NMR spectrum from crude of 17-cyano-*rac*-sparteine hydrolysis

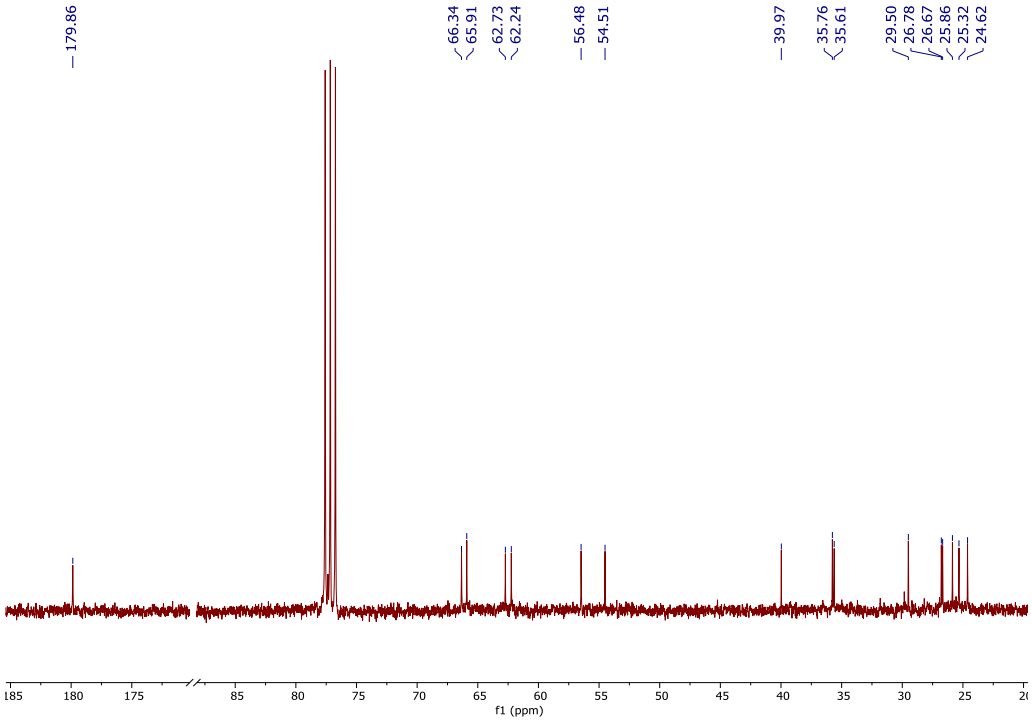

Figure 5.42: ^{13}C NMR spectrum from crude of 17-cyano-*rac*-sparteine hydrolysis

5.8.3 17-dehydrolupaninium triflate (13) characterization

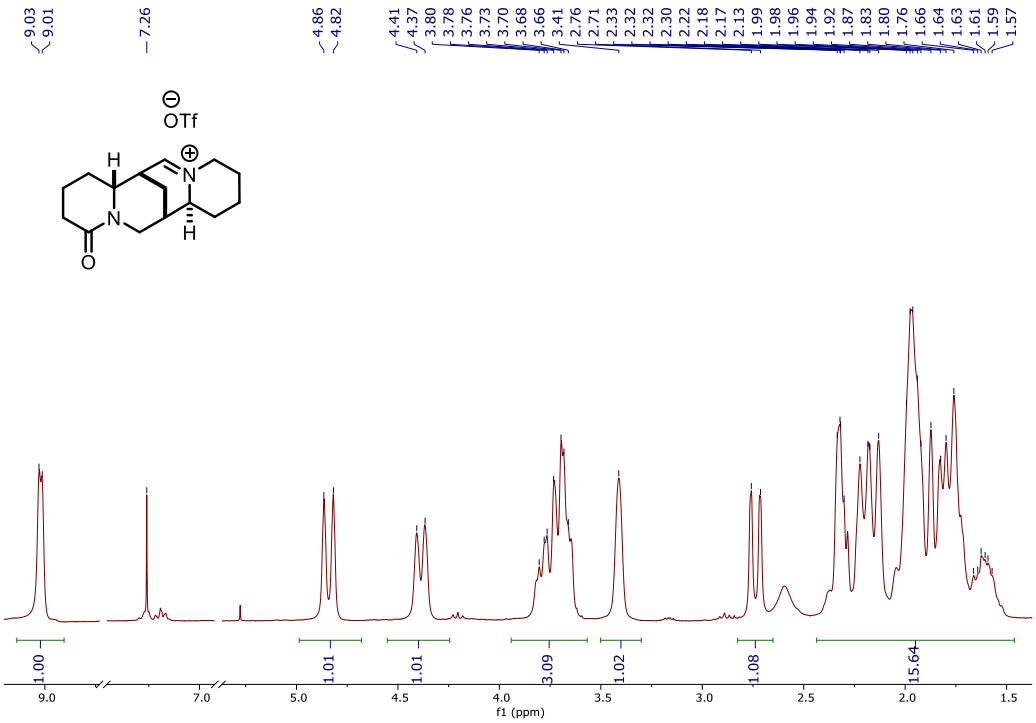

Figure 5.43: ^{1}H NMR spectrum of 17-dehydrolupaninium triflate (13)

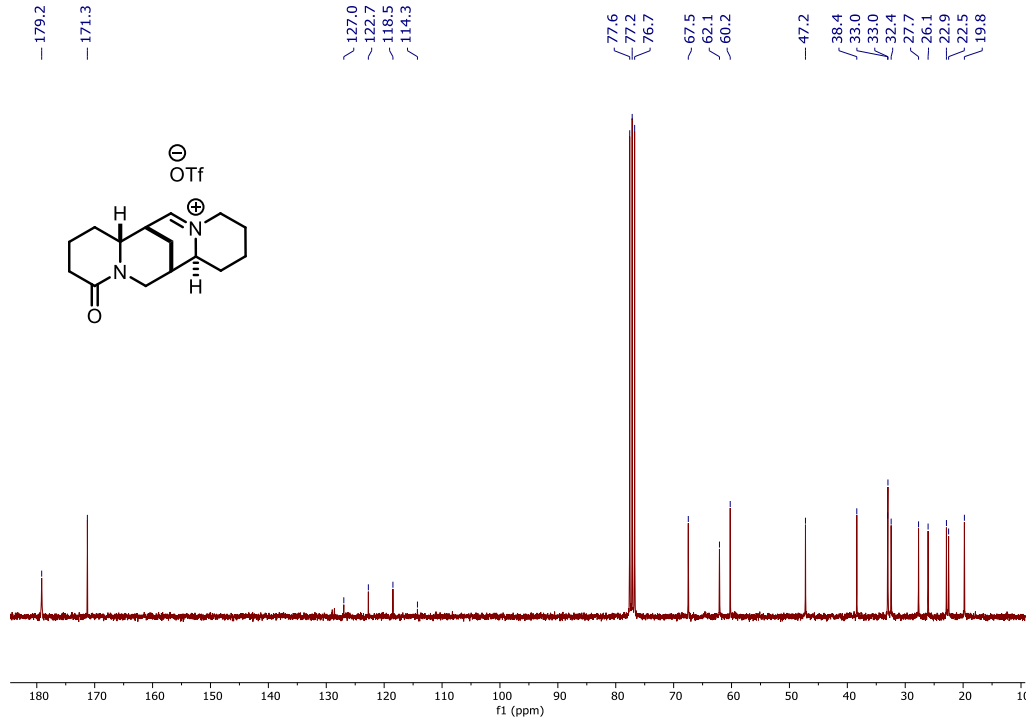

Figure 5.44: ^{13}C NMR spectrum of 17-dehydrolupaninium triflate (13)

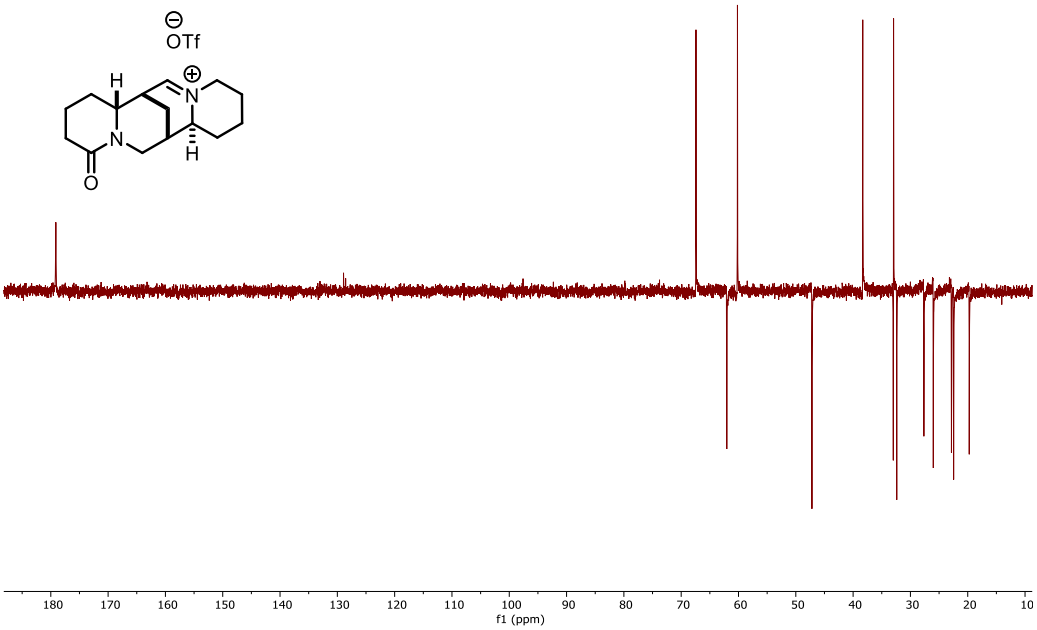

Figure 5.45: APT DEPT of 17-dehydrolupaninium triflate (13)

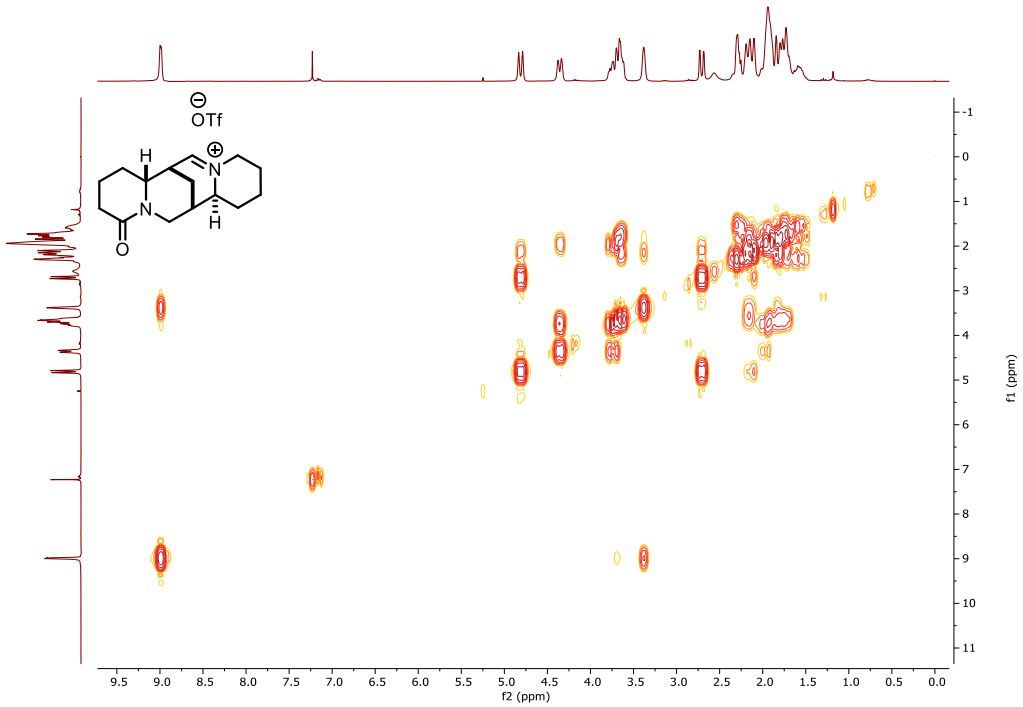

Figure 5.46: COSY spectrum of 17-dehydrolupaninium triflate (13)

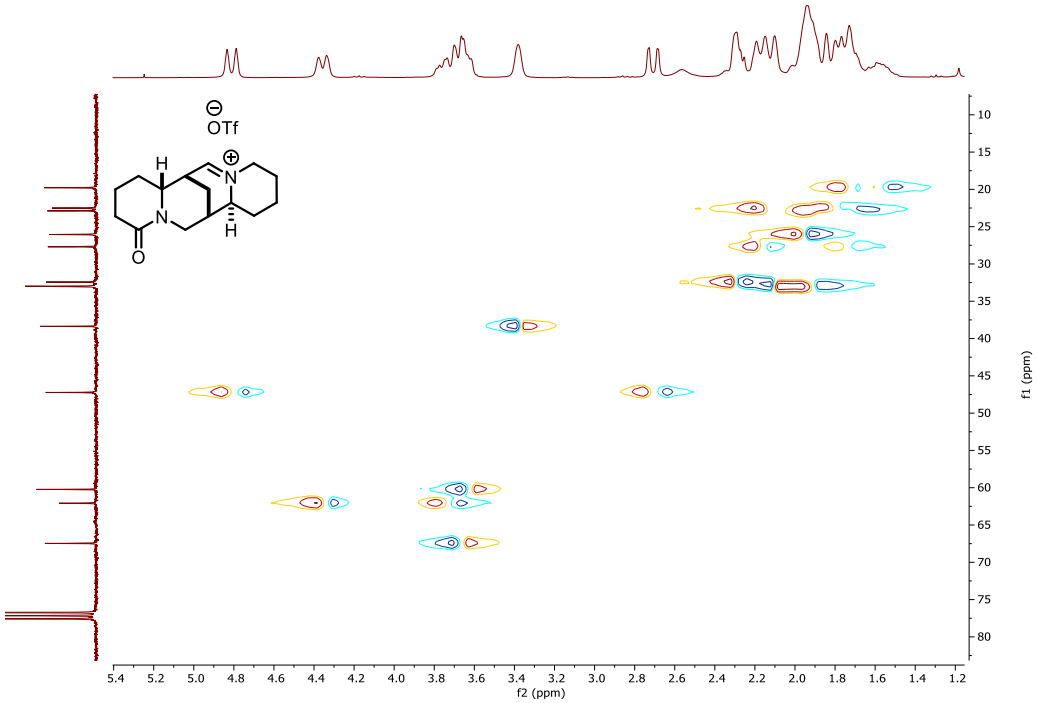

Figure 5.47: HSQC spectrum of 17-dehydrolupaninium triflate (13)

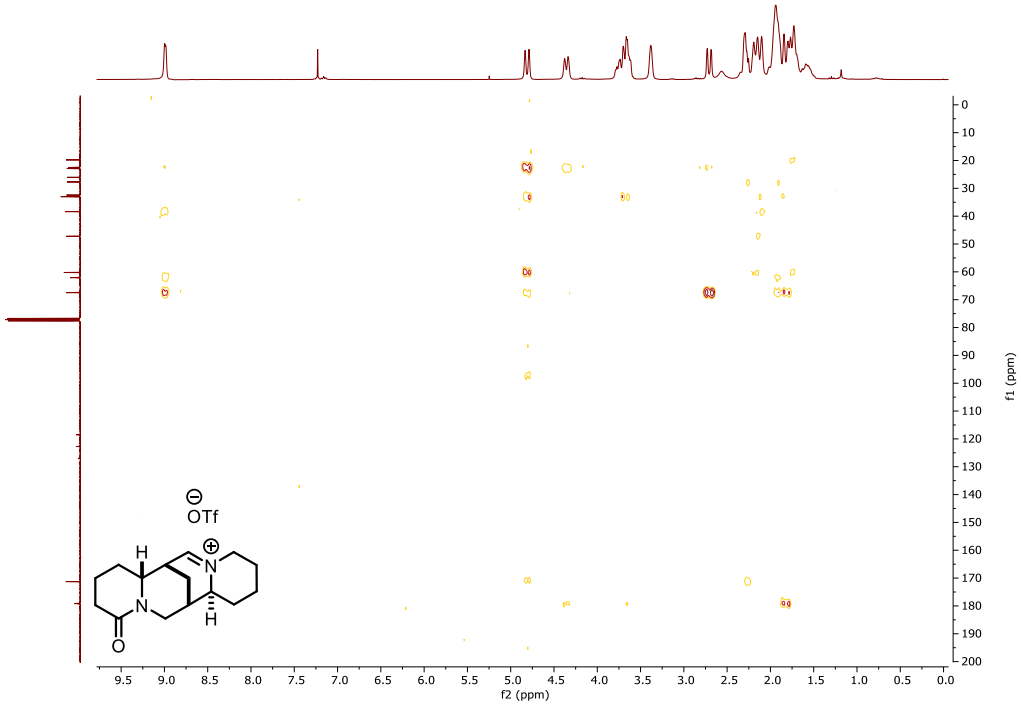

Figure 5.48: HMBC spectrum of 17-dehydrolupaninium triflate (13)

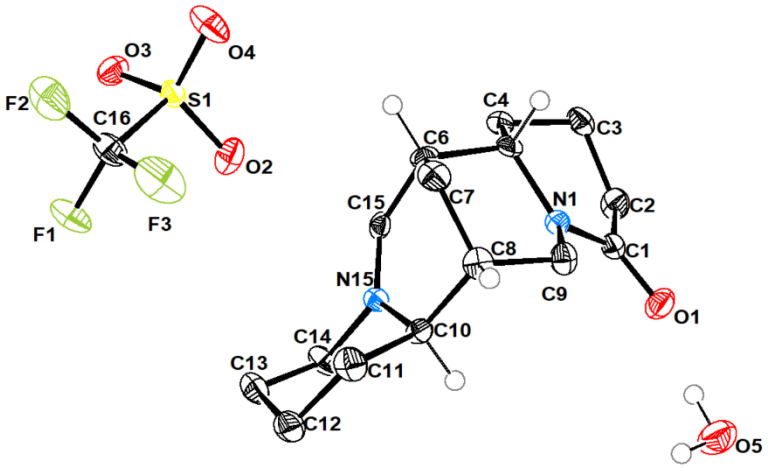

Figure 5.49: X-ray characterization of 17-dehydrolupaninium triflate (13)

5.8.4 Tetrazole Synthesis

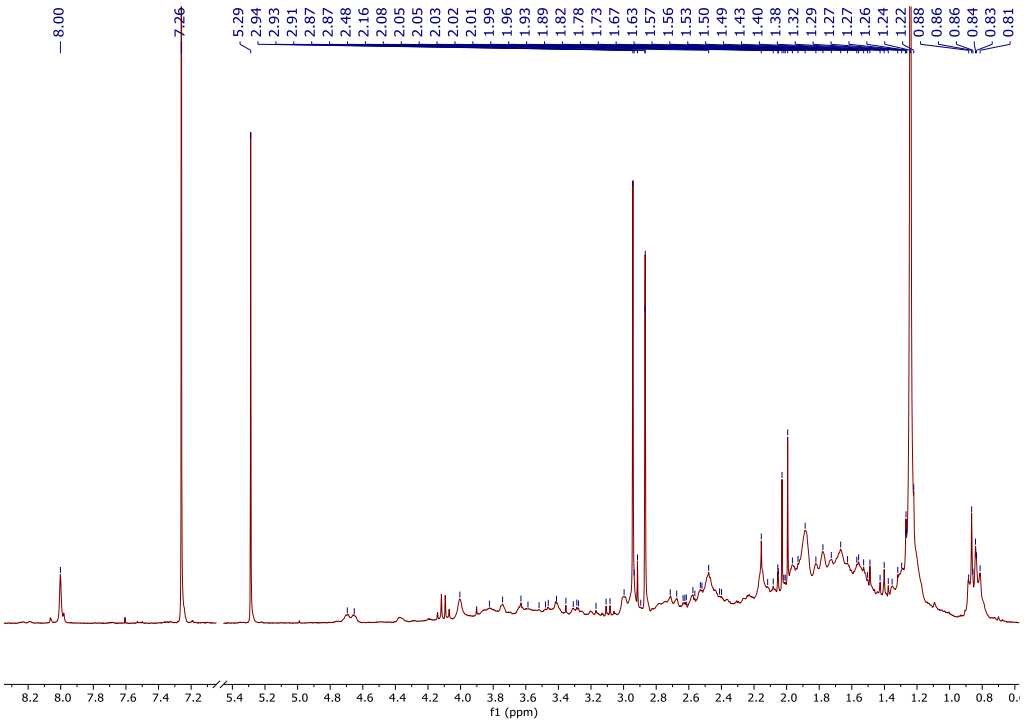

Figure 5.50: ^{1}H NMR crude of tetrazole synthesis, using as starting material 17-cyano-*rac*-sparteine

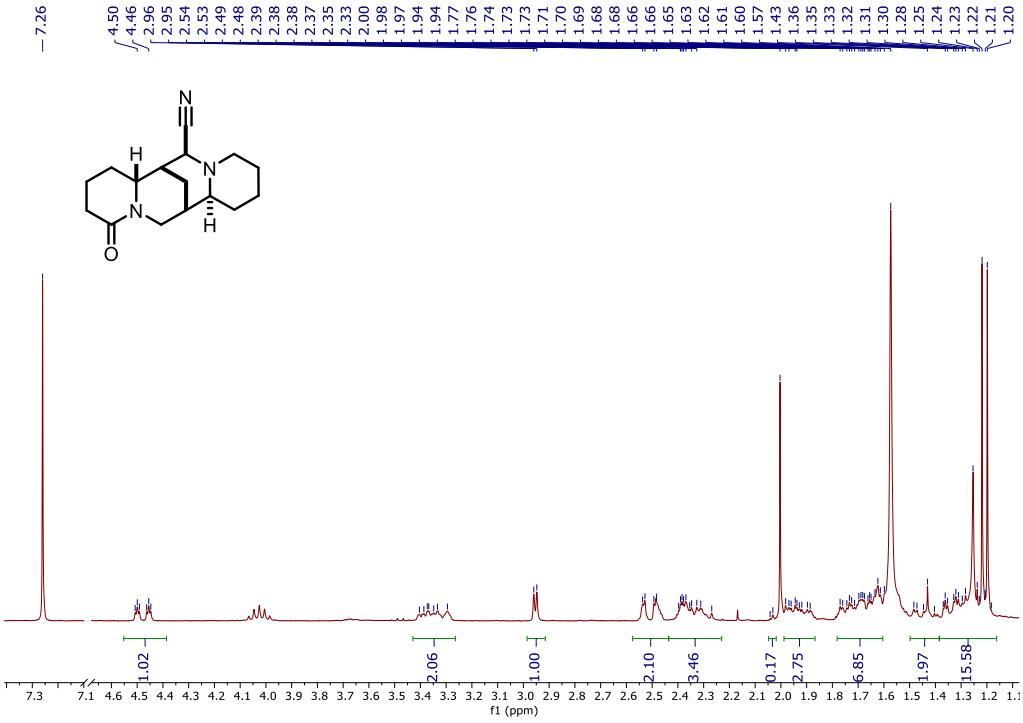

Figure 5.51: ^{1}H NMR spectrum of 17-cyano-*rac*-lupanine (10) from 17-cyano-*rac*-lupanine tetrazole synthesis

5.9 Appendix 9: Pharmacological activity of natural products containing the labdane skeleton

Structure	Natural Source	Biological Activity
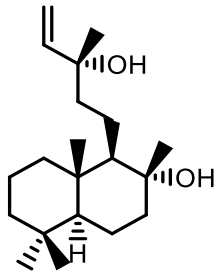	Leaves of *Cistus incanus* (Cistaceae)	Antibacterial
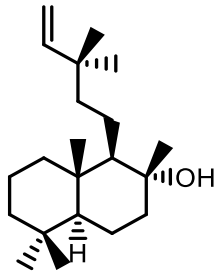	*Cistus incanus* (Cistaceae)	Antibacterial
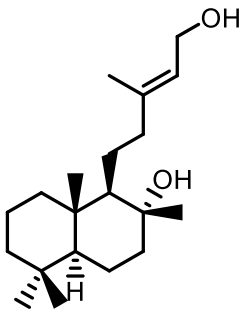	*Cistus incanus* (Cistaceae)	Antibacterial
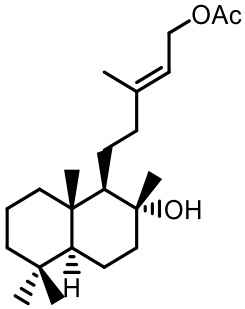	*Cistus incanus* (Cistaceae)	Antibacterial

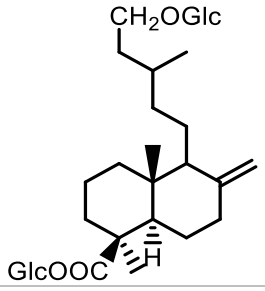	Leaves of *Viburnum suspensum* (Caprifoliaceae)	Antibacterial
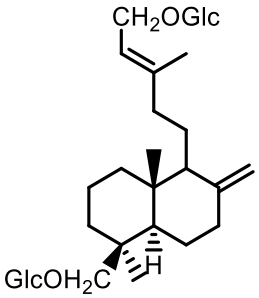	Leaves of *Viburnum suspensum* (Caprifoliaceae)	Antibacterial
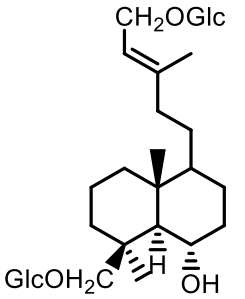	Leaves of *Viburnum suspensum* (Caprifoliaceae)	Antibacterial
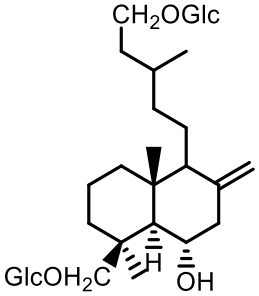	Leaves of *Viburnum suspensum* (Caprifoliaceae)	Antibacterial
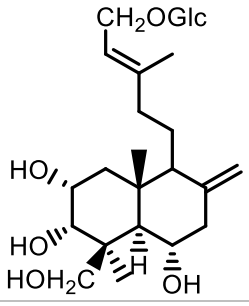	Leaves of *Viburnum suspensum* (Caprifoliaceae)	Antibacterial
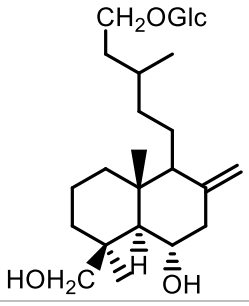	Leaves of *Viburnum suspensum* (Caprifoliaceae)	Antibacterial

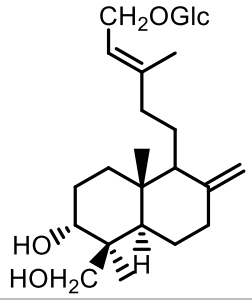	Leaves of *Viburnum suspensum* (Caprifoliaceae)	Antibacterial
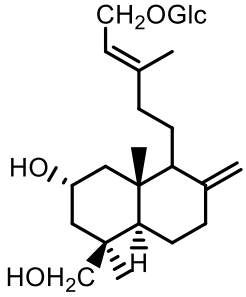	Leaves of *Viburnum suspensum* (Caprifoliaceae)	Antibacterial
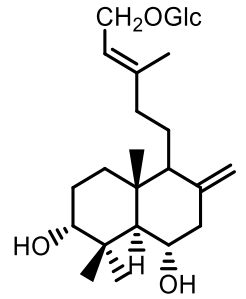	Leaves of *Viburnum suspensum* (Caprifoliaceae)	Antibacterial
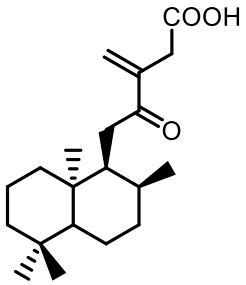	*Premna oligotricha* (Verbenaceae)	Antimicrobial
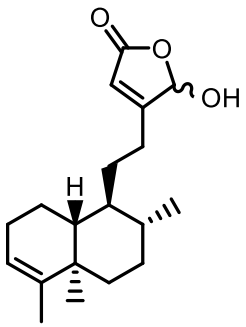	*Premna oligotricha* (Verbenaceae)	Antimicrobial
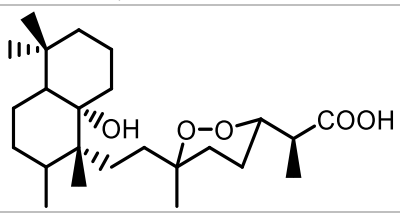	Thai sponge of the *Mycale* genus	Antibacterial Antiviral

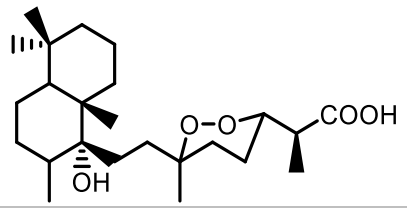	Thai sponge of the *Mycale* genus	Antibacterial Antiviral
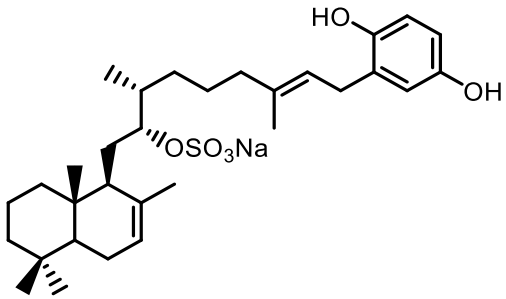	Dark brown sponge (Halichondriidae)	Antimicrobial Antifungal Antibacterial
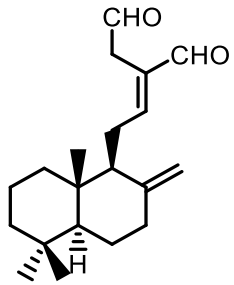	Seeds from *Alpinia galangal and Aframomun daniellii,* and rhizomes of *Hedychium coronarium* (Zingiberaceae)	Antifungal and Cytotoxic
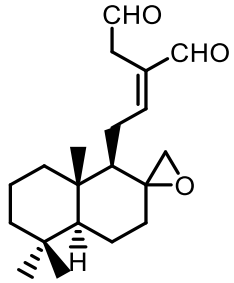	Seeds from *Alpinia galangal* and *Aframomun daniellii* (Zingiberaceae)	Antifungal
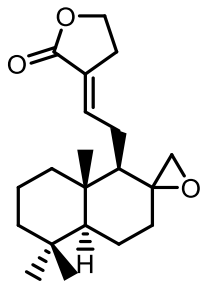	Seeds of *Alpinia galangal* (Zingiberaceae)	Antifungal
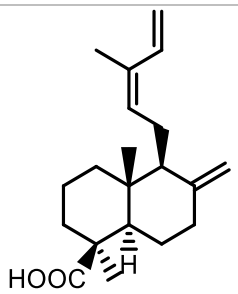	Leaves of *Cryptomeria japonica* (Taxodiaceae)	Anti-inflammatory
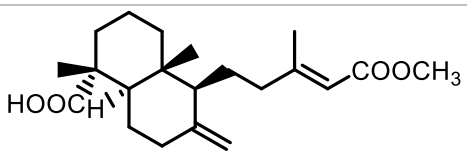	Stem bark of *Polyalthia macropoda* (Annonaceae)	Antileishmanial

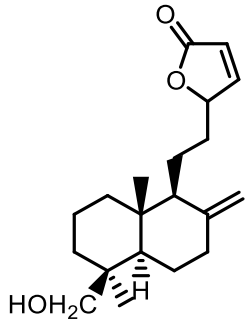	Root of *Melodinus monogynus* (Apocyanaceae)	Cardiotonic Activity
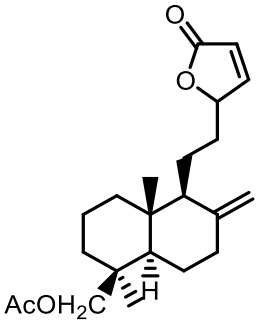	Root of *Melodinus monogynus* (Apocyanaceae)	Cardiotonic Activity
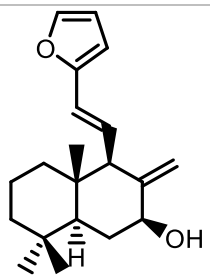	Rhizomes of *Hedychium coronarium* (Zingiberaceae)	Cytotoxic
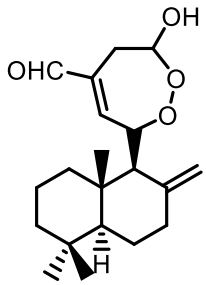	Rhizomes of *Hedychium coronarium* (Zingiberaceae)	Cytotoxic
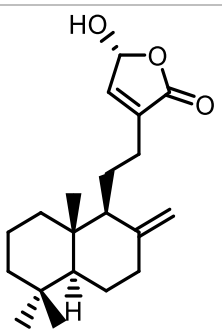	Rhizomes of *Hedychium coronarium* (Zingiberaceae)	Cytotoxic

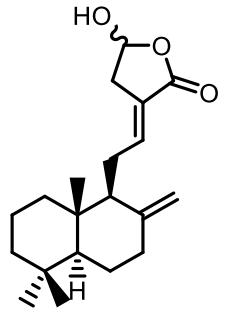	Rhizomes of *Hedychium coronarium* (Zingiberaceae)	Cytotoxic
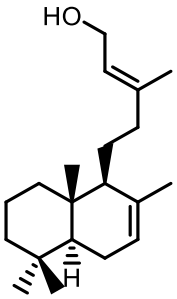	*Cistus creticus* (Cistaceae)	Cytotoxic
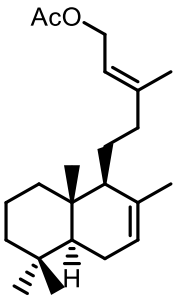	*Cistus creticus* (Cistaceae)	Cytotoxic
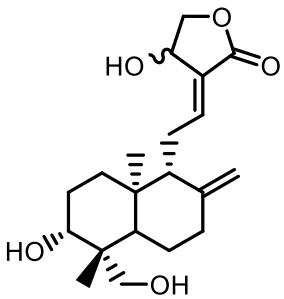	Aerial parts of *Andrographis paniculate* (Acanthaceae)	Cell differentiation inducer/ phagocytosis inducer
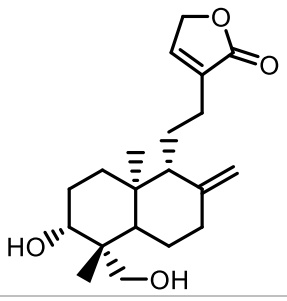	Aerial parts of *Andrographis paniculate* (Acanthaceae)	Cell differentiation inducer/ phagocytosis inducer
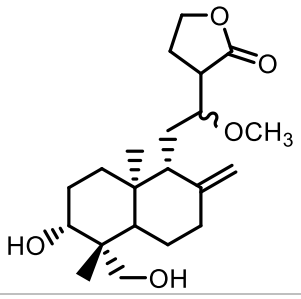	Aerial parts of *Andrographis paniculate* (Acanthaceae)	Cell differentiation inducer/ phagocytosis inducer

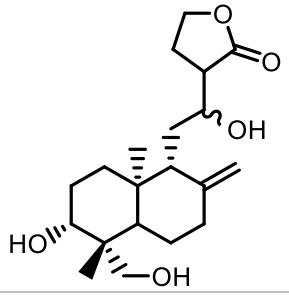	Aerial parts of *Andrographis paniculate* (Acanthaceae)	Cell differentiation inducer/ phagocytosis inducer
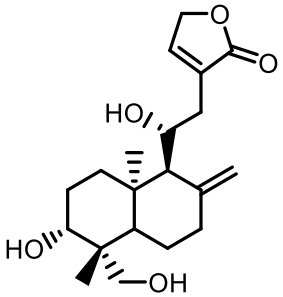	Aerial parts of *Andrographis paniculate* (Acanthaceae)	Cell differentiation inducer/ phagocytosis inducer
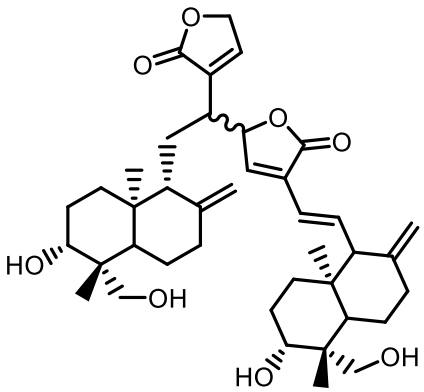	Aerial parts of *Andrographis paniculate* (Acanthaceae)	Cell differentiation inducer/ phagocytosis inducer
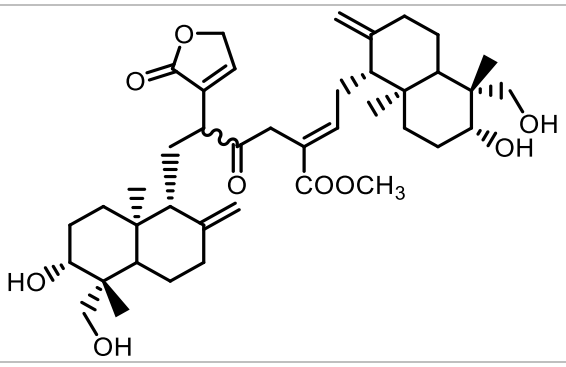	Aerial parts of *Andrographis paniculate* (Acanthaceae)	Cell differentiation inducer/ phagocytosis inducer
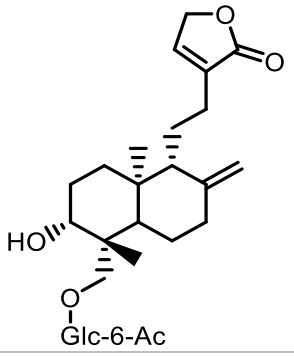	Aerial parts of *Andrographis paniculate* (Acanthaceae)	Cell differentiation inducer/ phagocytosis inducer

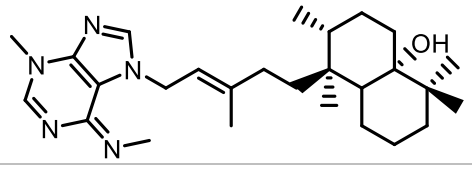	Marine orange sponge *Agelas mauritiana*	Cytotoxicity α – adrenergic blockers Ca^{2+} channel antagonists
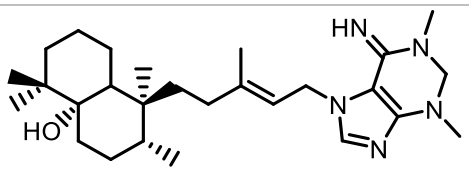	Marine orange sponge *Agelas mauritiana*	Cytotoxicity α – adrenergic blockers Ca^{2+} channel antagonists
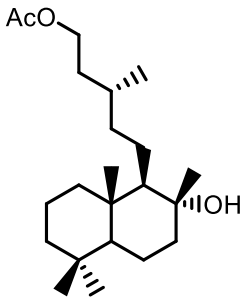	Synthesized form labdanediol (isolated form *Oxylobus glanduliferus*)	Anti-inflammatory
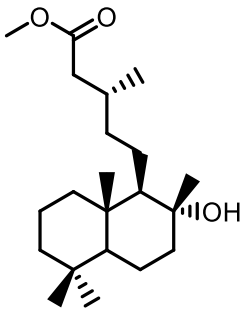	Synthesized form labdanediol (isolated form *Oxylobus glanduliferus*)	Anti-inflammatory
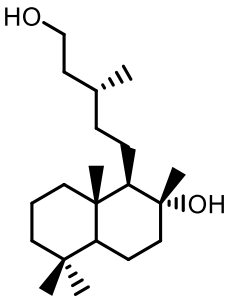	*Oxylobus glanduliferus*	Cytotoxic
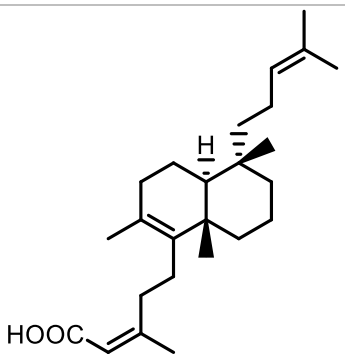	Marine sponge genus *Dysidea*	Inhibitor of aldose reductase

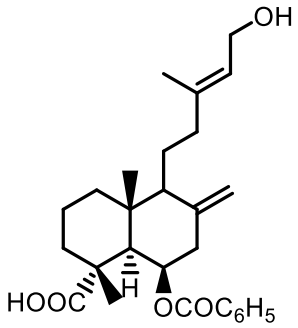	Roots of *Scoparia dulcis* (Scrophulariaceae)	Inhibitor of β - glucuronidase